

***GOME-2 / Metop-A Level 1B Product Validation  
Report No. 5: Status at Reprocessing G2RP-R2***

Doc.No. : EUM/OPS-EPS/REP/09/0619  
Issue : v1F  
Date : 18 June 2012  
WBS :

EUMETSAT  
Eumetsat-Allee 1, D-64295 Darmstadt, Germany  
Tel: +49 6151 807-7  
Fax: +49 6151 807 555  
<http://www.eumetsat.int>

***This page intentionally left blank.***

## Document Change Record

<i>Issue / Revision</i>	<i>Date</i>	<i>DCN. No</i>	<i>Changed Pages / Paragraphs</i>
1	13/01/2012		First version.
1C	02/04/2012		Remove redundant pages
1D	12/04/2012		Initial version for review/comment.
1E	29/05/2012		Updates following DRR: <ul style="list-style-type: none"> <li>• Add bullet on scan-angle dependent biases in section 1.1</li> <li>• PMD band settings, section 4.2</li> <li>• Band 1A/B separation and settings, section 4.2</li> <li>• Added information on predicted OSV information used during reprocessing in section 6.2.2</li> <li>• Added statistical information on FRESCO+/AVHRR collocation in section 6.2.4</li> <li>• Editorial changes and minor textual comments included</li> </ul>
1F	06/18/2012		Formatting changes only, <ul style="list-style-type: none"> <li>• Rebuilt reference tables.</li> </ul>

## Table of Contents

<b>1</b>	<b>Introduction .....</b>	<b>11</b>
1.1	Purpose and Scope .....	11
1.2	Description of Validation Environment .....	11
<b>2</b>	<b>Applicable Documents .....</b>	<b>12</b>
<b>3</b>	<b>Reference Documents .....</b>	<b>12</b>
3.1	Acronyms and Abbreviations Used in this Document .....	13
<b>4</b>	<b>The Global Ozone Monitoring Experiment 2 (GOME-2) .....</b>	<b>14</b>
4.1	The Instrument.....	14
4.2	GOME-2 Optical Layout ([AD2]) .....	15
4.2.1	Polarisation Measurement Device (PMD) band settings.....	17
4.3	GOME-2 Specifications Summary.....	19
4.4	GOME-2 Level 1b products .....	19
4.5	GOME-2 Level 2 Products.....	19
4.6	Other Useful links .....	20
<b>5</b>	<b>Dataset and Instrument References .....</b>	<b>21</b>
5.1	Main dataset identifiers.....	21
5.1.1	G2RP-R2 processor version.....	21
5.1.2	G2RP-R2 reference period.....	21
5.1.3	G2RP-R2 product and format version .....	21
5.2	Main instrument and platform events .....	21
5.3	Main processor and configuration differences to G2RP-R1 (PPF 4.0) .....	23
<b>6</b>	<b>Validation Strategy .....</b>	<b>24</b>
6.1	Target parameters within the scope of current validation .....	24
6.2	Target parameters outside the scope of current validation .....	25
6.2.1	Geo-referencing (A2.6, A3.2).....	25
6.2.2	PPG correction (A2.11, A3.5) .....	27
6.2.3	Stray light correction (A2.19, A3.9).....	27
6.2.4	Cloud properties (FRESCO+) (A3.15).....	28
<b>7</b>	<b>Validation of target parameters.....</b>	<b>31</b>
7.1	Instrument Dark Signal Correction (A2.8, A2.9, A3.3).....	31
7.1.1	Description.....	31
7.1.2	Analysis.....	31
7.1.3	Interpretation.....	32
7.1.4	Assessment .....	39
7.2	Thermal Performance Monitoring (Overlap-point stability, PMD-P/S ratio -sensitivity, spectral calibration stability).....	40
7.2.1	Description .....	40
7.2.2	Analysis.....	42
7.2.3	Interpretation.....	42
7.2.4	Assessment .....	44
7.3	Instrument spectral calibration (A2.13-A2.15, A3.6).....	45
7.3.1	Definition.....	45
7.3.2	Analysis.....	45
7.3.3	Interpretation.....	45
7.3.4	Assessment .....	49
7.4	Instrument Etalon Correction (A2.16, A2.17, A3.7) .....	50
7.4.1	Description.....	50
7.4.2	Analysis.....	51
7.4.3	Interpretation.....	51
7.5	Instrument polarisation correction (Stokes Fractions) (A2.21, A3.10).....	54
7.5.1	Monitoring Stokes Fractions for Special Earth Viewing Geometries.....	54
7.5.2	Monitor Stokes Fractions for Earthshine Scanning Measurements – Limiting Atmosphere approach .....	59
7.6	Instrument diffuser performance (A2.20, A3.12) .....	62
7.6.1	Description.....	62

---

7.6.2	Analysis.....	62
7.6.3	Interpretation.....	63
7.7	Level 1B data record consistency and long-term signal variation for sun and earthshine radiances (A3.11, A3.12) .....	64
7.7.1	Solar Measurements.....	64
7.7.2	Solar Measurements for PMD and main channels at individual wavelength .....	66
7.7.3	Earthshine long-term degradation .....	71
7.7.4	Results for reflectivity degradation from G2RP-R2 .....	81
7.7.5	Degradation signatures from G2RP-R2 for band 1a (Channel 1) .....	84
7.8	Differences with Respect to the Extended G2RP-R1 (January 2007 to January 2011; PPF 4.0).....	88
7.8.1	Homogeneity with respect to NRT: differences for the solar path .....	88
7.8.2	Differences with respect to R1: Earthshine path – Stokes fractions.....	92
7.8.3	Differences with respect to R1: Earthshine Path.....	99
7.8.4	Differences with respect to R1: Reflectivity degradation rates. ....	105
<b>8</b>	<b>Conclusions .....</b>	<b>109</b>
8.1	Product Validation Summary .....	109
8.1.1	Product Validation Open Issues .....	110
8.1.2	Processor Open Issues .....	110
8.1.3	Instrument Performance .....	110
8.1.4	Calibration Key Data.....	110
8.2	Recommendations.....	110

## Table of Tables

Table 1: Channel characteristics of GOME-2 spectral coverage and resolution .....	16
Table 2: Main channel band settings of GOME-2. The band separation shift between band 1A and B occurred during orbit 11119 on 10 December 2008.....	16
Table 3: Default GOME-2 PMD band definitions (v1.0) valid from launch to 11 March 2008 in orbit 7226.....	18
Table 4: GOME-2 PMD band definitions (v3.1). This set of definitions has been uploaded for orbit on 11 March 2008 during orbit 7227. ....	18
Table 5: Product and format type list .....	20
Table 6: Metop-A/GOME-2 FM3 instrument events and operations .....	21
Table 7: GOME wavelength range per pixel for all main channels.....	32
Table 8: Validity region of the etalon correction.....	50

## Table of Figures

Figure 1: The Global Ozone Monitoring Experiment–2 (GOME-2) Instrument.....	14
Figure 2: GOME-2 transmittance as derived from the GOME-2 level 1b radiance product. Selected spectral regions with absorption signatures used for various trace gas products as derived from GOME-2 level-1b radiances are shown. ....	15
Figure 3: GOME-2 optical layout. The optics lie in one plane (except insets A and B). Nadir is in -Z direction. ....	17
Figure 4: Along-track (left panels) and across-track (right panels) shifts of geo-referencing parameters as evaluated from co-location to AVHRR signals. Note the two different date ranges: February 2007 and October 2011. ....	26
Figure 5: Detector pixel-to-pixel gain (PPG) contribution for channel 1 (blue), 2 (red), 3 (green), 4 (yellow) over the reference period.....	27
Figure 6: GOME-2/Metop-A FRESCO+ R2 cloud fraction values (left panel) for one orbit in February 2007 (upper panels) and in October 2011 (lower panels).....	28
Figure 7: Correlations for GOME-2 /Metop-A FRESCO+ R2 versus GOME-2 footprint equivalent cloud fractions derived from AVHRR (albedo test using visible AVHRR channels) for one orbit in February 2007 (left panel) and in October 2011 (right panel).....	29
Figure 8: Comparison of Zonal Means for GOME-2 /Metop-A FRESCO+ R2 versus GOME-2 footprint equivalent cloud fractions derived from AVHRR (albedo test using visible AVHRR channels) for one orbit in February 2007 (left panel) and in October 2011 (right panel).....	29
Figure 9: FRESCO+ fit flagging statistics for one orbit in February 2007 (left panel) and in October 2011 (right panel). Fail flag=0: successful fit; Fail flag=1: reflectivity out of range; Fail flag=2: solar zenith angle out of range; Fail flag=3: Satellite Zenith angle out of range; Fail flag=4: non-convergence of fit; Fail flag=5: missing input data. ....	30
Figure 10: Band 1A averaged offset (blue points) and leakage current (green points).....	32
Figure 11: Averaged offset (blue points) and leakage current green points) for Bands 1B–Band 2B...	33
Figure 12: Averaged offset (blue points) and leakage current green points) for Bands 3 and Band 4..	34
Figure 13: Averaged offset (blue points) and leakage current (green points) for Bands PMD-P and PMD-S. ....	35
Figure 14: Averaged noise for Band 1. ....	36
Figure 15: Averaged noise for Band 2. ....	36
Figure 16: Averaged noise for Band 4. ....	37
Figure 17: Averaged noise for Band 5. ....	37
Figure 18: Averaged noise for Band 6 .....	38
Figure 19: Averaged noise for Band 7. ....	38
Figure 20: Averaged noise for PMD-S.....	39
Figure 21: Instrument main channels (upper panel) and PMD (lower panel) detector temperatures during the time covered by G2RP-R1. Temperature-related spikes appear in all channels (other main channel colours are hidden by channel 4; green) .....	40
Figure 22: Instrument Optical bench temperature for the reference time period. The orbital variation is about 1 K. ....	41
Figure 23: Relative percentage difference between PMD-P and PMD-S detector temperatures during the time covered by G2RP-R1. ....	41
Figure 24: Overlap point position for the transition between channel 1 and 2 in detector pixel space..	42

Figure 25: Overlap-point position for the transition between channel 1 and 2 in wavelength space.....	43
Figure 26: Overlap-point position for the transition between channel 2 and 3 in detector pixel space .	43
Figure 27: Overlap-point position for the transition between channel 2 and 3 in wavelength space.....	44
Figure 28: Spectral stability for the complete reprocessing period for main channels at 240 nm. ....	45
Figure 29: Spectral stability for the complete reprocessing period for main channels at 283 nm .....	46
Figure 30: Spectral stability for the complete reprocessing period for main channels at 311 nm (upper panel), and PMD channels at 311 nm (mid and lower panels). ....	46
Figure 31: Spectral stability for the complete reprocessing period for main channels at 380 nm (upper panel), and PMD channels at 380 nm (mid and lower panels). ....	47
Figure 32: Spectral stability for the complete reprocessing period for main channels at 420 nm (upper panel), and PMD channels at 420 nm (mid and lower panels). ....	47
Figure 33: Spectral stability for the complete reprocessing period for main channels at 570 nm (upper panel), and PMD channels at 570 nm (mid and lower panels). ....	48
Figure 34: Spectral stability for the complete reprocessing period for main channels at 745 nm (upper panel), and PMD channels at 745 nm (mid and lower panels). ....	48
Figure 35: Spectral stability of the co-registration between PMD-P and PMD-S in percentage of fractional detector pixels around 311 nm. ....	49
Figure 36: Spectral stability of the co-registration between PMD-P and PMD-S in percentage of fractional detector pixels around 745 nm. Note the different scales of the range axis .....	49
Figure 37: Typical Etalon correction derived from a daily WLS measurement.....	51
Figure 38: Typical etalon correction derived from daily WLS measurement over the reference period in channel 1 (lower panel) and 2 (upper panel). ....	52
Figure 39: Relative change of the WLS spectrum with respect to the beginning of the reference period (February 2007). The left column shows main channel 1 to 4 (in rows, bottom to top) results not corrected with the derived etalon signature. The right column shows the same but with the etalon correction applied. ....	53
Figure 40: Stokes fractions calculated for special earth viewing geometries averaged over the full reference period for G2RP-R2 January 2011. ....	55
Figure 41: Stokes fractions calculated for special Earth-viewing geometries over the full reference period and per PMD bands 1-6 for G2RP-R2 January 2011. ....	56
Figure 42: Stokes fractions calculated for special Earth-viewing geometries over the full reference period and per PMD bands 7-12 for G2RP-R2 January 2011. ....	57
Figure 43: Stokes fractions calculated for special Earth-viewing geometries over the full reference period and per PMD bands 13-15 for G2RP-R2 January 2011. ....	58
Figure 44: Limiting atmosphere plot for earthshine q-Stokes fractions and for all PMD bands. The data is derived from one orbit on 31 July 2007. ....	59
Figure 45: Limiting atmosphere plot for earthshine q-Stokes fractions and for all PMD bands. The data is derived from one orbit on 31 July 2008 .....	60
Figure 46: Limiting atmosphere plot for earthshine q-Stokes fractions and for all PMD bands. The data is derived from one orbit on 31 July 2009. ....	60
Figure 47: Limiting atmosphere plot for earthshine q-Stokes fractions and for all PMD bands. The data is derived from one orbit on 31 July 2010. ....	61
Figure 48: Limiting atmosphere plot for earthshine q-Stokes fractions and for all PMD bands. The data is derived from one orbit on 31 July 2011. ....	61
Figure 49: Limiting atmosphere plot for earthshine q-Stokes fractions and for all PMD bands. The data is derived from one orbit on 31 July 2011. ....	61
Figure 50: SMR spectra for all four main channels, for the whole reference period and normalised to January 2007.....	65
Figure 51: SMR spectra for the PMD-P (left panel) and the PMD-S channels, for the entire reference period and normalised to January 2007.....	65
Figure 52: Solar mean reference (SMR) spectra for all four main channels normalised to January 2007. The red and the blue curve are ratios before and after the second throughput test in September 2009, respectively. The green curve is the ratio on 31 July 2011 .....	66
Figure 53: Solar mean reference (SMR) spectra for the PMD-P to S ratio, for the whole reference period and normalised to January 2007.....	67
Figure 54: SMR signals normalised to February 2007 at 310 nm in channel 1 for both main channel (blue curve) and PMD-P and PMD-S signals (red and green curve) .....	68

Figure 55: SMR signals normalised to February 2007 at 311 nm in Channel 2 for both main channel (blue curve) and PMD-P and PMD-S signals (red and green curve) .....	68
Figure 56: SMR signals normalised to February 2007 at 330 nm in channel 2 for both main channel (blue curve) and PMD-P and PMD-S signals (red and green curve) .....	69
Figure 57: SMR signals normalised to February 2007 at 380 nm in channel 2 for both main channel (blue curve) and PMD-P and PMD-S signals (red and green curve) .....	69
Figure 58: SMR signals normalised to February 2007 at 420 nm in channel 3 for both main channel (blue curve) and PMD-P and PMD-S signals (red and green curve) .....	70
Figure 59: SMR signals normalised to February 2007 at 570 nm in channel 3 for both main channel (blue curve) and PMD-P and PMD-S signals (red and green curve) .....	70
Figure 60: SMR signals normalised to February 2007 at 745 nm in channel 4 for both main channel (blue curve) and PMD-P and PMD-S signals (red and green curve) .....	71
Figure 61: "Stable" target areas used for the routine NRT monitoring as well as the evaluation of reprocessed earthshine data. For the evaluation of G2RP-R2 we consider only the Sahara area, which provides the most stable situation and best statistics (most clear-sky cases).....	72
Figure 62: Earthshine signals normalised to the mean of 2007 at 310 nm in Channel 1 and for every second scanner position (coloured curves). The SMR normalised signal, a dashed black line, is provided as a reference.....	73
Figure 63: Earthshine signals normalised to the mean of 2007 at 310 nm in Channel 1 and for every second scanner position (coloured curves). The SMR normalised signal, a dashed black line, is provided as a reference. A 3-day moving average is applied for smoothing. ....	74
Figure 64: Temporally smoothed earthshine signals normalised to the mean of 2007 at 311 nm in Channel 2 and for every second scanner position (coloured curves). The SMR normalised signal, a dashed black line, is provided as a reference.....	74
Figure 65: Temporally smoothed earthshine signals normalised to the mean of 2007 at 330 nm in Channel 2 and for every second scanner position (coloured curves). The SMR normalised signal, a dashed black line, is provided as a reference.....	75
Figure 66: Temporally smoothed earthshine signals normalised to the mean of 2007 at 380 nm in Channel 2 and for every second scanner position (coloured curves). The SMR normalised signal, a dashed black line, is provided as a reference.....	75
Figure 67: Temporally-smoothed earthshine signals normalised to the mean of 2007 at 420 nm in Channel 3 and for every second scanner position (coloured curves). The SMR normalised signal, a dashed black line, is provided as a reference.....	76
Figure 68: Temporally smoothed earthshine signals normalised to the mean of 2007 at 570 nm in Channel 3 and for every second scanner position (coloured curves). The SMR normalised signal, a dashed black line, is provided as a reference.....	76
Figure 69: Temporally smoothed earthshine signals normalised to the mean of 2007 at 745 nm in Channel 4 and for every second scanner position (coloured curves). The SMR normalised signal, a dashed black line, is provided as a reference.....	77
Figure 70: Earthshine signal degradation rate per year for the period before the second throughput test (left panel) and after the throughput test (right panel) at 310 nm (channel 1). The plots also show the corresponding degradation rate of SMR at scanner position 16. ....	78
Figure 71: Earthshine signal degradation rate per year for the period before the second throughput test (left panel) and after the throughput test (right panel) at 311, 330, and 380 nm (channel 2)..	79
Figure 72: Earthshine signal degradation rate per year for the period before the second throughput test (left panel) and after the throughput test (right panel) at 420 and 570 nm (Channel 3) and 745 nm (Channel 4). The plots also show the corresponding degradation rate of SMR at scanner position 16. See text for detailed explanation. ....	80
Figure 73: GOME-2/Metop-A reflectivity degradation rate per year for the period before the second throughput test (left panel) and after test (right panel) at 310 nm (Channel 1). ....	81
Figure 74: GOME-2/Metop-A reflectivity degradation rate per year for the period before the second throughput test (left panel) and after the test (right panel) at 311, 330 and 380 nm (Channel 2). ....	82
Figure 75: GOME-2/Metop-A reflectivity degradation rate per year for the period before the second throughput test (left panel) and after the test (right panel) at 420 and 570 nm (Channel 2) and 745 nm (Channel 4).....	83
Figure 76: Earthshine signals normalised to the mean of 2007 at 260 nm in channel 1 (band 1a) and for all three forward scanner positions (coloured lines: red, yellow and green). The SMR normalised signal, a dashed black line, is provided as a reference.....	85

Figure 77: Earthshine signals normalised to the mean of 2007 at 280 nm in channel 1 (band 1a) and for all three forward scanner positions (coloured curves). The SMR normalised signal, a dashed black line, is provided as a reference. ....	85
Figure 78: Earthshine signal degradation rate per year for the period before the second throughput test (left panel) and after the throughput test (right panel) at 260 and 280 nm (channel 1; band 1a). The plots also show the corresponding degradation rate of SMR at forward scan position 2 (for details see text). ....	86
Figure 79: GOME-2 / Metop-A reflectivity degradation rate per year for the period before the second throughput test (left panel) and after the throughput test (right panel) at 260 nm and 280 nm (Channel 1; Band 1a). ....	87
Figure 80: GOME-2/Metop-A: Difference (per cent) between solar mean reference spectra in Channels 1 and 2, derived from the near-real time (NRT) time series and the G2RP-R2 time series. ....	89
Figure 80: GOME-2/Metop-A: Difference (per cent) between solar mean reference spectra in Channels 1 and 2, derived from the near-real time (NRT) time series and G2RP-R2. ....	89
Figure 81: GOME-2/Metop-A: Difference (per cent) between solar mean reference spectra in Channels 3 and 4, derived from the NRT time series and G2RP-R2. ....	90
Figure 82: GOME-2/Metop-A: Difference (per cent) between solar mean reference spectra for PMD-P and S, derived from the NRT time series and G2RP-R2. ....	91
Figure 83: Stokes fractions for special geometries as for Figure 41 to Figure 43 and derived from PMD band 1. The left panel shows the time series for the extended R1+ products. The right panel shows the results for R2. ....	91
Figure 84: Stokes fractions for special geometries as for Figure 41 to Figure 43 and derived from PMD bands 2, 3, and 4. The left panel shows the time series for the extended R1+ products. ....	93
Figure 85: Stokes fractions for special geometries as for Figure 41 to Figure 43 and derived from PMD bands 5, 6, and 7. The left panel shows the time series for the extended R1+ products. The right panel shows the results for R2. ....	94
Figure 86: Stokes fractions for special geometries as for Figure 41 to Figure 43 and derived from PMD bands 8, 9, and 10. The left panel shows the time series for the extended R1+ products. The right panel shows the results for R2. ....	95
Figure 87: Stokes fractions for special geometries as for Figure 41 to Figure 43 and derived from PMD bands 11, 12, and 13. The left panel shows the time series for the extended R1+ products. The right panel shows the results for R2. ....	96
Figure 88: Stokes fractions for special geometries as for Figure 41 to Figure 43 and derived from PMD bands 14 and 15. The left panel shows the time series for the extended R1+ products. The right panel shows the results for R2. ....	97
Figure 89: Stokes fractions for special geometries as for Figure 40 averaged over the complete time series, for both the extended R1+ (left panel) and R2 (right panel) products. Note difference in scale of the y-axis. ....	98
Figure 90: Percentage difference between reprocessed time-series R1+ and R2 (R1-R2) of calibrated earthshine spectra for main channels at every second scanner position (left panel) and for the most extreme positions. Data derived at a wavelength of 310 nm (Channel 1). ....	99
Figure 91: Percentage difference between reprocessed time-series R1+ and R2 (R1-R2) of calibrated earthshine spectra for main channels at every second scanner position (left panel) and for the most extreme positions east, nadir, and west corresponding to readout number 2, 12 and 24. Here we show data derived at wavelengths of 311, 330 and 380 nm (channel 2). ....	100
Figure 92: Percentage difference between reprocessed time-series R1+ and R2 (R1-R2) of calibrated earthshine spectra for main channels at every second scanner position (left panel) and for the most extreme positions east, nadir, and west corresponding to readout number 2, 12 and 24. Here we show data derived at wavelengths of 420, 570 and 745 nm (channel 2). ....	101
Figure 93: Percentage difference between reprocessed time-series R1+ and R2 (R1-R2) of calibrated earthshine spectra for PMD-P (left panel) and PMD-S (right panel) for the most extreme positions east, nadir, and west corresponding to readout number 2, 12 and 24 for main channels. Here we show data derived from PMD bands closest to the main channel wavelength. ....	102
Figure 94: Percentage difference between reprocessed time-series R1+ and R2 (R1-R2) of calibrated earthshine spectra for PMD-P (left panel) and PMD-S (right panel) for the most extreme positions east, nadir, and west corresponding to readout number 2, 12 and 24 for main channels. Data derived from PMD bands closest to the main channel wavelengths. ....	103

Figure 95: Percentage difference between reprocessed time-series R1+ and R2 (R1-R2) of calibrated earthshine spectra for PMD-P (left panel) and PMD-S (right panel) for the most extreme positions east, nadir, and west corresponding to readout number 2, 12 and 24 for main channels. Here we show data derived from PMD bands closest to the main channel wavelengths of 420, 570, and 745 nm. .... 104

Figure 96: Reflectivity degradation rates at 310 nm (Channel 1) before (left panels) and after (right panels) the second throughput test. The top row shows yearly rates derived from R1+ and the bottom row of panels show the results from the recent R2 campaign. .... 105

Figure 97: Reflectivity degradation rates at 330 nm (Channel 2) before (left panels) and after (right panels) the second throughput test. The top row shows yearly rates derived from R1+ and the bottom row of panels show the results from the recent R2 campaign. .... 106

Figure 98: Reflectivity degradation rates at 420 nm (Channel 3) before (left panels) and after (right panels) the second throughput test. The top row shows yearly rates derived from R1+ and the bottom row of panels show the results from the recent R2 campaign. .... 107

Figure 99: Reflectivity degradation rates at 745 nm (Channel 4) before (left panels) and after (right panels) the second throughput test. The top row shows yearly rates derived from R1+ and the bottom row of panels show the results from the recent R2 campaign. .... 108

## 1 Introduction

### 1.1 Purpose and Scope

This document describes the status of GOME-2 Cal/Val activities relevant to the GOME-2 reprocessed dataset G2RP-R2. Release 2 of the dataset has been produced using the GOME-2 level 0-to-1B operational processor version 5.3 [RD6].

The reprocessing of dataset R2 serves five main purposes:

- to remove any spurious effects on the level 1B data quality due to processor and auxiliary-data changes,
- to serve the consistent evaluation and validation of level 2 data processing over multiple seasonal cycle,
- to consistently evaluate the long-term degradation of the instrument,
- to support the analysis of the origin of scan-angle dependent biases as observed in level 2 products,
- to support the development of a level 1C processor and product, mitigating the effects of long-term instrument degradation [RD5], and
- to assist in the preparation and execution of atmospheric composition and climate monitoring studies (extension of the GOME-1 and SCIAMACHY datasets).

For details about the dataset, its specific identifiers, as well as instructions for ordering R2 data, please see the referenced document [AD1].

### 1.2 Description of Validation Environment

The data has been verified and validated using the output of the EPS GOME-2 reprocessing system (G2RPS) and its database (G2RP-DB) installed and executed in the EUMETSAT reprocessing environment for EPS data (R-EPS). For details related to G2RPS and R-EPS see reference documents: [RD1], [RD2] and [RD3].

## 2 Applicable Documents

- [AD1] GOME-2 / Metop-A Reprocessed L1B-R2 dataset User Guide, EUM/OPS-EPS/DOC/09/0618 v1
- [AD2] GOME-2 Level 1 Product Generation Specification, EPS.SYS.SPE.990011 v7
- [AD3] GOME-2 Level 1 Product Format Specification, EPS.MIS.SPE.97232 v9

## 3 Reference Documents

- [RD1] Reprocessing Environment - High Level User Requirements, EUM/OPS/TEN/08/2458 v6
- [RD2] Reprocessing Environment System Design, EUM/OPS/TEN/08/3850 v2B
- [RD3] GOME-2 level 1 Reprocessing System - Implementation Plan, EUM/OPS-EPS/TEN/09/0572, v2
- [RD4] EPS GOME-2 Reprocessed L1B-R1 dataset, EUM/OPS-EPS/DOC/08/0345, v2A
- [RD5] Investigation on GOME-2 throughput degradation, EUM/LEO/REP/09/0732
- [RD6] GOME2 PPF 5.3 Software Release Note, EUM/OPS-EPS/DOC/09/0609, 1C
- [RD7] EPS Generic Product Format Specification (GPFS), EPS.GGS.SPE.96167, version 6.6
- [RD8] GOME2 PPF 4.0 Software Release Note, EUM/OPS-EPS/DOC/08/0213, June 2008
- [RD9] GOME-2 Calibration and Validation Plan, EPS.SYS.PLN.01.010
- [RD10] GOME-2 Level 1B Product Validation Report No. 4: Status at Reprocessing G2RP-R1, EUM/MET/REP/08/0327, v2
- [RD11] MetOp GOME-2 In-Orbit Verification Plan, ML-PL-ESA-GO-0506
- [RD12] GOME Annual In-Flight Performance Review 2011, EUM/OPS-EPS/REP/11/0057, v1.
- [RD13] GOME-2 PMD Band Definitions 3.0 and PMD Calibration, EUM/OPS-EPS/DOC/07/0601, v8.
- [RD14] Cai, et al, Characterization and Correction of Global Ozone Monitoring Experiment-2 Ultraviolet Measurements and Application to Ozone Profile Retrievals, JGR, submitted, 2012.
- [RD15] Cloud retrieval algorithm for GOME-2: FRESCO+, EUM/CO/09/4600000655/RM, 2011.
- [RD16] Support for upgrade to FRESCO+ in the GOME-2 PPF: Final Report, EUM/CO/09/4600000655/RM, 2011.
- [RD17] GOME-2 HCL CHECK OF THE FM3 ON-GROUND CALIBRATION, MO-TN-TPD-GO-0086, FM-3 Reanalysis campaign, June 2009.
- [RD18] GOME-2 FM3 Calibration: Instrument Performance Testing, MO-TR-TPD-GO-0094
- [RD19] GOME-2 Error Assessment Study Final Report, Phases I—IV, EUM/CO/01/901/DK, December 2002
- [RD20] GOME-2 Error Assessment Study Final Report, Phase V, EUM/CO/01/901/DK, April 2004
- [RD21] Dikty, et al., Support for Analysis of GOME-2 In-Orbit Degradation and Impacts on level 2 data Products – Final report, ITT 09/10000262, 2011
- [RD22] Hartmann, H.W., C.P. Tanzi, J.M. Krijger, and I. Aben, GOME-2 Polarisation Study - Phase C/D: Final Report, RP-GOME2-003SR, SRON, Utrecht, The Netherlands

### 3.1 Acronyms and Abbreviations Used in this Document

<i>Abbreviation/ Acronym</i>	<i>Meaning</i>
AVHRR	advanced very high resolution radiometer
CFR	cloud fractions
FFT	fast Fourier transform
FWHM	full width at half maximum
Ifov	instantaneous field of view
NRT	near real-time
PDU	product dissemination unit
PMD	polarization measurement device
PPF	level 0 to 1 product processing facility
SMR	solar mean reference
SZA	solar zenith angle
SIOV	satellite in-orbit verification phase
WLS	white light source

## 4 The Global Ozone Monitoring Experiment 2 (GOME-2)

### 4.1 The Instrument

The Global Ozone Monitoring Experiment–2 (GOME-2) is an optical spectrometer fed by a scan mirror which enables across-track scanning in nadir, as well as sideways viewing for polar coverage and instrument characterisation measurements using the moon. GOME-2 senses the earth's backscattered radiance and extraterrestrial solar irradiance in the ultraviolet and visible part of the spectrum (240–790 nm) at a high spectral resolution between 0.26–0.51 nm. Some 4096 spectral points from four detector channels are transferred per individual GOME-2 measurement (see Figure 1).

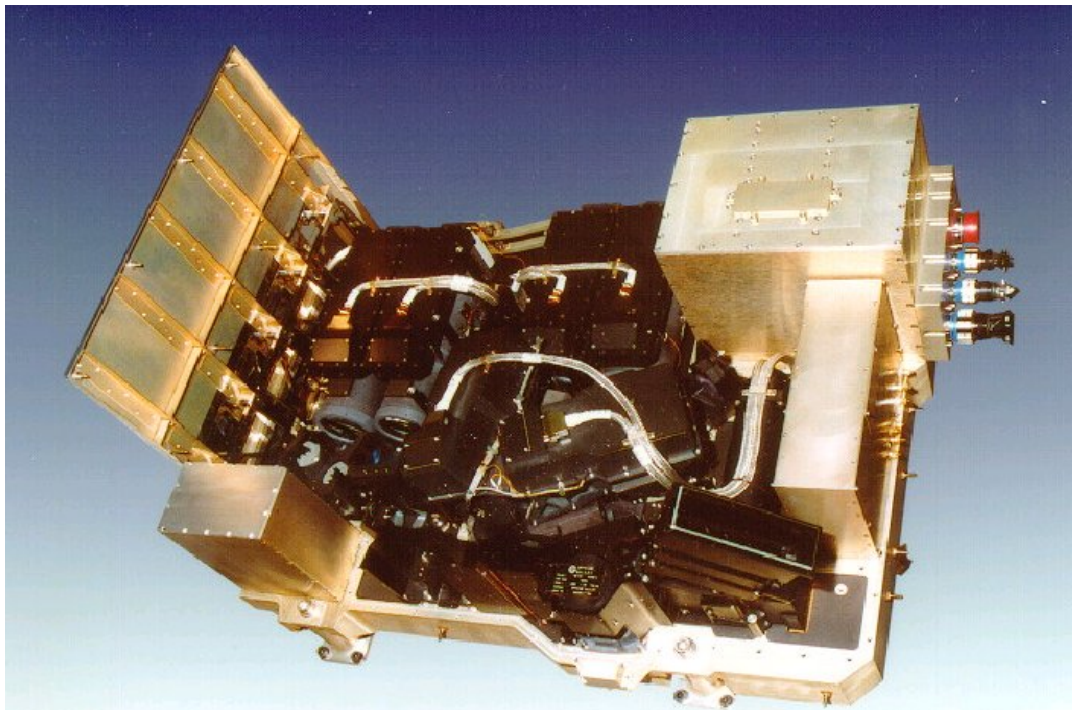


Figure 1: The Global Ozone Monitoring Experiment–2 (GOME-2) Instrument

The footprint size is 80 x 40 km for main channel data. The instrument also measures the state of linear polarisation of the backscattered earthshine radiances in two perpendicular directions. The polarisation data is down-linked in 15 spectral bands covering the region from 312 nm–800 nm for both polarisation directions with a footprint of 10 x 40 km.

The recorded spectra are used to derive a detailed picture of the total atmospheric content of ozone and the vertical ozone profile in the atmosphere. They also provide accurate information on the total column amount of nitrogen dioxide, sulphur dioxide, water vapour, oxygen /oxygen dimer, bromine oxide and other trace gases, as well as aerosols and cloud optical properties (Figure 2).

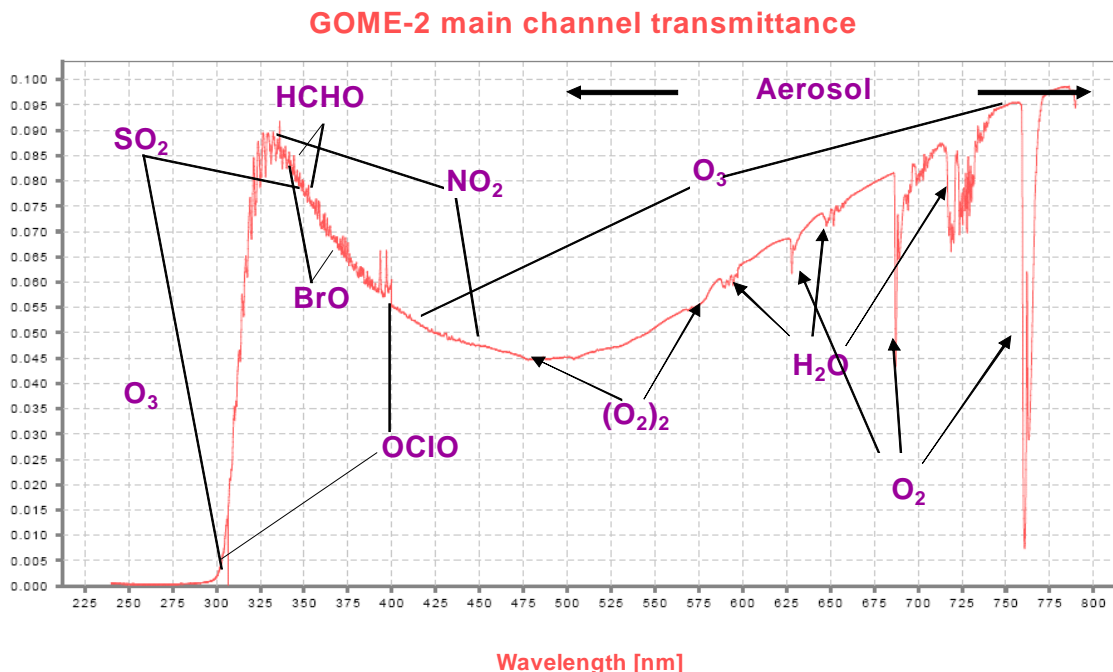


Figure 2: GOME-2 transmittance as derived from the GOME-2 level 1b radiance product. Selected spectral regions with absorption signatures used for various trace gas products as derived from GOME-2 level-1b radiances are shown.

The GOME-2 instrument has been developed by SELEX/Galileo Avionica in Florence, Italy, under a joint contract from EUMETSAT and ESA.

## 4.2 GOME-2 Optical Layout ([AD2])

The four main channels of the GOME-2 instrument provide continuous spectral coverage of the wavelengths between 240 nm and 790 nm with a spectral resolution full width at half maximum (FWHM) between 0.26 nm and 0.51 nm. Channel characteristics are listed in Table 1. The optical configuration of the instrument is shown in Figure 3. Light enters the two-mirror telescope system via the scan mirror. The telescope projects the light beam onto the slit, which determines the instantaneous field-of-view (IFOV) of 0.28° x 2.8° (across-track x along-track). After it has passed the slit, the beam is collimated again and enters a double Brewster prism for partial split-off to PMD-S, followed by the pre-disperser prism which has two functions. Brewster reflection at the back of the prism splits off part of the p-polarisation direction to PMD-P. The prism furthermore forms a low-dispersion spectrum which is subsequently separated at the channel separator prism into three parts going to Channels 1 (transmitted beam), 2 (reflected beam), and 3 and 4, respectively. The separation between channels 3 and 4 is performed by a dichroic filter.

A grating in each channel then further disperses the light, which is subsequently focused onto the detector array. Each PMD channel contains a dispersion prism and two additional folding prisms and collimating lenses. PMD-P measures intensity polarised parallel to the spectrometer's slit, and PMD-S measures intensity polarised perpendicular to the spectrometer's slit. The two PMD channels are designed to ensure maximum similarity in their optical properties. The wavelength-dependent dispersion of the prisms causes a much higher spectral resolution in the ultraviolet than in the red part of the spectrum.

In Table 1, values are given for GOME-2 FM3. For the overlap regions between the main channels, the wavelengths are given for the 10 % intensity points. For example, at 310 nm, 10 % of the signal is registered in channel 2, and 90 % in channel 1. At 314 nm, 10 % of the signal is registered in Channel 1, and 90% in Channel 2. Spectral resolution varies slightly across each main channel; the given values are channel averages.

Table 1: Channel characteristics of GOME-2 spectral coverage and resolution

<i>Channel</i>	<i>Spectral range [nm]</i>	<i>Detector Pixel size [nm]</i>	<i>FWHM [nm]</i>
1	240 - 314	0.12	0.26
2	310 – 403	0.12	0.27
3	397 – 604	0.21	0.51
4	593 – 790	0.21	0.48
PMD-P PMD-S	312 – 790	0.62 (312nm)–8.8 (790nm)	2.9 (312 nm)–37 (790nm)

The GOME-2 channels can be separated in different bands operating at different integration times. The latter can also vary over the orbit. Nominal integration times in band 1A are 1.5 seconds (6 seconds at high solar zenith angles) and 0.1875 seconds for band 1B to 4 (1.5 and 0.75 seconds at high SZA). For details on the exact integration times per band during one instrument timeline series, we refer to the GOME-2 monitoring pages in the timelines sub-section at this address:

[gome.eumetsat.int](http://gome.eumetsat.int).

The separation between band 1A and band 1B has been shifted 10 December 2008 (see Table 2). Previously, band 1A/B was separated at 307 nm. After 10 December 2008, the separation has been shifted to 283 nm, in accordance with the GOME-1 and SCIAMACHY instrument specifications.

Table 2: Main channel band settings of GOME-2. The band separation shift between band 1A and B occurred during orbit 11119 on 10 December 2008.

<i>Channel</i>	1	1	2	2	3	4	5/6
<i>Band</i>	1A	1B	2A	2B	3	4	PMD P/S
<i>Used Pixels</i>	877/659 <sup>1</sup>	147/365	71	953	1024	1024	256
<i>Spectral Range (nm)</i>	240-307/283 <sup>1</sup>	307/283-315 <sup>1</sup>	290-300	300-412	401-600	590-790	290-790
<i>nm/pixel</i>	0.07	0.07	0.09	0.09	0.2	0.2	2
<i>Predefined dark signal electronic offset (BU)</i>	1501	1501	1503	1503	1495	1492	1503/1499

<sup>1</sup> Changed settings 10 December 2008.

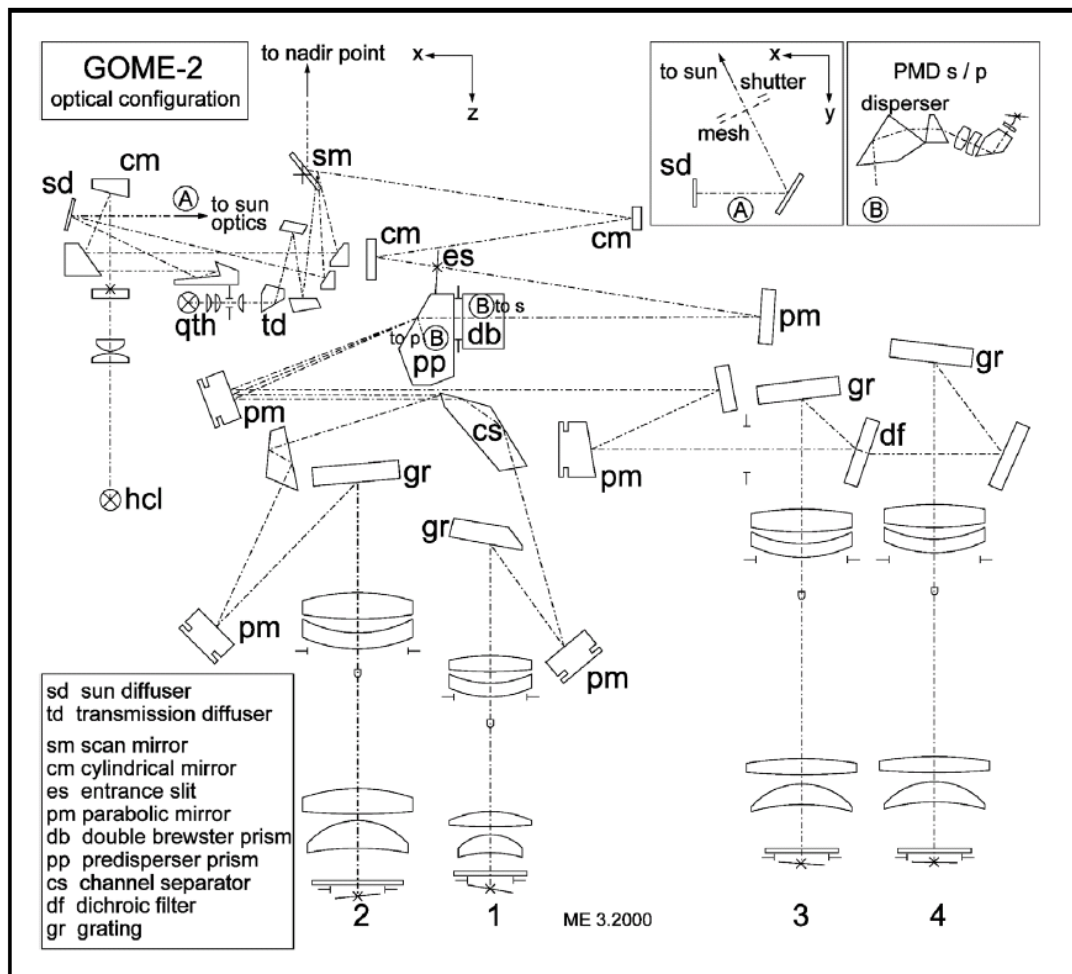


Figure 3: GOME-2 optical layout. The optics lie in one plane (except insets A and B). Nadir is in  $-Z$  direction.

#### 4.2.1 Polarisation Measurement Device (PMD) band settings

The 256 detector pixels of both PMD devices of block C,D, and E (for details we refer to [AD2]) are co-added on board in spectral space and for nominal earthshine measurements in 15 PMD spectral bands. Before 11 March 2008, both PMD detectors (PMD-P and PMD-S) used the same band settings as listed in Table 3.

Table 3: Default GOME-2 PMD band definitions (v1.0) valid from date of launch to 11 March 2008 in orbit 7226

Band	First pixel in band from C-start	Number of pixels in Band	Start Wavelength $\lambda$ (nm)	Stop Wavelength $\lambda$ (nm)
0	19	2	309.2	309.9
1	23	5	311.7	314.4
2	31	4	317.0	319.1
3	37	12	321.2	329.5
4	50	5	331.1	334.3
5	56	43	335.9	377.7
6	100	4	380.1	383.7
7	115	20	399.3	428.4
8	138	43	435.5	552.5
9	183	2	553.6	557.5
10	187	22	569.6	678.6
11	217	2	742.3	750.2
12	219	1	758.2	758.2
13	223	1	792.1	792.1
14	228	1	838.8	838.8

On 11 March 2008 in orbit 7227, updated PMD band settings, with different settings for PMD-P and PMD-S have been uploaded in order to improve the spectral co-registration of both PMDs and to optimise for the usage of PMD bands for level 2 data retrieval. See Table 4.

Table 4: GOME-2 PMD band definitions (v3.1). This set of definitions has been uploaded for orbit on 11 March 2008 during orbit 7227.

Band-S					Band-P				
No.	pix1	pixw.	wav1	wav2	No.	pix1	pixw.	wav1	wav2
0	22	5	311.709	314.207	0	20	5	311.537	313.960
1	30	4	316.762	318.720	1	29	4	317.068	318.983
2	37	12	321.389	329.139	2	36	12	321.603	329.267
3	50	6	330.622	334.443	3	49	6	330.744	334.560
4	57	6	336.037	340.161	4	56	6	336.157	340.302
5	84	17	360.703	377.873	5	83	17	361.054	378.204
6	102	4	380.186	383.753	6	101	4	380.502	384.049
7	117	19	399.581	428.585	7	116	19	399.921	429.239
8	138	27	434.083	492.066	8	137	27	434.779	492.569
9	165	18	494.780	548.756	9	164	18	495.272	549.237
10	183	2	552.474	556.262	10	182	2	552.967	556.769
11	187	11	568.070	612.869	11	186	11	568.628	613.680
12	198	9	617.867	661.893	12	197	9	618.711	662.990
13	218	4	744.112	768.269	13	217	4	745.379	769.553
14	224	2	794.080	803.072	14	223	2	795.364	804.351

For more details on the PMD calibration and PMD band settings we refer to [RD13]].

### 4.3 GOME-2 Specifications Summary

<i>Item</i>	<i>Specification</i>
Spectral band (nm)	240-790
Spectral resolution (nm)	0.26-0.51
Spatial resolution (km <sup>2</sup> )	80 x 40 (main channels) 80 x 10 (PMD)
Earth coverage (km)	120-1920
Spectral channels	4096 (in 4 separated optical channels)
Polarization channels	30 (in 2 separated optical channels)
Calibration system	Spectral lamp, white lamp, solar diffuser
Dimensions	600 mm x 800 mm x 500 mm
Weight	68 kg
Main bus voltage	22-37 V
Power consumption	50 W
Data rate interface	400 kbit

### 4.4 GOME-2 Level 1b products

- sun-normalised nadir radiance
- absolute nadir radiance
- absolute sun radiance
- spectral calibration parameters
- sun mean reference spectrum
- effective cloud fraction
- cloud-top pressure
- geo-reference parameters

### 4.5 GOME-2 Level 2 Products

The responsibility for extraction of meteorological or geophysical (level 2) products from GOME-2 lies with the Satellite Application Facility on Ozone Monitoring (O3MSAF) at this address:

[o3msaf.fmi.fi/](http://o3msaf.fmi.fi/)

For detailed off- and online validation of GOME-2 level-2 products, go to:

<http://lap.physics.auth.gr/eumetsat/index.php>

A “quick-look” imagery of GOME-2 level 2 data is also available here:

<http://atmos.caf.dlr.de/gome2/index.html>

A product and format list follows in Table 5. The product format type, either HDF5 and/or binary universal form for the representation of meteorological data (BUFR), is indicated for each product:

Table 5: Product and format type list

<i>Product</i>	<i>Format Type</i>
Total column ozone	HDF5 and BUFR
Ozone profiles	HDF5 and BUFR
NO2	HDF5
NO2 tropics	HDF5
BrO, SO2	HDF5
HCHO	HDF5
OCIO, Aerosol Absorbing Index	HDF5
Clear Sky UV fields	HDF5
UV fields with Clouds and Albedo	HDF5
Total Water Vapour Column	HDF5

Level 2 products being planned for future operational provision by the O3MSAF include tropospheric ozone and BrO, CHOCHO, amongst others.

#### **4.6 Other Useful links**

For more detailed descriptions, see the GOME-2 Products Guide and ESA's GOME-2 page. The GOME-2 Product Quality Monitoring website provides summary information about GOME-2 level 1 products, including availability, daily and orbit reports, timelines in use, and product quality. Here is the intranet address:

[Home > Service Status > Product Quality Monitoring > GOME-2 instrument](#)

## 5 Dataset and Instrument References

### 5.1 Main dataset identifiers

For in-depth details on the dataset identifiers, refer to [AD1]. In the sections that follow, we list only the details which are relevant for this validation document.

#### 5.1.1 G2RP-R2 processor version

<i>GOME-2 L1 PPF Software version</i>	<i>Introduced on CGSI</i>	<i>Comments</i>
5.3.0	24/01/2012	

#### 5.1.2 G2RP-R2 reference period

<i>Start Date</i>	<i>End Date</i>	<i>Start Sensing Time (UTC)</i>	<i>Stop Sensing Time (UTC)</i>
25 January 2007	25 January 2012	20070125 01:00:11	20120125 01:20:45

#### 5.1.3 G2RP-R2 product and format version

<i>Release Date</i>	<i>Reprocessing Version</i>	<i>Product Format Version</i>	<i>PGS version</i>	<i>PFS version</i>
6 June 2012	2.0	12.0	7	9

### 5.2 Main instrument and platform events

This table is part of the continuously-updated GOME-2 / Metop-A instrument, PPF and auxiliary-data change history available at this internet address:

[gome.eumetsat.int](http://gome.eumetsat.int)

*Note:* The events' start/stop times do not necessarily coincide with near real-time (NRT) data dissemination start/stop times.

Table 6: Metop-A/GOME-2 FM3 instrument events and operations

<i>Start date</i>	<i>End date</i>	<i>Orbit Start</i>	<i>Orbit End</i>	<i>Instrument Event/Operation</i>	<i>Type</i>
02/03/2007 19:50:55 UTC	06/03/2007 12:32:54 UTC	1905	1958	Instrument switch-off due to single event set-up	Instrument anomaly
08/04/2007 23:05:56 UTC	10/04/2007 15:29:59 UTC	2433	2457	Instrument switch-off due to single event set-up	Instrument anomaly
20/04/2007 08:38:55 UTC	26/04/2007 09:24:30 UTC	2594	2681	Satellite platform switch-off due to single event set-up	Platform anomaly
17/09/2007 05:11:57 UTC	20/09/2007 14:17:55 UTC	4723	4772	Satellite platform switch-off due to single event set-up	Platform anomaly
08/10/2007 08:02:59 UTC	09/10/2007 09:23:59 UTC	5024	5039	Test upload of PMD band definitions version 2.1 [AD4]	Instrument operations

<i>Start date</i>	<i>End date</i>	<i>Orbit Start</i>	<i>Orbit End</i>	<i>Instrument Event/Operation</i>	<i>Type</i>
16/01/2008 13:32:59 UTC	19/01/2007 10:50:59 UTC	6447	6488	Satellite platform switch-off due to single event set-up	Platform anomaly
29/01/2008 11:53:48 UTC	31/01/2008 12:53:11 UTC	6632	6661	Degraded spectral calibration for FPA channel 2 and PMDs between 300 and 400 nm.	Instrument anomaly
05/02/2008 09:26:55 UTC	06/02/2008 15:51:22 UTC	6730	6747	Test upload of PMD band definitions version 3.0 [AD4].	Instrument operations
11/03/2008 10:43:20 UTC	n/a	7227	n/a	Final upload of PMD band definitions version 3.1 [AD4].	Instrument operations
19/03/2008 21:50:54 UTC	22/03/2008 12:26:56 UTC	7347	7385	Satellite platform switch-off due to single event set-up.	Platform anomaly
02/09/2008 07:17:56 UTC	03/09/2008 15:35:54 UTC	9712	9730	On-board software co-adding patch I.	Instrument operations
10/09/2008 07:53:57 UTC	11/09/2008 14:29:59 UTC	9826	9843	On-board software co-adding patch II.	Instrument operations
10/12/2008 07:53:59 UTC	n/a	11119	n/a	Shift of FPA band 1a/b separation to pixel detector pixel 658 at 283 nm.	Instrument operations
27/01/2008 06:40:00 UTC	29/01/2008 16:06:00 UTC	11800	11833	Test of instrument throughput behaviour.	Instrument operations
16/02/2009 21:38:55 UTC	18/02/2009 12:40:00 UTC	12092	12117	Instrument macro-command error – EQSOL.	Instrument anomaly
03/03/2009 08:00:00 UTC	04/03/2009 17:45:00 UTC	12998	12318	On-board software co-adding patch III.	Instrument operations
07/09/2009 06:16:00	12/09/2009 09:50:00	14968	15041	Second test of instrument throughput behaviour and instrument out-gassing.	Instrument operations
04/01/2011 09:45:00 UTC	04/01/2011 10:20:00 UTC	21846	21846	Old spectral calibration applied due to sudden drop in on-board temperatures because of ASCAT anomaly (switched to calibration mode).	Instrument (ASCAT) anomaly
05/04/2011 10:44:00 UTC	05/04/2011 16:41:00 UTC	23139	23143	Wrong channel 2 band separation settings due to erroneous command of the instrument.	Instrument operations
19/04/2011 23:20:00 UTC	20/04/2011 00:20:00 UTC	23346	23346	Timeline failed executing. Orbit contains only dark measurements.	Instrument operations
01/05/2011 02:20:00 UTC	01/05/2011 03:59:00 UTC	23504	23505	In-plane collision avoidance manoeuvre	Instrument operations

<i>Start date</i>	<i>End date</i>	<i>Orbit Start</i>	<i>Orbit End</i>	<i>Instrument Event/Operation</i>	<i>Type</i>
22/10/2011 21:54:00 UTC	25/10/2011 13:15:00 UTC	25987	26024	Metop-A payload switch-off	Platform anomaly

### 5.3 Main processor and configuration differences to G2RP-R1 (PPF 4.0)

The G2RP-R2 is based on the level 0-to-1 processor Version 5.3.0. A detailed summary of all changes applied to the calibration of GOME-2 level 0 data between Version 4.0 and Version 5.3 is provided on this intranet site:

[Home](#) > [Service Status](#) > [Product Quality Monitoring](#) > [GOME-2 instrument](#) > [Documentation](#) > [Processor change history](#)

Here are the six main changes to the processor used for G2RP-R2 that impact the provided product quality and maturity, with respect to G2RP-R1 (January 2007 to January 2009):

1. improved polarisation correction for the full mission
2. improved and additional instrument key-data (especially for PMD signals)
3. improved geo-referencing, including geo-locations for PMD measurements
4. random noise contribution instead of absolute errors reported in the product
5. product format 12.0
6. homogenous dataset, removing the impact of previous processor changes

The main impact on product quality and the homogeneity of the derived time-series is expected to originate from points one, two, and six above. For a detailed description of these differences, see Section 7.8.

## 6 Validation Strategy

### 6.1 Target parameters within the scope of current validation

Validation and verification have been performed in a manner consistent with those activities outlined in the GOME-2 Cal/Val plan ([RD9]), which are relevant for the purposes of the dataset as outlined in Section 1.1. Validation activities have been carried out by examining the long-term consistency of the following group of essential calibration quantities which are applied during level 0-to-1 processing of radiance data:

<i>Quantity</i>	<i>Section in Cal/Val Plan</i>
Instrument dark-signal correction	A2.8, A2.9, A3.3
Thermal response of the key processing parameters (Overlap-point, Spectral calibrations)	
Instrument spectral calibration	A2.13–A2.15, A3.6
Instrument etalon correction	A2.16, A2.17, A3.7
Instrument polarisation correction (Stokes Fractions)	A2.21, A3.10
Instrument diffuser degradation	A2.20, A3.12
Level 1B data record consistency and long-term signal variation for sun and earthshine radiances	A3.11, A3.12
Differences with respect to G2RP-R1	

All of these calibration quantities are potentially affected by the observed instrument throughput degradation ([RD5]) except for the dark-signal correction (offset and read-out noise). In addition, these quantities can be affected by any other instrument and/or platform anomaly which has occurred during the reprocessing period. No attempt has been made during this reprocessing campaign to mitigate the effects of any instrument or platform anomaly. A table of instrument and platform anomalies during the reference period is provided in Section 5.2 as outlined in Section 1, the current validation shall confirm that G2RP-R2 has removed any spurious effects of level 0-to-1 processor changes and anomalies up to version 5.3 (operational since 24 January 2012) for both main channel and polarisation measurement device (PMD) channel data. See also Section 4. Furthermore, the validation shall confirm the overall consistency of the data with respect to the latest version of the product generation specification, in this case PGS v.7. The PGS Algorithm reference numbers are given in brackets for the individual target parameters) [AD2]. This validation will also confirm a deviation from the original signal levels after launch due to instrument degradation within the previously identified limits. For more details on this topic, see [RD5].

## 6.2 Target parameters outside the scope of current validation

The following list of level 0-to-1 calibration components are not part of the current validation.

<i>Component</i>	<i>Section in Cal/Val Plan</i>
Geo-referencing data	A2.6, A3.2
PPG correction	A2.11, A3.5
Stray light correction	A2.19, A3.9
Cloud properties (FRESCO+)	A3.15

These parameters have been processed within the pre-defined quality limits as specified by the PGS 7 during the whole reprocessing. The following sections (6.2.1–6.2.4) provide some example results for verification only. These parameters and results are not meant to be a validation.

### 6.2.1 Geo-referencing (A2.6, A3.2)

Geo-location parameters are processed during level 0-to-1B processing both for a fixed grid of 32 read-outs per scan and for an individual grid based on the actual integration time of an instrument band. For reference, GOME-2 channels 1 and 2 are separated into two bands each, as are the PMD channels—both short-wave and main PMD bands—such that there are ten bands in total that potentially can be commanded with different integration times, leading to different ground footprints. In practice, GOME-2 instrument timelines include only four different integration times per scan:

- IT1 for band 1a
- IT2 for band 1b to 4
- IT3 for PMD main channels
- IOT4 for PMD short-wave channels.

However, IT1 and IT2 change over the orbit from longer to shorter integration times along decreasing solar zenith angles.

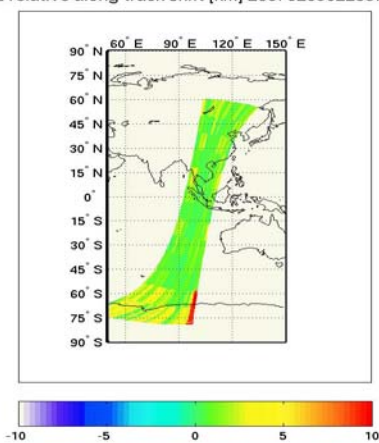
For GOME-2 level 1 reprocessing, the predicted orbit state vectors as used for near real-time processing are also used in the reprocessing campaign. The accuracy of the predicted orbit is significantly less than 100 m. Therefore an upper limit bias on the calculated geo-referencing parameters of 1% of across-track pixel size for PMDs (0.25 % along track) and 0.6% for main channels (0.25 % along track) are estimated with respect to dedicated corrected orbits for reprocessing. The effect is considered negligible with respect to the pointing accuracy of the instrument. Using the predicted orbits as for NRT also provides continuity between the reprocessed dataset and NRT data.

The main changes to the geo-location processing during the lifetime of the mission were the resolution of EUM/OPS/AR/12454 with PPF 4.5, as well as the introduction of geo-location records for PMD measurements with PPF 5.0. Both changes are included in PPF 5.3.0 used for G2RP-R2. Here, we show the results of the verification of the geo-location reference data in G2RP-R2 for one case at the beginning of the time-series (February 2007) as well as for a more recent case (October 2011). GOME-2 radiances in channels 3 and 4 are merged with the AVHRR spectral response function and compared to the averaged radiometric signal from AVHRR within one GOME-2 ground pixel (using IT2 for channel 3 and 4). The geo-location data for the GOME-2 ground pixel box is then modified and the averaged AVHRR radiances within the box are fitted until an optimal correlation is achieved. Along-track, the delta on the GOME-2 geo-location data should be zero, whereas across-track there is a fixed offset of 10 % of the pixel size expected due to spatial aliasing. Spatial aliasing can be defined as the time that has to be accounted for during the duration of reading out the detector arrays of GOME-2, a time period during which the space-craft moves. For more details, see PGS 7, Section 5.3.16 [AD2].

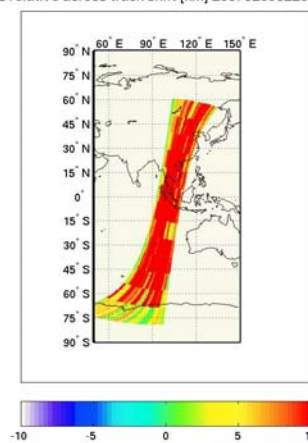
Below, Figure 4 shows the along-track and across-track offsets over the orbit for February 2007 and October 2011. The scatter in the results is due to the differences in fit residuals, depending on the “information content” of the scene. For a scene with a lot of albedo variations (broken cloud fields, for example) one GOME-2 measurement covers a large variation in signal level as measured by AVHRR and therefore provides a more robust (smaller fitting error) correlation result. Note, that because of the latter, multiple pixels at the same scanner position for each product dissemination unit (PDU), for example 30 GOME-2 measurements at a time, are used for the optimisation procedure (striping along-track). As expected, the along-track offset is close to zero and the across-track offset is close to 10 % for the beginning and the end of the reference period.

**Feb 2007**

/HRR/GOME-2 relative along track shift [km] 20070205022357 20070205040557

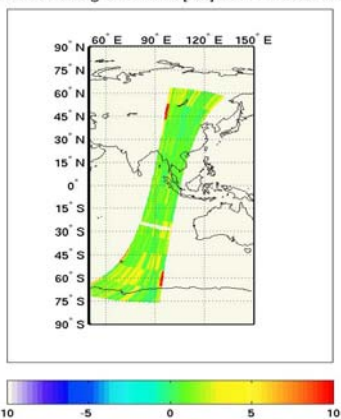


AVHRR/GOME-2 relative across track shift [km] 20070205022357 20070205040557



**Oct 2011**

/HRR/GOME-2 relative along track shift [km] 20111012024158 20111012042358



AVHRR/GOME-2 relative across track shift [km] 20111012024158 20111012042358

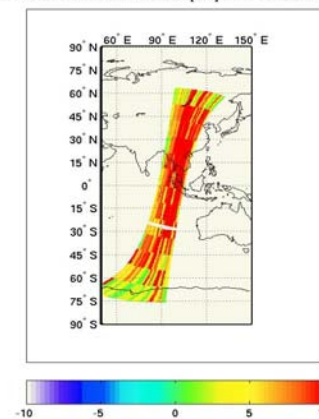


Figure 4: Along-track (left panels) and across-track (right panels) shifts of geo-referencing parameters as evaluated from co-location to AVHRR signals. Note the two different date ranges: February 2007 and October 2011.

### 6.2.2 PPG correction (A2.11, A3.5)

The processing of LED signals in the level 0-to-1B processor has not been changed since the launch of Metop-A. For details of this processing, see the commissioning report for GOME-2 level 1B data for details [RD10].

Figure 5 shows the contribution of the detector pixel-to-pixel gain for detector pixel 650 and channel 1 to 4 over the reference period. The contribution of PPG is at the  $10^{-4}$  level and increases for channel 1 and 2 (blue and red curves) towards the end of the time period—and especially after throughput test number 2 in September 2009. The contribution of this signal to the overall throughput degradation and variation of calibrated radiances is small, however.

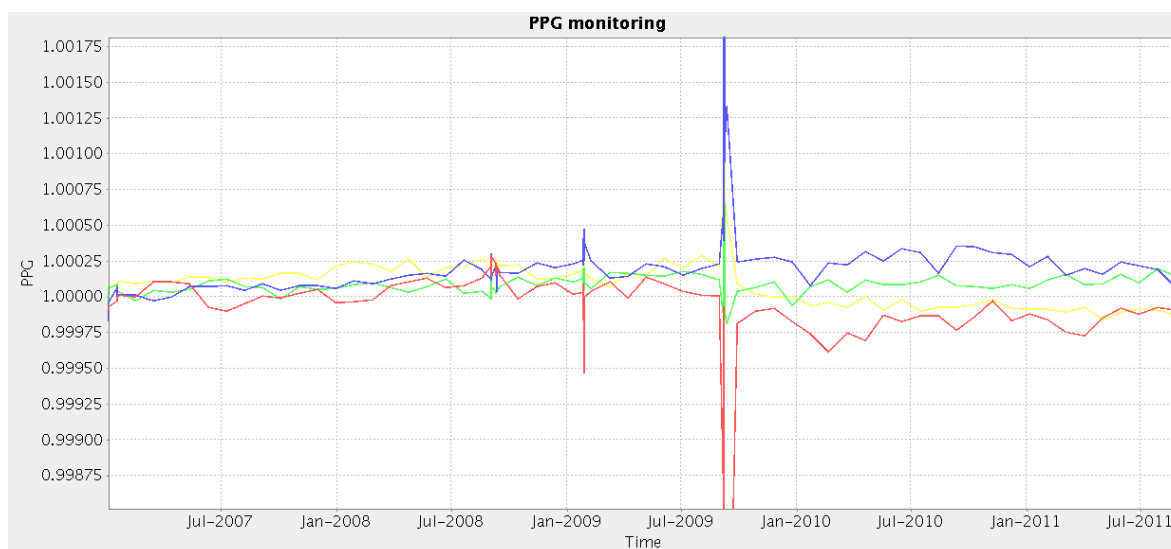


Figure 5: Detector pixel-to-pixel gain (PPG) contribution for channel 1(blue), 2 (red), 3 (green), 4 (yellow) over the reference period

### 6.2.3 Stray light correction (A2.19, A3.9)

Two types of stray light contributions are taken into account during the level 0-to-1B processing of GOME-2 data. Uniform stray light originates in diffuse scatter inside the instrument and generates a slowly varying or nearly uniform stray light across a detector array. Ghost stray light originates in specular reflection from optical components within the instrument. It is essentially focused on the detector array (for details, see Section 5.7.16 in [AD2]).

The characterisation of stray light level is done using on-ground calibration data measurements. The latter have not been changed during the reference period of G2RP-R2.

However, several users indicated that increasing fit-residual biases, especially for channel one, and increasing towards lower wavelength, may be due to increasing stray light levels during the reference period [RD3]. Uniform stray light is corrected using on-ground characterisation data. No significant stray light ghosts were found during on-ground characterisation. No attempt has been made to quantify and correct for any changes in the stray light performance of the instrument during G2RP-R2. Stray light characterisation key data are used as delivered. The evaluation and/or validation of the effect should be carried out based on G2RP-R2 output.

### 6.2.4 Cloud properties (FRESCO+) (A3.15)

The level 1B product provides basic information on cloud optical properties such as CFR (cloud fraction) and CTP (cloud top pressure). The parameters are derived using FRESCO+ ([RD15]), which has been implemented with version 5.0 of the processor. For a detailed validation of the FRESCO+ output in the level 1B product we refer to [RD16]. Since the FRESCO+ parameter is essentially a level-2 retrieval based on calibrated level 1B radiances and not used in the level 0-to-1b processing, these parameters are not validated here.

We verify cloud-fraction values from GOME-2 with co-located CFRs derived from AVHRR for the beginning and the end of the reference period. In Figure 6, the left panels show the GOME-2 footprint equivalent cloud fraction derived from AVHRR (albedo test using visible AVHRR channels). Differences in data gaps are due to differences in treating snow-covered surfaces at high latitudes and failure in fit convergence for FRESCO+ at some mid-latitudes in February 2007.

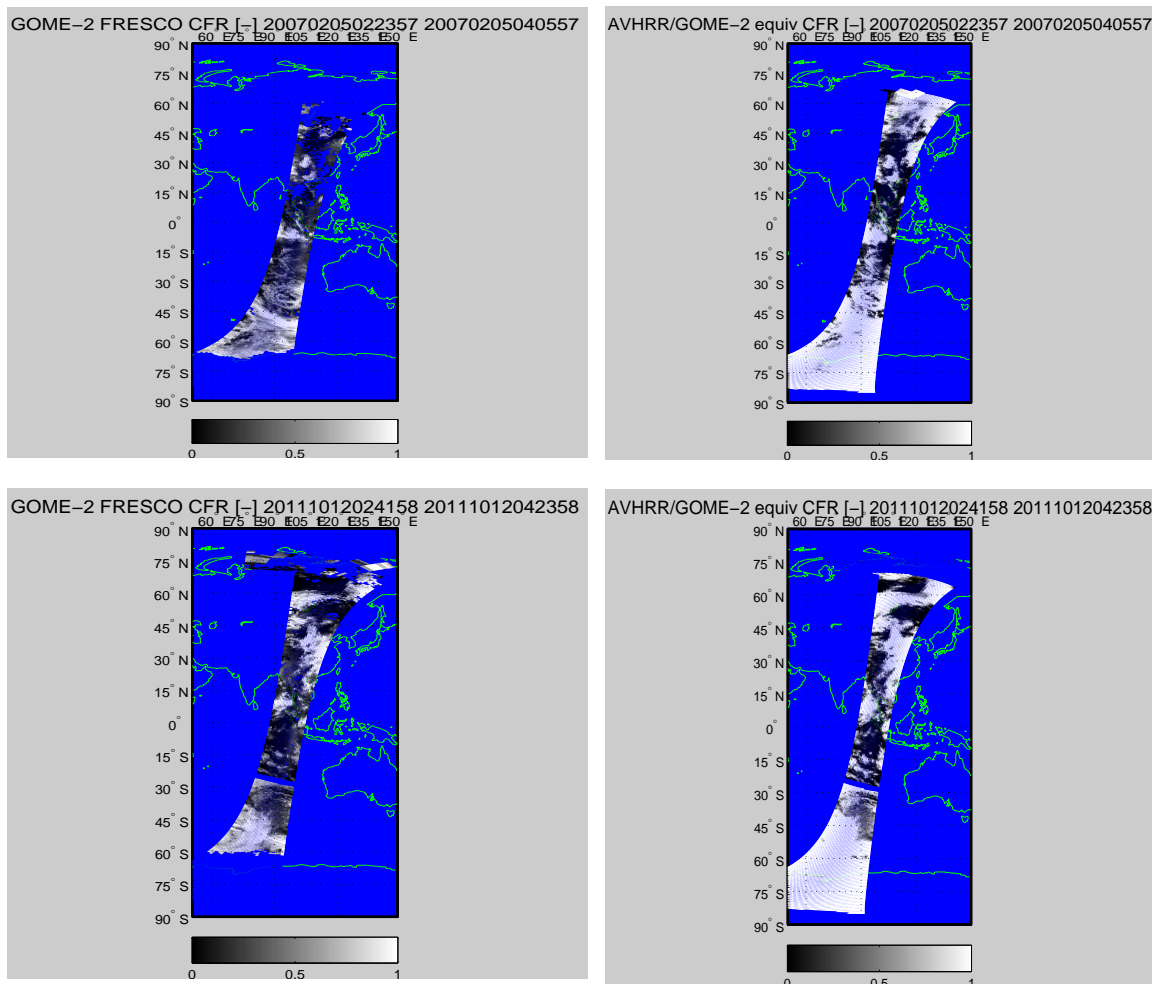


Figure 6: GOME-2/Metop-A FRESCO+ R2 cloud fraction values (left panel) for one orbit in February 2007 (upper panels) and in October 2011 (lower panels).

Figure 6 shows cloud fractions (CFR) as provided by the G2RP-R2 level 1b products for GOME-2 (left panels) derived by FRESKO+ and for February 2007 and October 2011. We compare the results with equivalent CFR values derived from AVHRR co-located cloud products using the albedo test (visible AVHRR channels). Apart from differences in treating snow/ice covers and some failures of convergence of the FRESKO+ algorithm at mid-latitudes for February 2007, the results look comparable with the expected higher CFRs for AVHRR (due to the radiative versus geometric retrieval approach for FRESKO+ and ACVHRR respectively).

The correlations for these two orbits are shown in Figure 7 and do not show significant changes between the beginning and the end of the R2 time period. There is a slight improvement in correlation coefficients from 0.8 to 0.85 and in the offset from 0.18 and 0.19, though the latter cannot be considered significant. The same is true for the comparison of the zonal means presented in Figure 8.

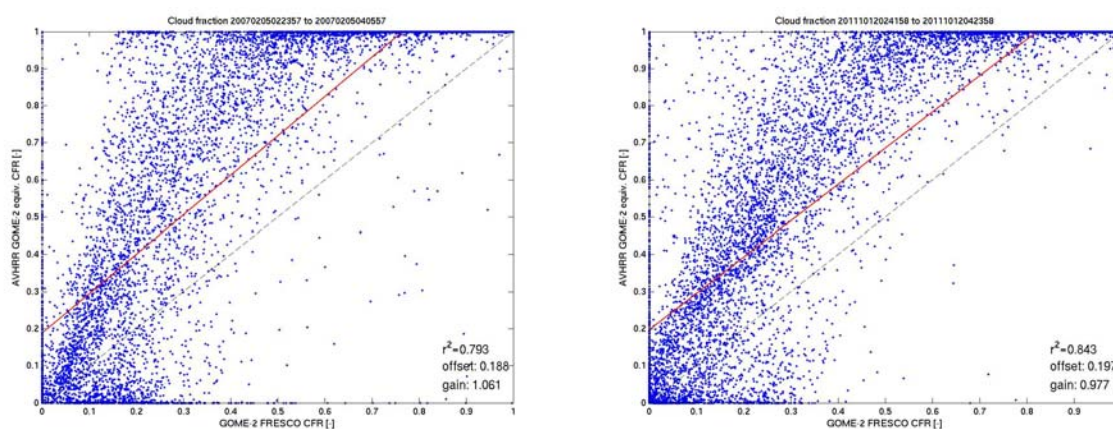


Figure 7: Correlations for GOME-2 /Metop-A FRESKO+ R2 versus GOME-2 footprint equivalent cloud fractions derived from AVHRR (albedo test using visible AVHRR channels) for one orbit in February 2007 (left panel) and in October 2011 (right panel).

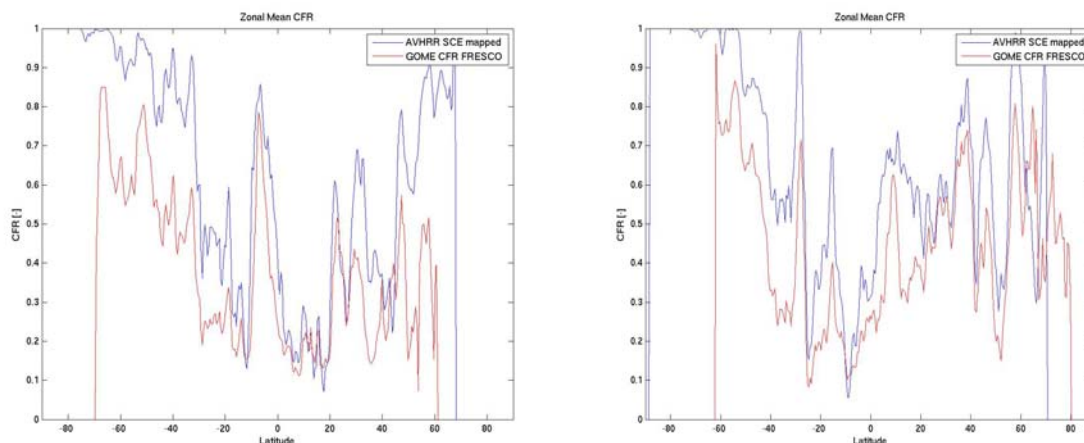


Figure 8: Comparison of Zonal Means for GOME-2 /Metop-A FRESKO+ R2 versus GOME-2 footprint equivalent cloud fractions derived from AVHRR (albedo test using visible AVHRR channels) for one orbit in February 2007 (left panel) and in October 2011 (right panel).

Overall, the statistics for FRESCO+ error flagging improved over the reference period with 91 % successful fits at the beginning of 2007 and roughly 7 % of failed fits to more than 97 % successful fits and less than 3 % failed by the end of 2011 (and only for the orbits investigated here). See Figure 9.

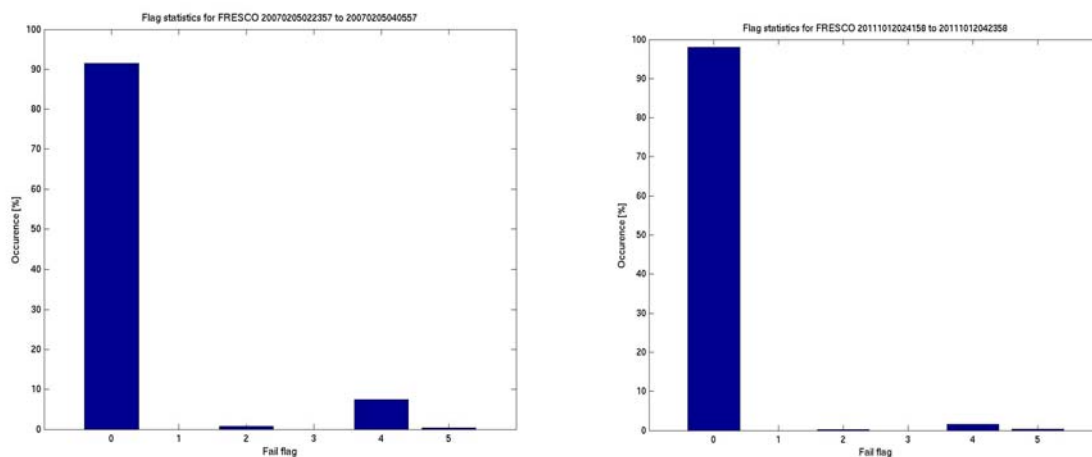


Figure 9: FRESCO+ fit flagging statistics for one orbit in February 2007 (left panel) and in October 2011 (right panel). Fail flag=0: successful fit; Fail flag=1: reflectivity out of range; Fail flag=2: solar zenith angle out of range; Fail flag=3: Satellite Zenith angle out of range; Fail flag=4: non-convergence of fit; Fail flag=5: missing input data.

## 7 Validation of target parameters

### 7.1 Instrument Dark Signal Correction (A2.8, A2.9, A3.3)

The status of the dark-signal performance is regularly reviewed by the annual GOME-2 instrument review [RD12]. The following section follows the structure of these performance reviews but using data for G2RP-R2.

#### 7.1.1 Description

The dark signal noise, dark signal offset and leakage are evaluated from dedicated dark measurements on the dark side of the orbit. Dark measurements are taken for the different integration times used during calibration and nominal earth scanning measurements and averaged over the valid integration period. The dark signal results are stored in the in-flight calibration file during processing for different temperatures and applied only for the relevant integration time and within a narrow range of the actual temperature.

The dark signal offset and leakage are specified in the PGS to be determined by the level 0-to-1b processor from mean dark signal readouts using a linear fit over integration time. During the analysis of data from the second throughput test, it has been found that this assumption on linearity is valid for the current operational temperatures of the main detectors, but breaks down at temperatures significantly above 280 K and for integration times longer than three seconds. To ensure a robust fit, the following analysis has been based on dark measurements with integration times shorter than three seconds. The post-processing of the results from data derived from the operational monitoring database makes sure that results are provided only if a significant amount of measurement is found to ensure a robust fitting result. For band 1A, during parts of the year not enough measurements for a certain integration time are available since they are taken outside of eclipse. Results close to these data gaps are therefore also not trustworthy (because the eclipse might be too shallow at this point in time).

**Note:** Based on these fitting criteria, the only other operations-induced change visible in the data is the turning on and off of co-adding in channel 3. Co-adding has been re-introduced at the 3 March 2009 with the introduction of new timelines: co-adding had been turned off earlier in March 2007 shortly after spacecraft in orbit verification (SIOV).

#### 7.1.2 Analysis

The following plots show band averaged results for dark signal electronic offset (blue line) and leakage signal (green line). Note that the dark-signal measurements for different integration times per band are taken at a different part of the orbit and therefore at different solar zenith angles (SZAs). Even though all dark measurements have so far been assumed to be taken (tagged as “valid”) well within eclipse, recent analysis of the timelines with the new GTL builder tool at EUMETSAT indicate that some of the dark measurements may suffer from (twilight) stray light, especially when taking the variation of the “shallowness” of the eclipse over the seasonal cycle into account. The latter is likely to cause the observed seasonal cycle in the noise signals, which varies significantly with integration time (which are related to different SZA or positions within the eclipse). The wavelength range covered per band is given in Table 7 below.

Table 7: GOME wavelength range per pixel for all main channels

Channel	1	1	2	2	3	4	5/6
Band	1A	1B	2A	2B	3	4	PMD P/S
Used Pixels	877/659 <sup>1</sup>	147/365 <sup>1</sup>	71	953	1024	1024	256
Spectral Range (nm)	240-307/283 <sup>1</sup>	307/283-315 <sup>1</sup>	290-300	300-412	401-600	590-790	290-790
nm/pixel	0.07	0.07	0.09	0.09	0.2	0.2	2
Predefined dark signal electronic offset (BU)	1501	1501	1503	1503	1495	1492	1503/1499

<sup>1</sup>Settings changed on 10 December 2008.

### 7.1.3 Interpretation

Unless otherwise stated in the figure notation, data in the following set of graphs (Figure 10 to Figure 13) are presented as follows:

- The band-averaged electronic offset signal (in BU) is in blue on the left axis.
- The leakage current (in BU/second) is in green on the right axis.
- The band-averaged dark signals (for all operationally used integration times) are plotted in blue points.
- The leakage current values are plotted as green points.

**Note:** Band 2A data are not reported. The data is outside the valid spectral range.

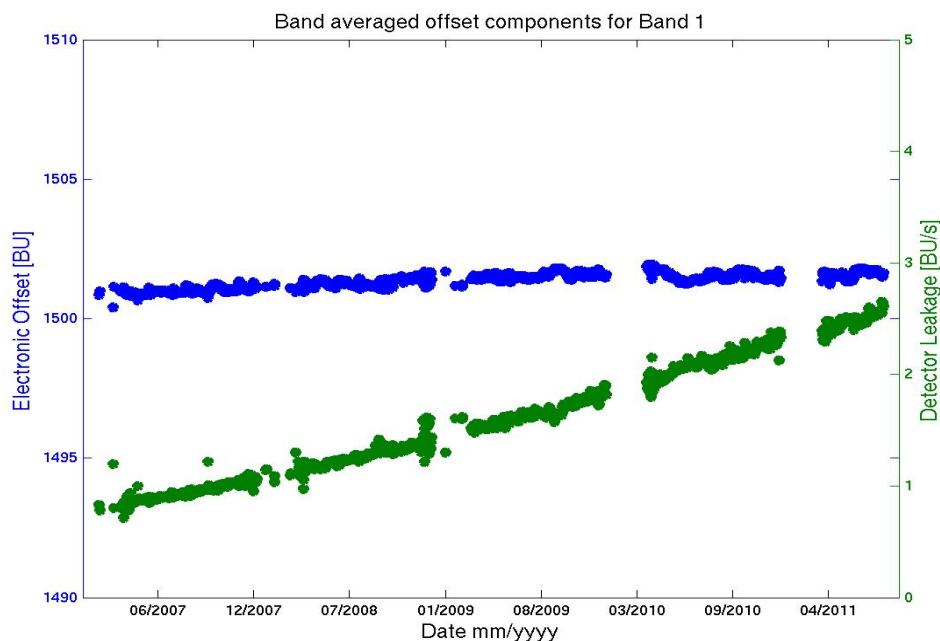
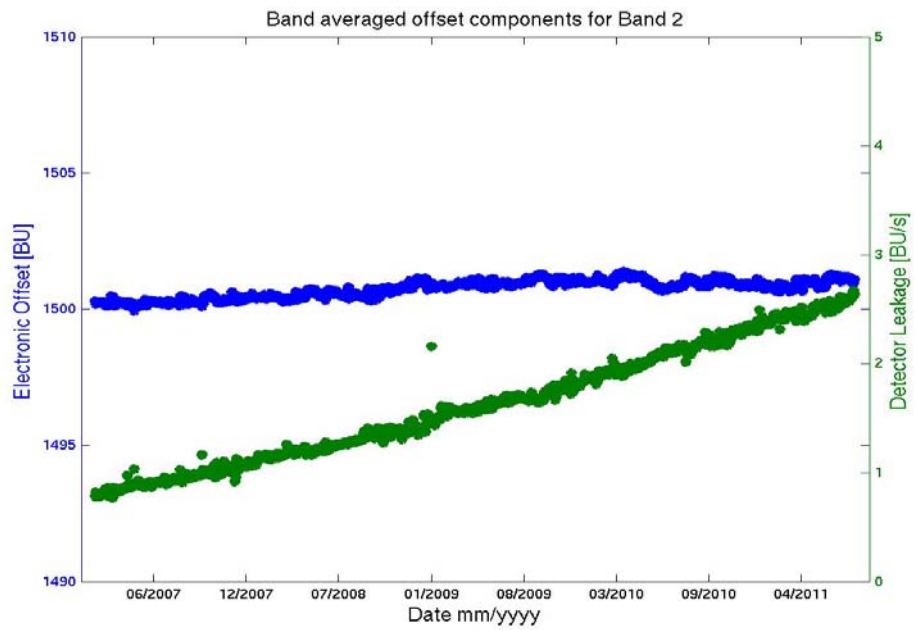


Figure 10: Band 1A averaged offset (blue points) and leakage current (green points)

**Band 1B**



**Band 2B**

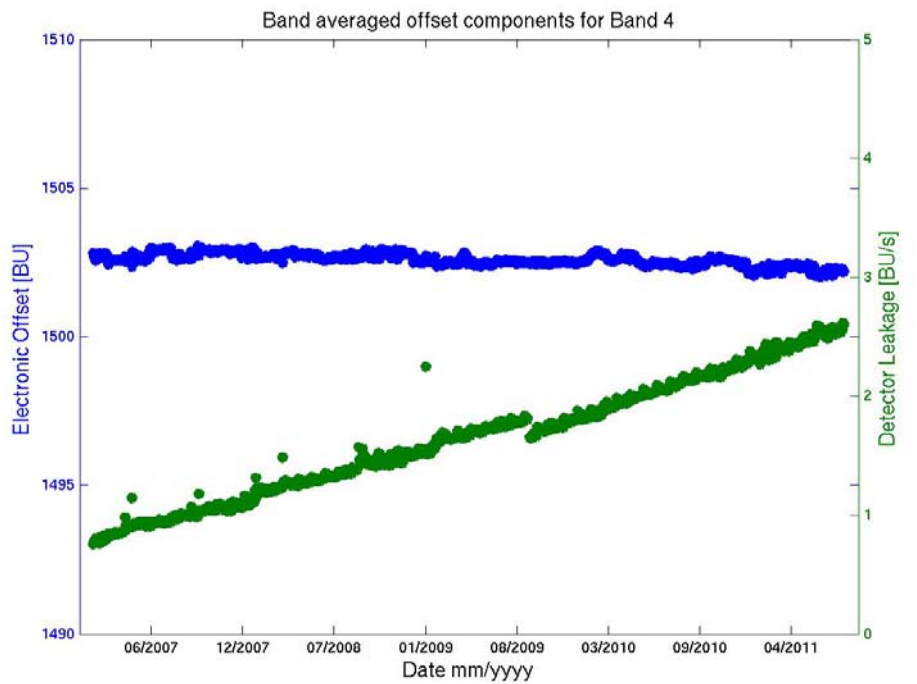


Figure 11: Averaged offset (blue points) and leakage current green points) for Bands 1B–Band 2B.

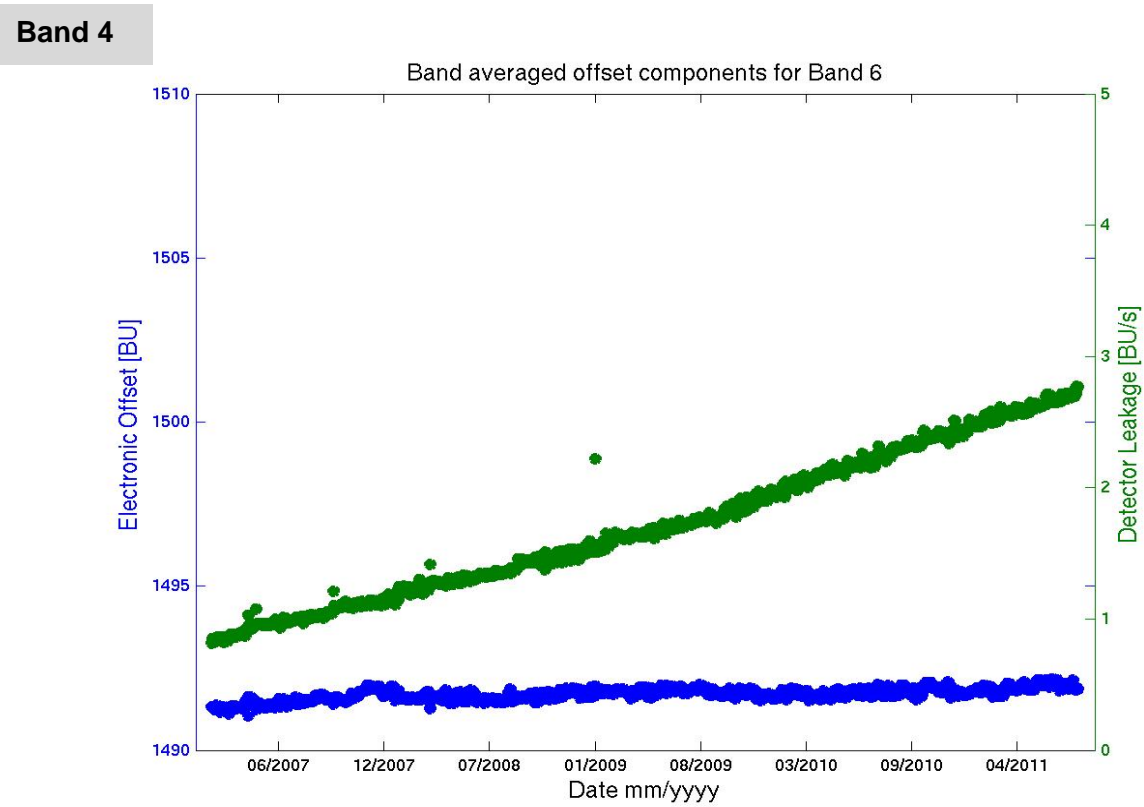
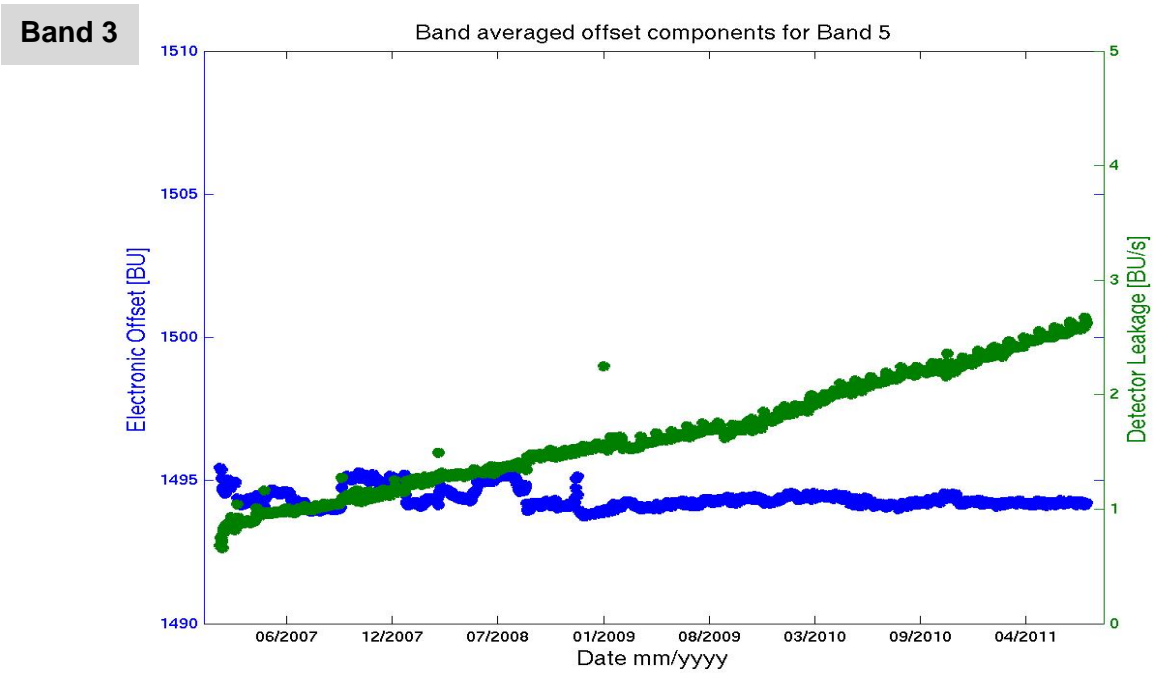
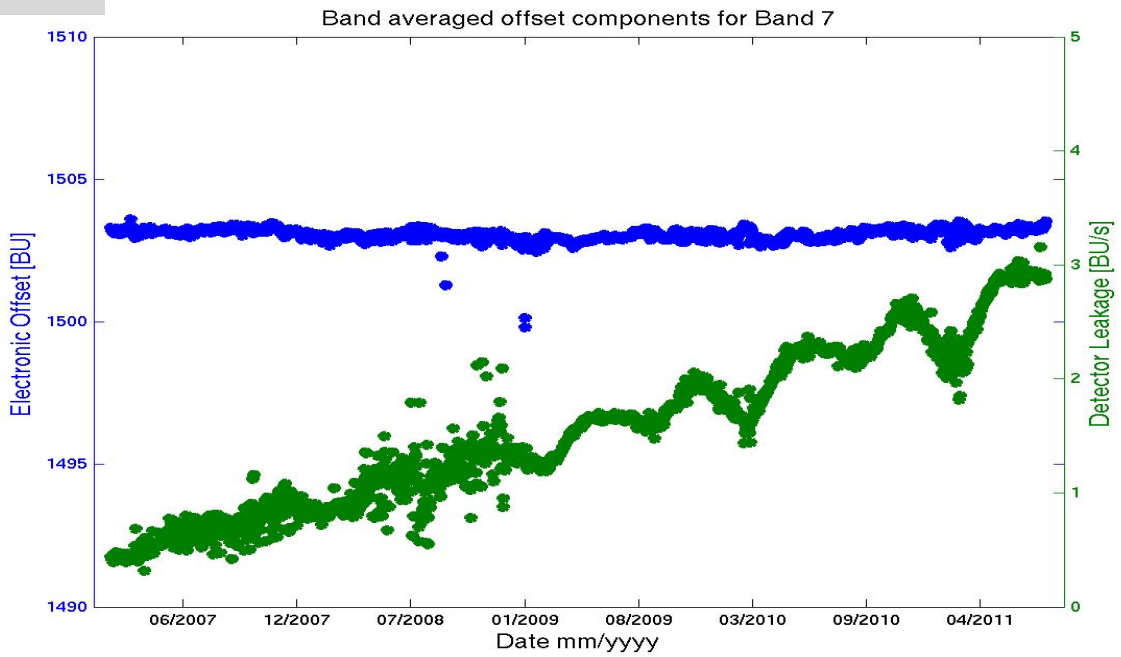


Figure 12: Averaged offset (blue points) and leakage current green points) for Bands 3 and Band 4.

**PMD-P**



**PMD-S**

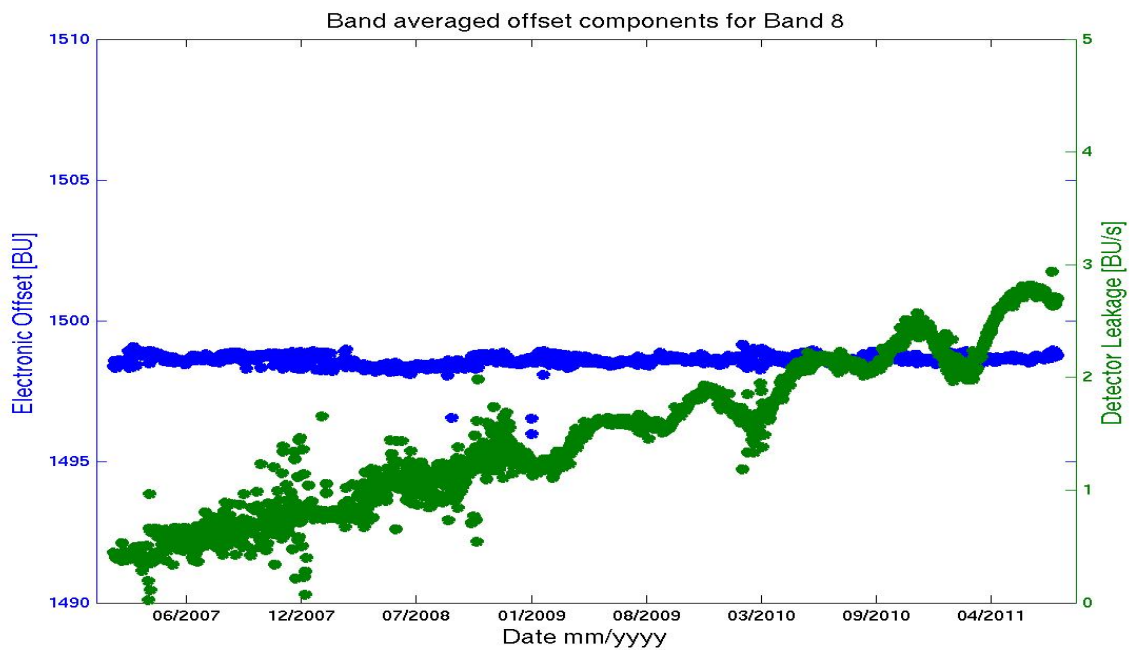


Figure 13: Averaged offset (blue points) and leakage current (green points) for Bands PMD-P and PMD-S.

**7.1.3 Interpretation (Continued)**

In the following series, Figure 14 to Figure 20, the band-averaged dark signal noise is presented for each of the seven bands.

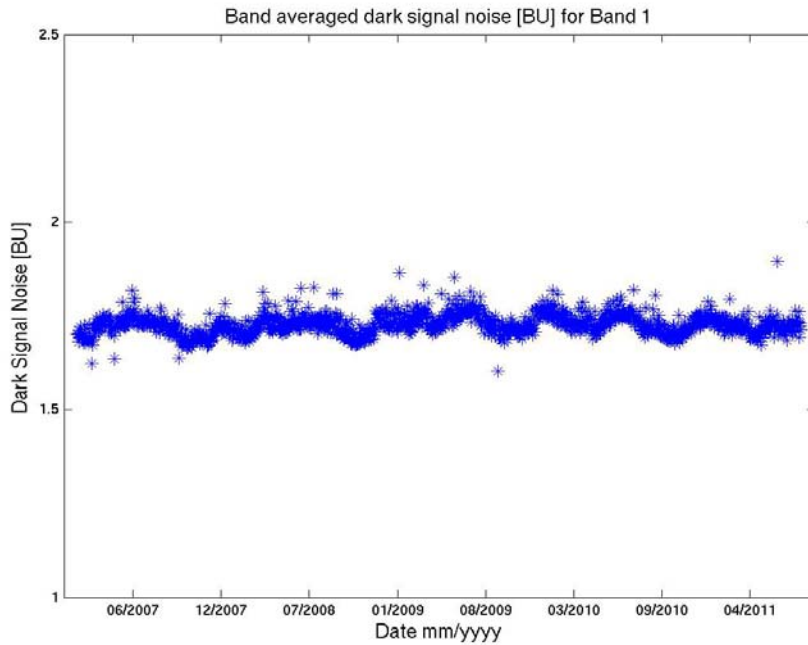


Figure 14: Averaged noise for Band 1.

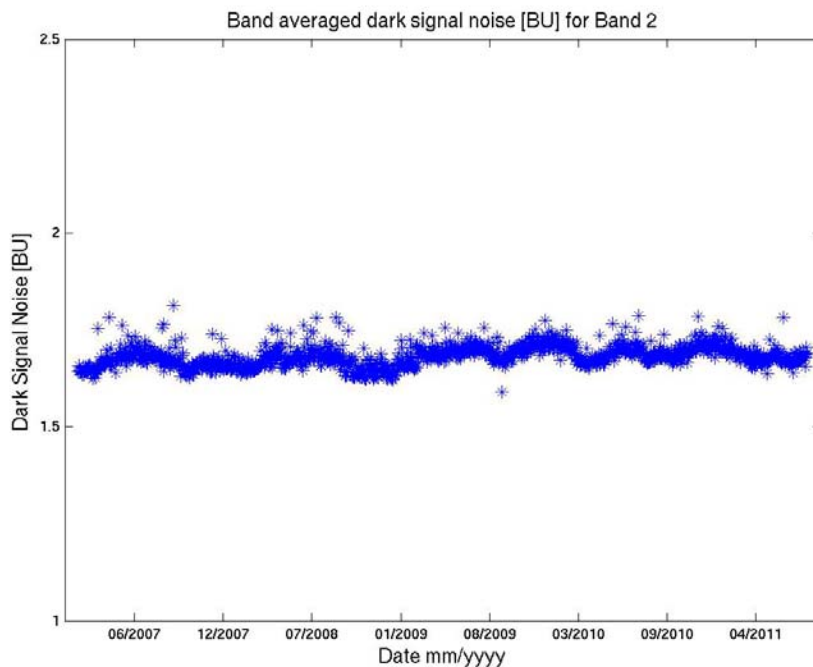


Figure 15: Averaged noise for Band 2.

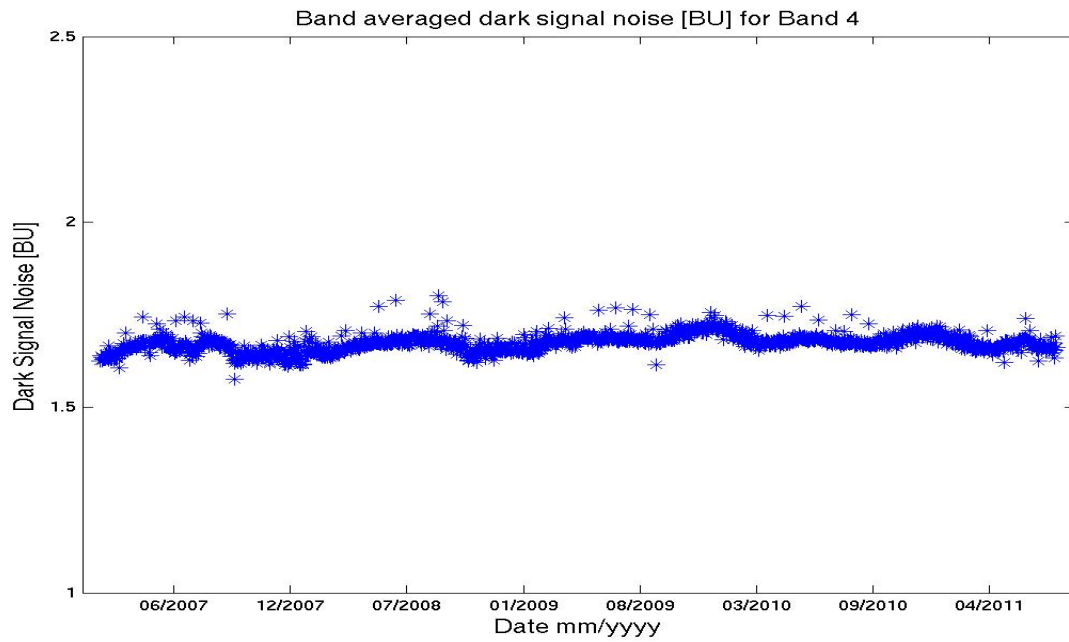


Figure 16: Averaged noise for Band 4.

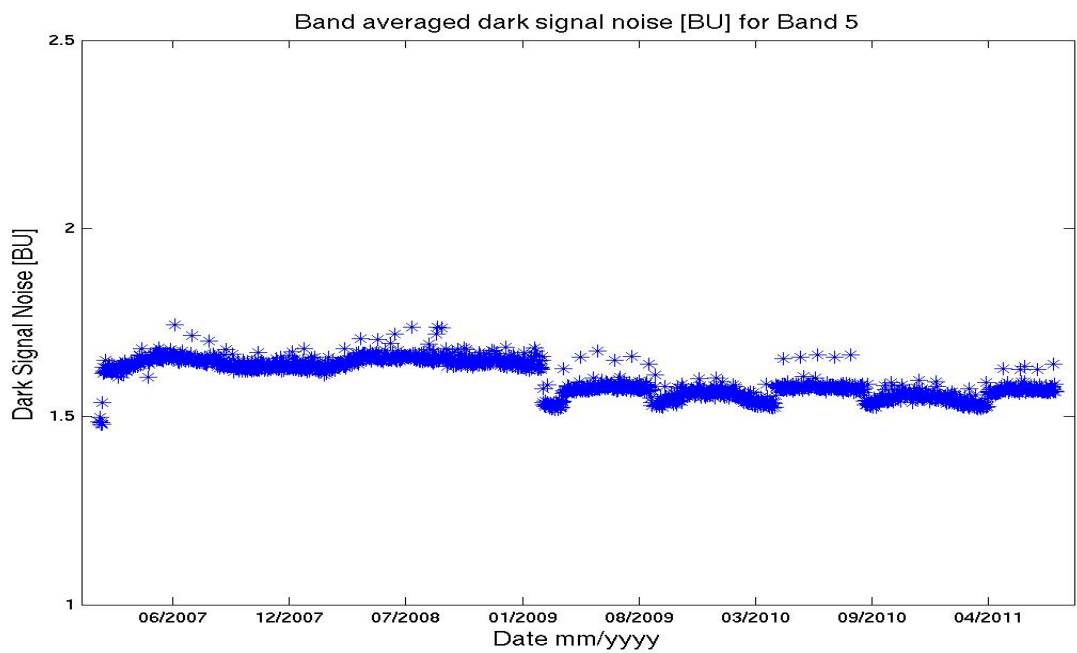


Figure 17: Averaged noise for Band 5.

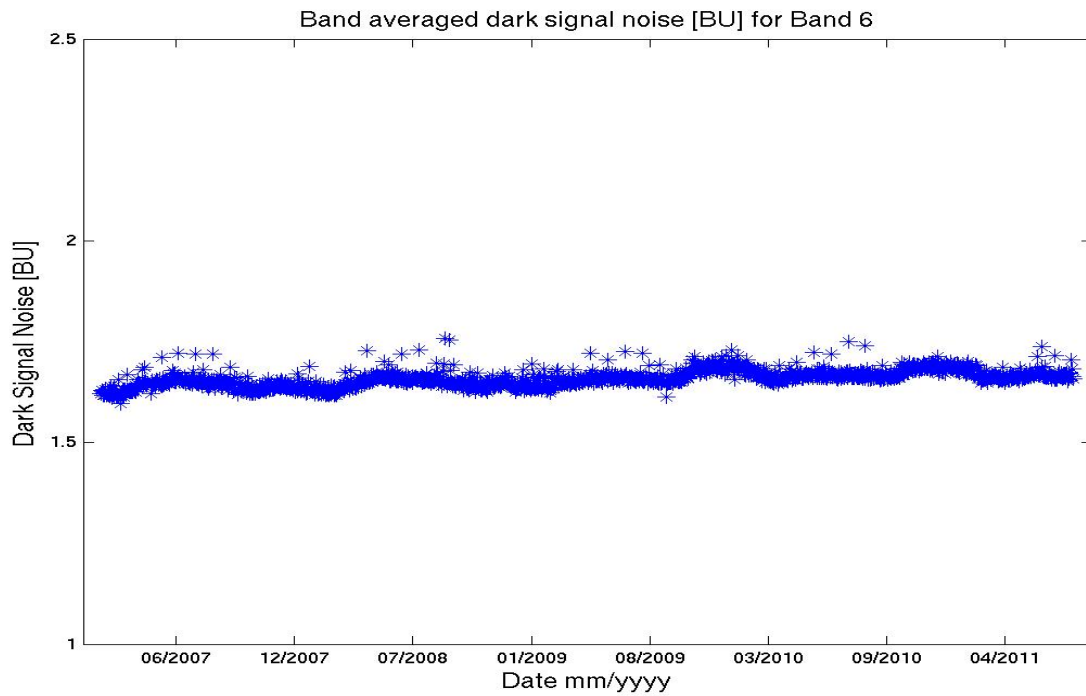


Figure 18: Averaged noise for Band 6

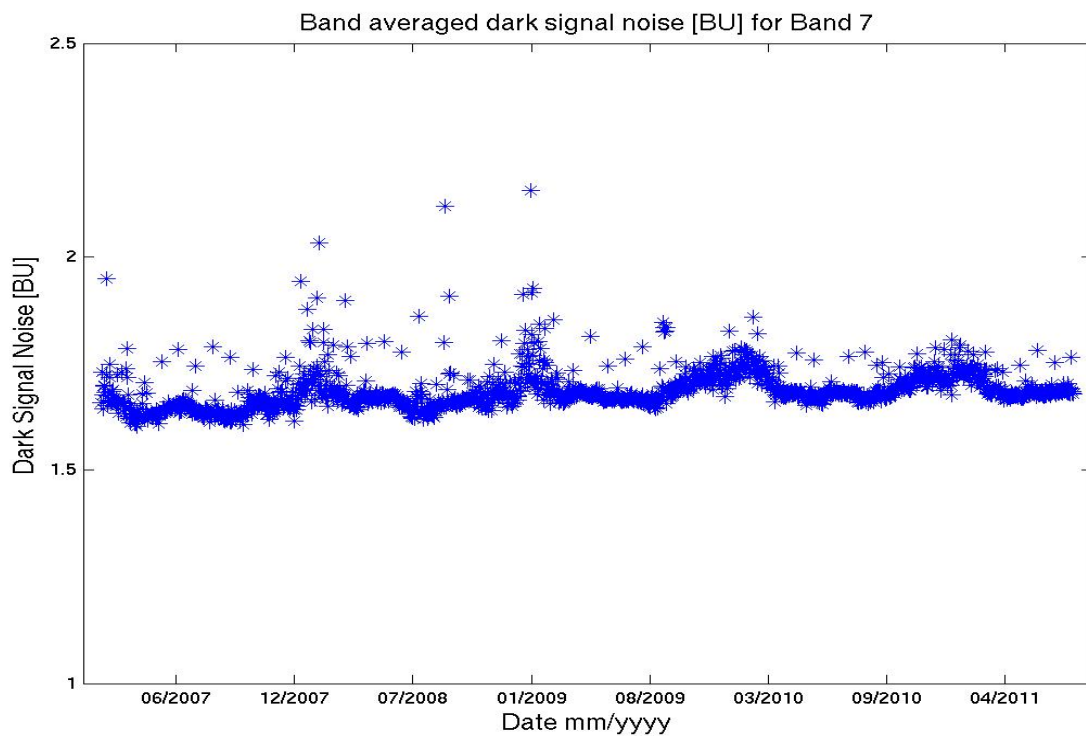


Figure 19: Averaged noise for Band 7.

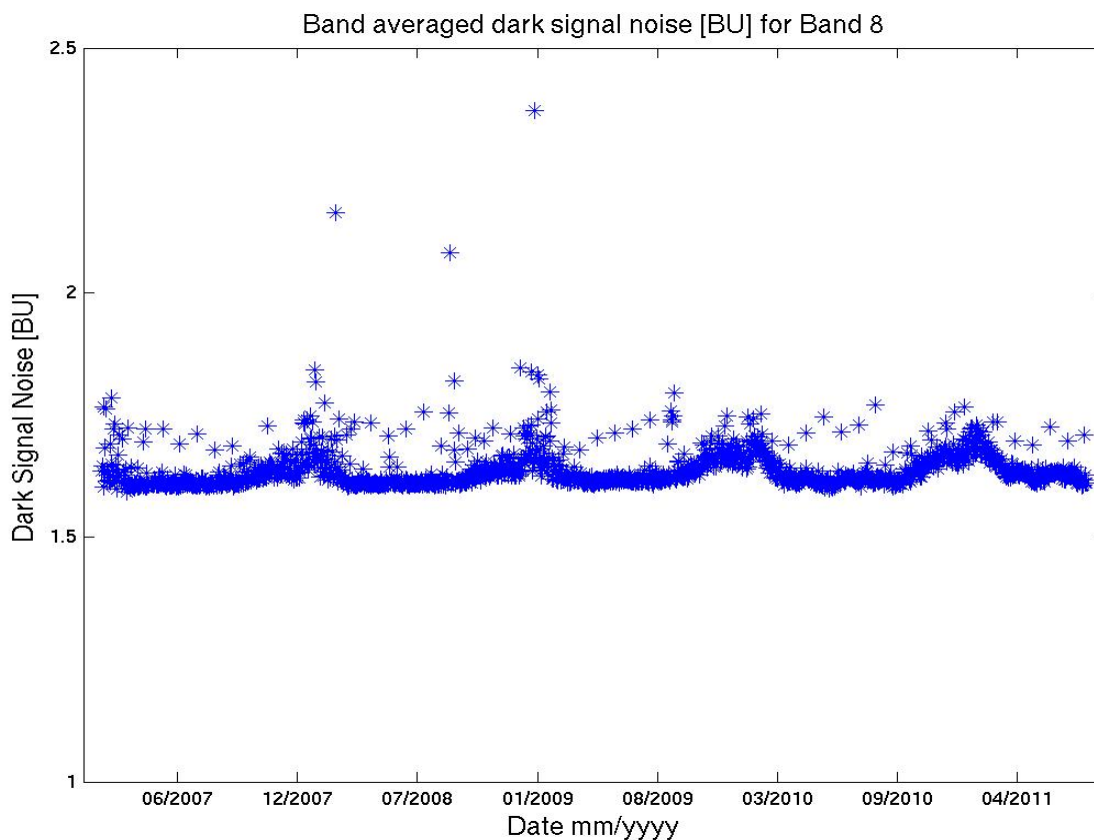


Figure 20: Averaged noise for PMD-S

#### 7.1.4 Assessment

The baseline for the electronic offset is steadily increasing for all bands. However, the increase is very small (individual BU level). The leakage current is increasing moderately and at a level of less than 0.5 BU/s per year, which is not unexpected for this type of detectors.

Apart from the seasonal cycle contributions depending on solar zenith angle (SZA) (related to specific integration times) within eclipse there is no significant other trending signal visible in the noise pattern. The seasonal cycle is related to the changing “shallowness” of the SZA within eclipse over the year. Overall, the noise pattern is very stable and slightly below 2 BU, as expected from pre-flight calibrations.

There is no negative impact from the very small increase in dark signal electronic offset on the product quality or the signal-to-noise ratio.

## 7.2 Thermal Performance Monitoring (Overlap-point stability, PMD-P/S ratio - sensitivity, spectral calibration stability)

Many on-board optical components and their performance are sensitive to on-board temperature changes. The main FPA detectors and the PMD detectors are therefore both actively cooled to 235 K and 231 K respectively, the FPAs in a closed-loop configuration and the PMD-S in an open-loop configuration.

### 7.2.1 Description

The following results on the long-term thermal signature of main instrument components will serve as a reference for the interpretation of signals especially for spectral calibration stability, etalon stability (overlap point shift) and the PMD-P/S ratio stability as used for the derivation of Stokes fractions (Section 7.5). Figure 21 below shows the main channel (FPA) and PMD temperatures during the time range covered by G2RP-R2.

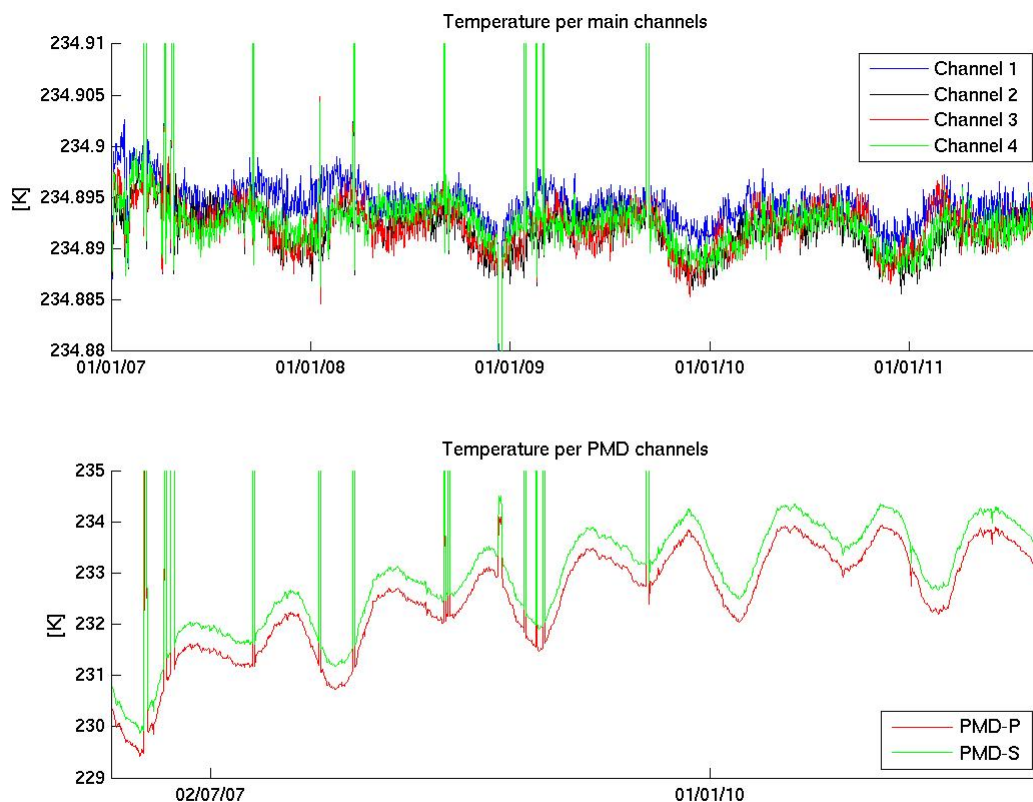


Figure 21: Instrument main channels (upper panel) and PMD (lower panel) detector temperatures during the time covered by G2RP-R1. Temperature-related spikes appear in all channels (other main channel colours are hidden by channel 4; green)

Whereas the FPA temperature for all main channels is very stable due to the closed loop cooling configuration, PMD temperatures vary somewhat during the current mission of Metop 2 and are closely linked to the optical bench temperature of the instrument. See Figure 22.

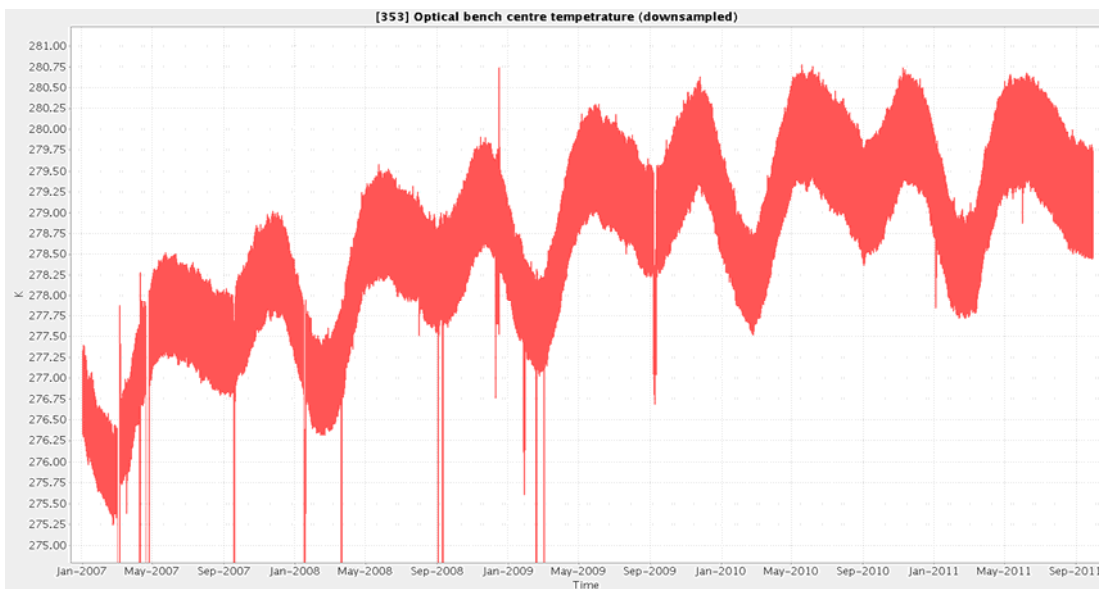


Figure 22: Instrument Optical bench temperature for the reference time period. The orbital variation is about 1 K.

Since the ratio of the PMD-P to PMD-S signals is frequently used in the derivation of the polarisation correction for main channel signals, Figure 23 shows the ratio of PMD-P to PMD-S detector temperature over the G2RP-R2 time period as an important reference frame for the interpretation of long-term instrument performance patterns. In an ideal situation, this ratio should be constant. The remaining observed differential temperature pattern, even though very small, may cause variations in the derived polarisation correction parameters during the observation period.

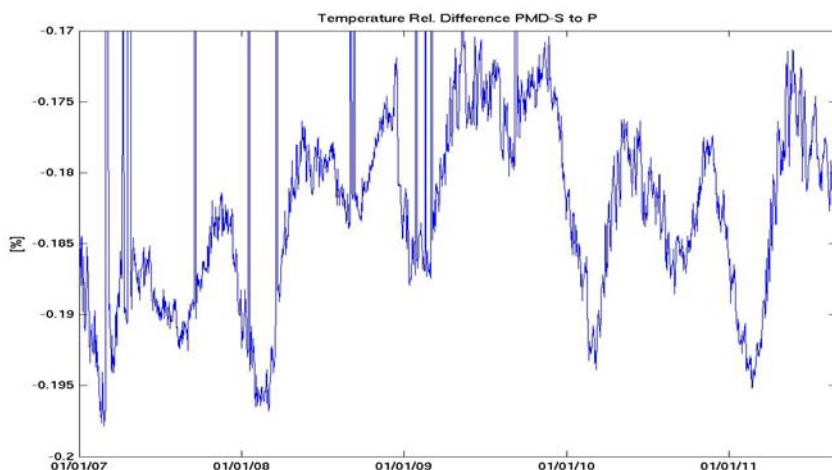


Figure 23: Relative percentage difference between PMD-P and PMD-S detector temperatures during the time covered by G2RP-R1.

### 7.2.2 Analysis

The point where the radiometric response of the instrument is equal for two physically separate detector arrays (channels) is called the “overlap point” between channels. The derived signals per channel are usually cut at this overlap point and concatenated in case radiances are used from spectral regions bridging a channel separation. This very often happens for the channel 1 and 2 overlap point around 311 nm. Many level 2 retrievals involving ozone and SO<sub>2</sub> are using radiances below and above this separation point. In addition, many radiometric corrections evaluated here are carried out only within the region of the overlap point avoiding low signal-to-noise ratio across this boarder and guaranteeing a homogenous transition from one channel to the other. However, it was noticed early in the mission that the overlap points are not stable with respect to detector pixels per channels but moving predominantly due to changing thermal stress on the optical bench. The latter predominantly influences the separation between channel 2 and 3, since the channel separation prism (see Figure 3), separating channel 1 and 2 from 3 and 4, is very sensitive to the thermal environment. Fortunately, the region between 395 nm and 405 nm is rarely used for level 2 retrievals. Also, the channel 1 and 2 overlap region is affected to some extent as shown in Figure 24.

### 7.2.3 Interpretation

Figure 24 to Figure 27 show the change of the overlap position in detector pixel and wavelength space both for channel transitions 1 and 2 and for channel transition 3 and 4 over the whole reference period.

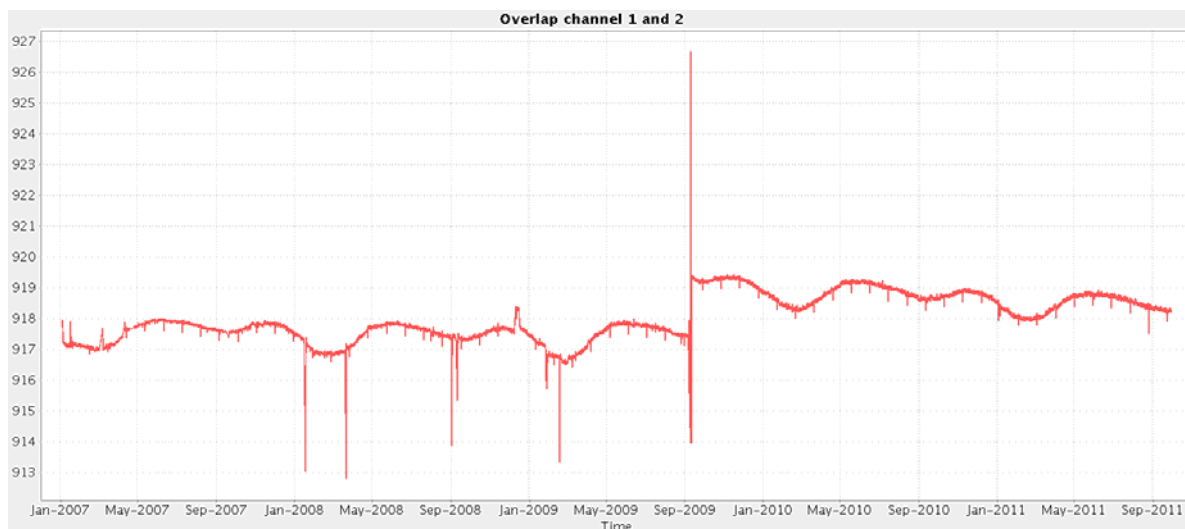


Figure 24: Overlap point position for the transition between channel 1 and 2 in detector pixel space



Figure 25: Overlap-point position for the transition between channel 1 and 2 in wavelength space

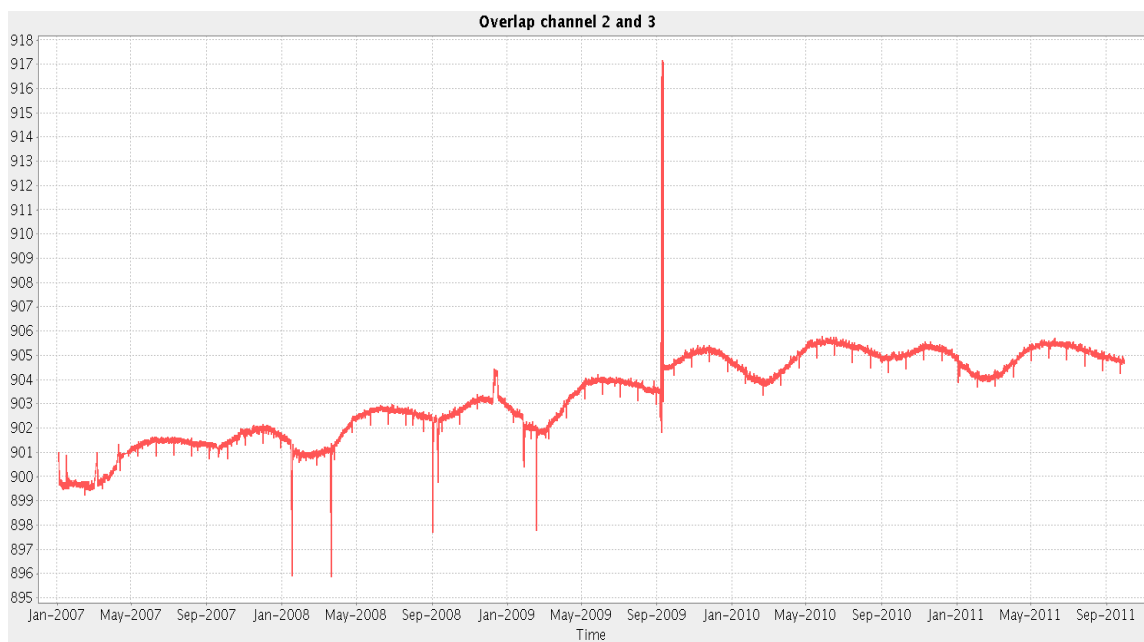


Figure 26: Overlap-point position for the transition between channel 2 and 3 in detector pixel space

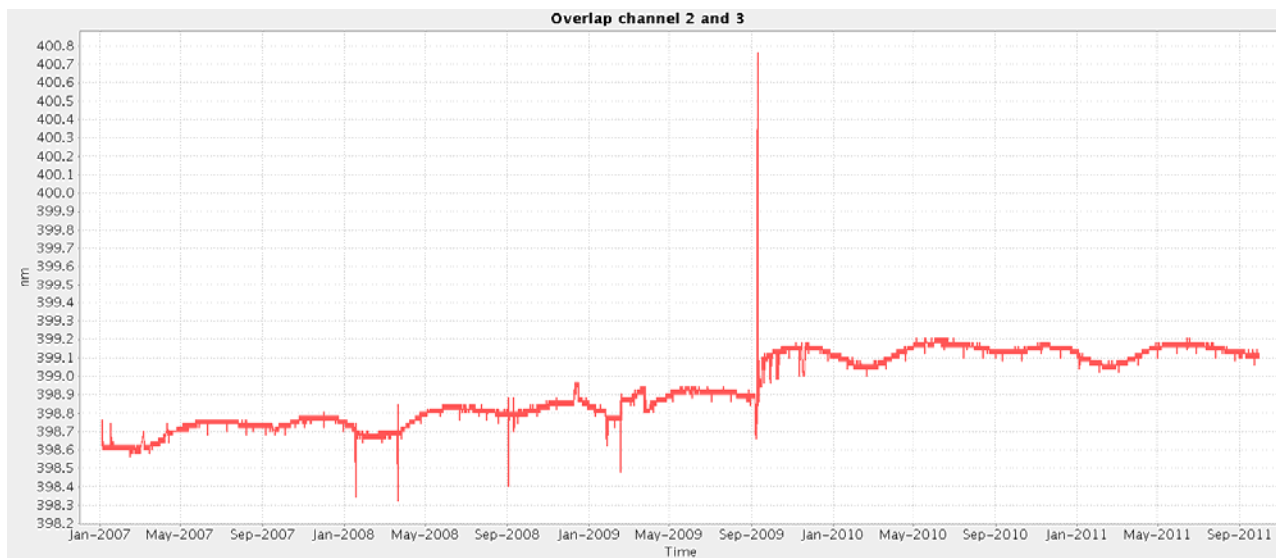


Figure 27: Overlap-point position for the transition between channel 2 and 3 in wavelength space.

#### 7.2.4 Assessment

The overlap point significantly shifted for the Channel 1 to Channel 2 transition following the second throughput test in September 2009. The shift was on the order of 0.1 nm and had some affect on the etalon correction (see Section 7.4). Thereafter, the overlap point gradually shifted back towards 311.5 nm—the position before the second throughput test.

### 7.3 Instrument spectral calibration (A2.13-A2.15, A3.6)

#### 7.3.1 Definition

GOME-2 spectral line source (SLS) measurements are used to derive spectral calibration parameters. Currently one spectral calibration is carried out on board every day. Spectral stability in orbit, which is a function of pre-disperser prism temperature, appears to be very good. The spectral calibration stability over the reference period for G2RP-R2 is well within the sub-detector pixel range (see Figure 28).

#### 7.3.2 Analysis

Only a very small, but abrupt, change in overall signal throughput of the SLS source signal is evident on 10 December 2008, following a short outage of the instrument and a delayed dale resistor switch-off (see instrument events list Section Main instrument and platform events). Otherwise, there is the significant drop in throughput also for the calibration lamp signal induced by the second throughput test. Both events caused a relative large shift ( $\sim 0.05$  nm, i.e.  $\sim 25\%$  per pixel) in the spectral assignment of channel 3 radiances in the blue part of the spectrum (see results for the 420 nm lines, Figure 32). This is usually the result of a different solution (change in coefficients) of the polynomial dispersion fitting for main channel spectral calibration.

#### 7.3.3 Interpretation

The spectral stability of the instrument is affected by the thermal environment. This is to be expected since changes in temperature will cause slight movement of the optical components of the instrument. Apart from the seasonal variation in spectral stability, it is also possible to see changes on short timescales due to switch-off events (Section 5.2).

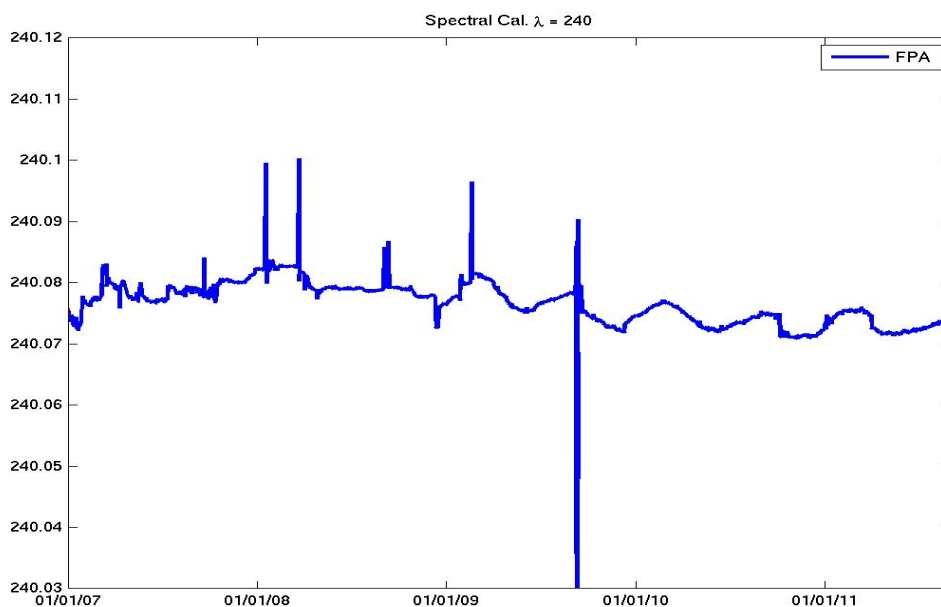


Figure 28: Spectral stability for the complete reprocessing period for main channels at 240 nm.

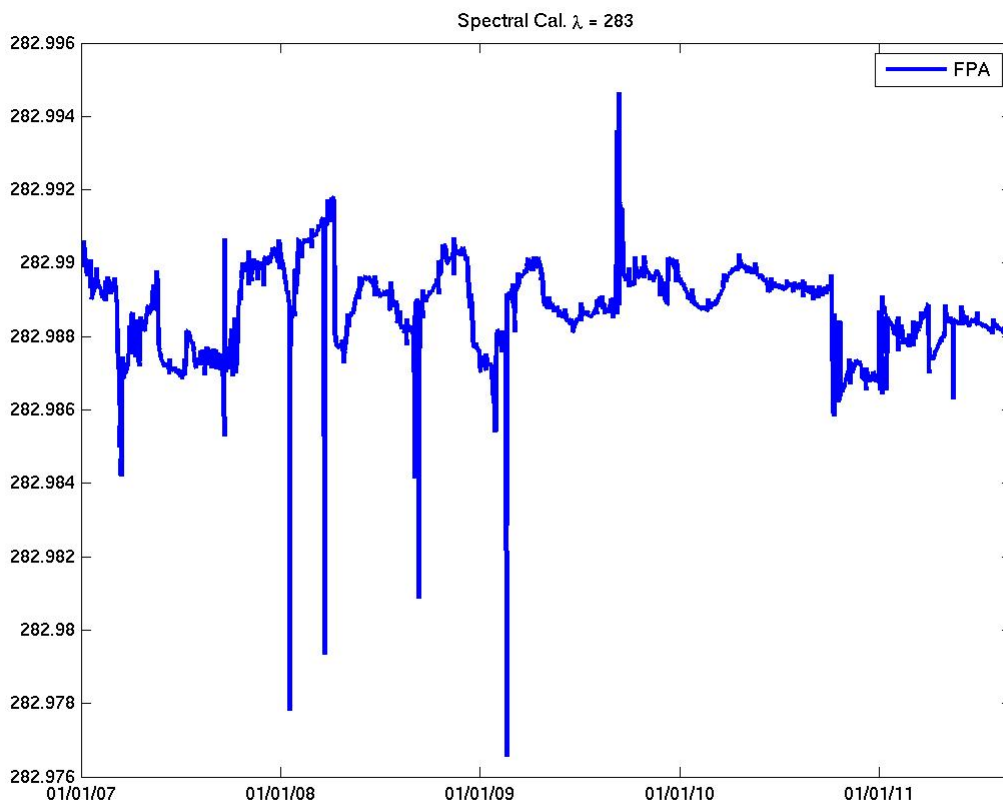


Figure 29: Spectral stability for the complete reprocessing period for main channels at 283 nm

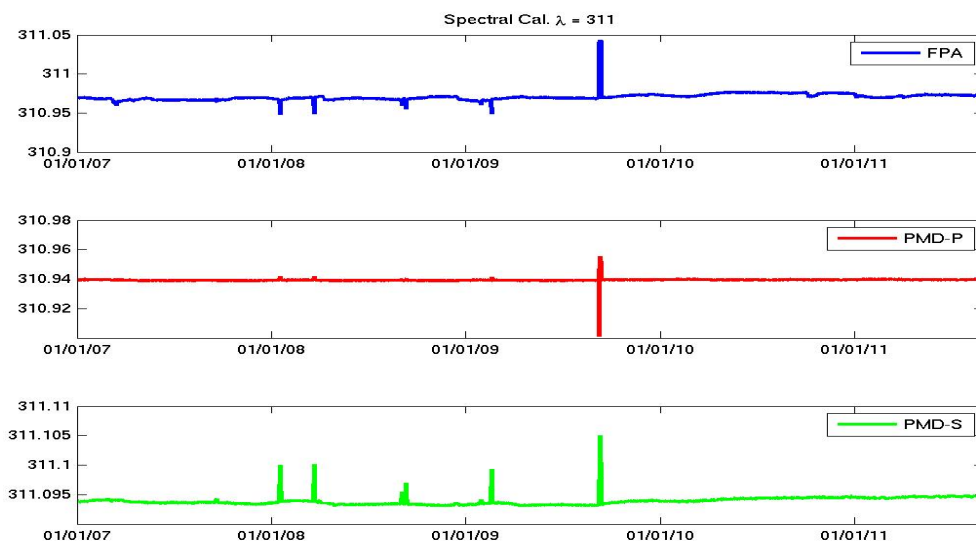


Figure 30: Spectral stability for the complete reprocessing period for main channels at 311 nm (upper panel), and PMD channels at 311 nm (mid and lower panels).

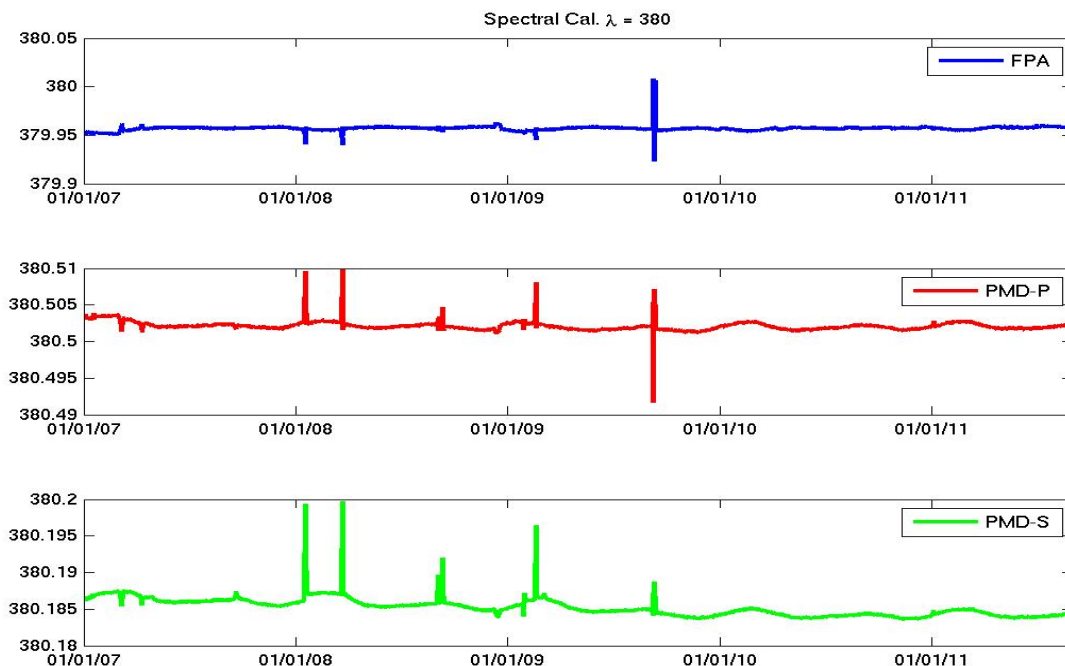


Figure 31: Spectral stability for the complete reprocessing period for main channels at 380 nm (upper panel), and PMD channels at 380 nm (mid and lower panels).

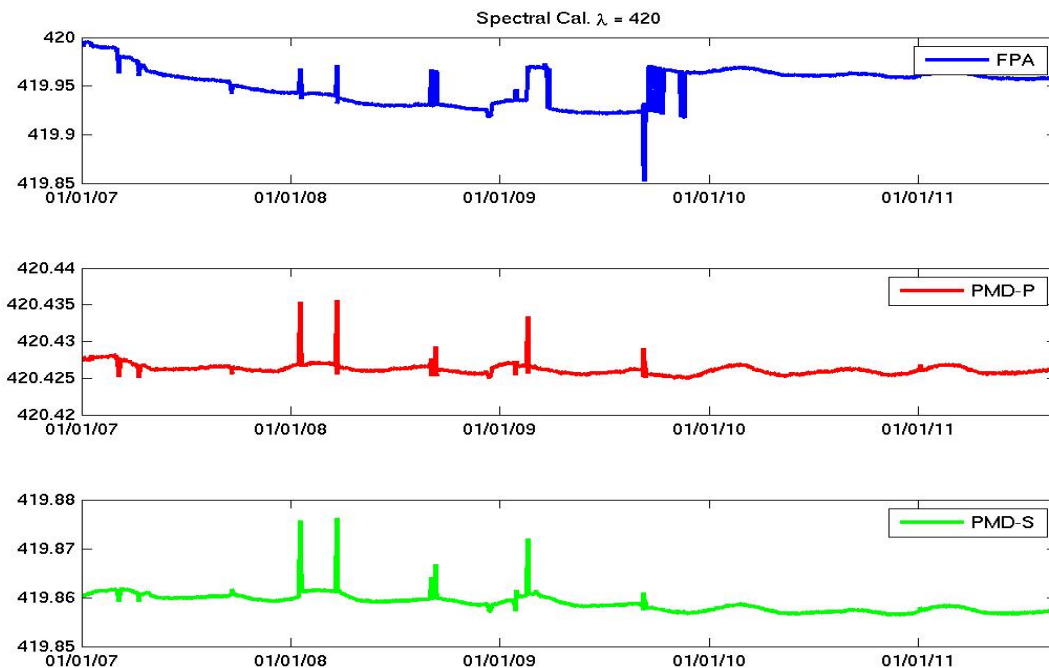


Figure 32: Spectral stability for the complete reprocessing period for main channels at 420 nm (upper panel), and PMD channels at 420 nm (mid and lower panels).

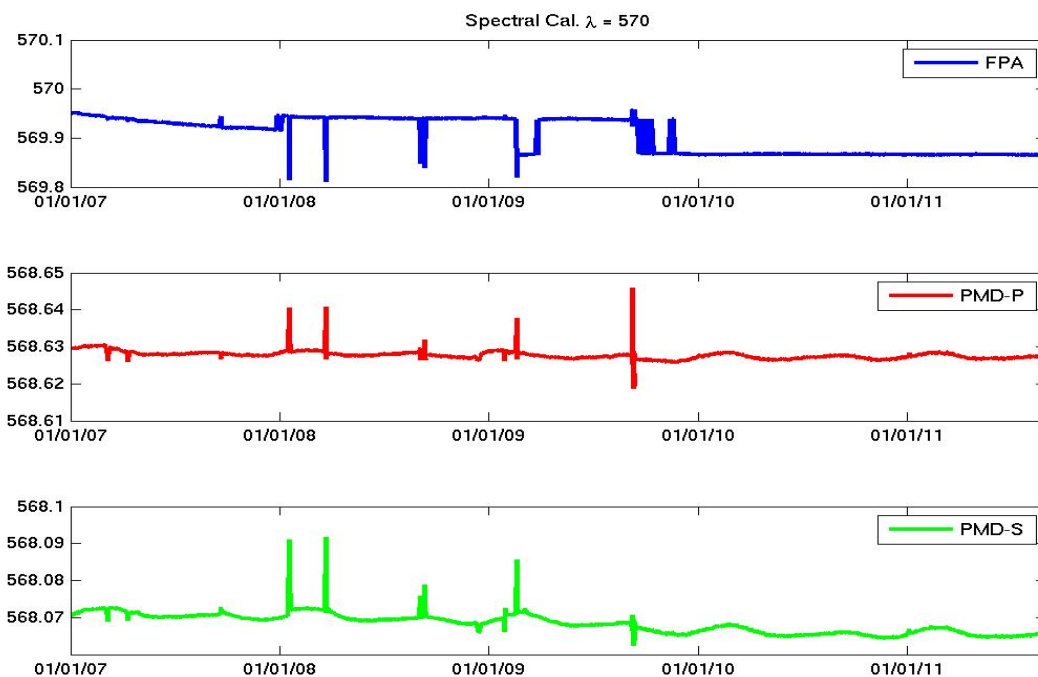


Figure 33: Spectral stability for the complete reprocessing period for main channels at 570 nm (upper panel), and PMD channels at 570 nm (mid and lower panels).

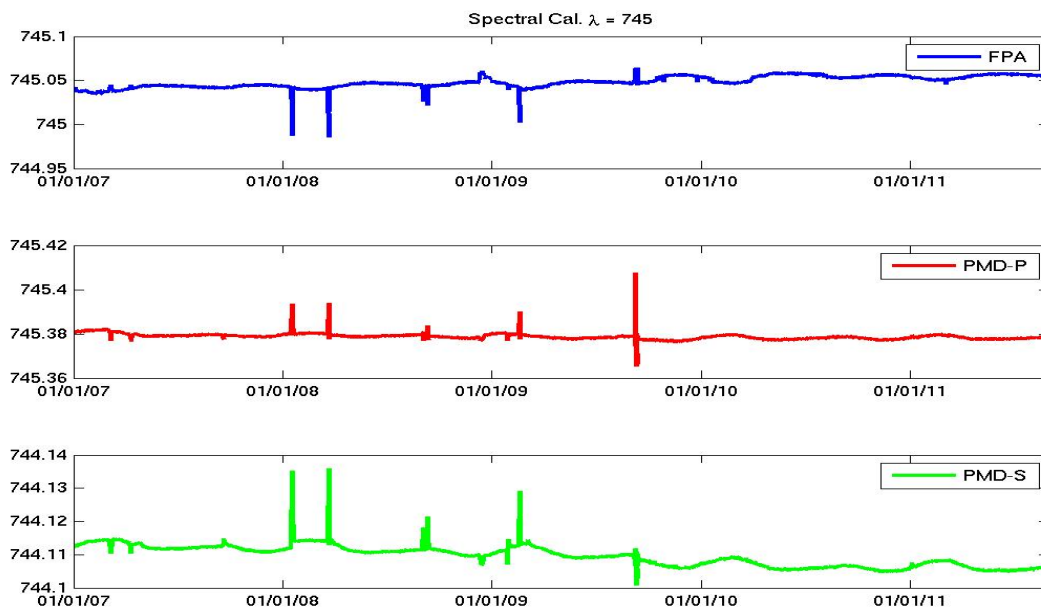


Figure 34: Spectral stability for the complete reprocessing period for main channels at 745 nm (upper panel), and PMD channels at 745 nm (mid and lower panels).

The spectral stability of PMP-P with respect to PMD-S is an important quantity since the stability of the “spectral co-registration” of the two polarisation detector grids affects the quality of the derived Stokes fraction quantities. The latter are in turn key to the accurate polarisation correction of main channel radiances. Figure 35 shows the spectral stability of PMD co-registration for G2RP-R2 in units of relative PMD detector pixel fractions.

### 7.3.4 Assessment

There is only a very small relative change visible over the whole reprocessing period (Figure 35 and Figure 36), which is negligible with respect to accuracy requirements for “q” Stokes fraction derivations. Note that the variation of spectral co-registration shows some correlation with the relative change in temperature between PMD-P and PMD-S.

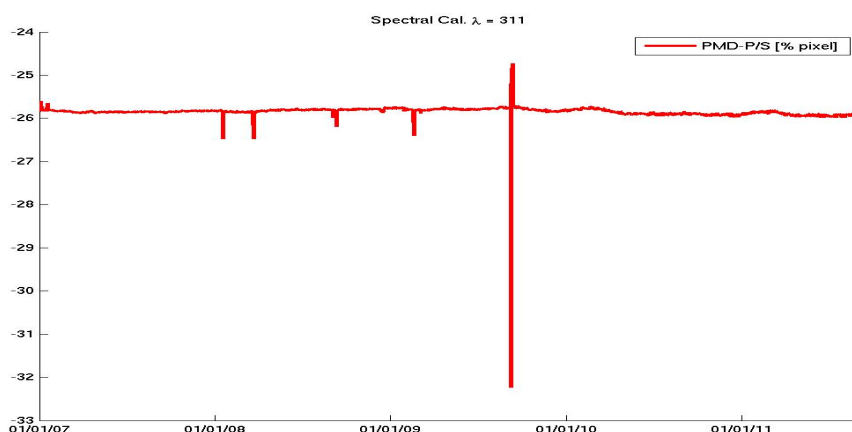


Figure 35: Spectral stability of the co-registration between PMD-P and PMD-S in percentage of fractional detector pixels around 311 nm.

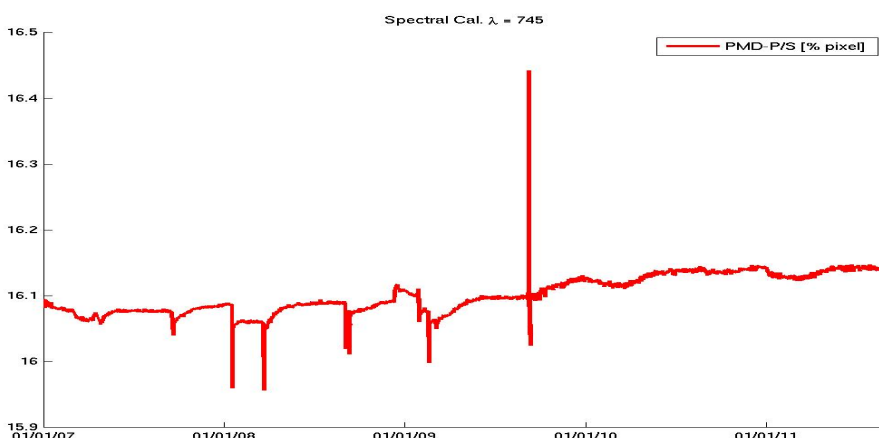


Figure 36: Spectral stability of the co-registration between PMD-P and PMD-S in percentage of fractional detector pixels around 745 nm. Note the different scales of the range axis

## 7.4 Instrument Etalon Correction (A2.16, A2.17, A3.7)

GOME-2 on-board white light source (WLS) measurements carried out daily are used to derive an etalon correction to account for potentially changing interference patterns caused by transparent layers on the instrument detectors. The WLS spectra measured in-orbit show a characteristic expected baseline shift as compared to on-ground measurements.

### 7.4.1 Description

The basis for the etalon correction is a baseline removed ratio of the on-ground reference WLS and the in-orbit lamp measurements assuming that the channel overlap point and hence the relative radiometric response of the two channels in the overlap point has not changed. However, as a result of the significant shift of the channel 1-2 and channel 2-3 overlap points from on-ground to in-orbit, it was necessary to correct the radiometric key data in these channel overlap regions using in-orbit WLS source measurements. This correction to the radiometric key data therefore includes an implicit etalon correction appropriate to the beginning of life. As a result, it is no longer possible to correct for transient changes in etalon with respect to the on-ground situation in these overlap regions (see Figure 37). In addition, changes in the overlap point due to thermal changes could affect the results (see Section 7.2). A valid etalon correction is therefore only available in the following regions.

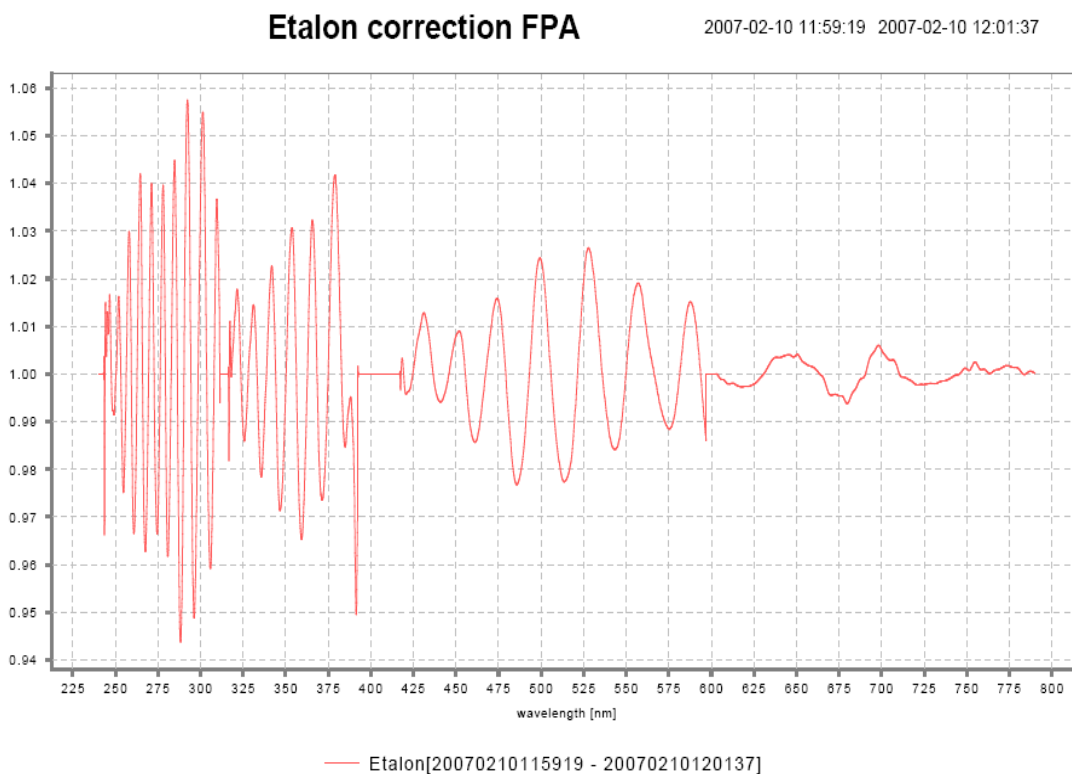
Table 8: Validity region of the etalon correction

<i>Channel Number</i>	<i>Detector Pixel Start/Stop</i>	<i>Approximate Wavelength Start/Stop [nm]</i>
1	310/935	243.4/312.8
2	210/850	316.5/392.1
3	120/1009	417.1/604.1
4	85/989	603.2/790.8
PMD-P	750/997	299.9/842.3
PMD-S	750/998	299.9/852.3

**7.4.2 Analysis**

The second throughput test in September 2009 has had a strong impact on the etalon amplitude and phase in all channels. The exact reason for an abrupt change in the detector transparent layer structure or the reason for any other sudden change of the etalon key parameters is still unknown [RD5] but might be linked also to a sudden shift of the overlap points between channels 1 and 2 as well as 3 and 4 (see Section 7.2). The consistency of the etalon correction (i.e. the correct removal of etalon-related structure from the observed spectra) is best evaluated by etalon correction of the WLS spectra, from which the etalon is derived. This essentially tests if the base-line correction and the fast Fourier transform (FFT) filtering of the WLS data is not introducing any artificial signatures, both in spectral as well as in temporal space.

Figure 37: Typical Etalon correction derived from a daily WLS measurement.



**7.4.3 Interpretation**

Figure 38 shows an example for the etalon correction derived once per day over the reference period and for the wavelength region of channel 2 (311 nm –400 nm). The abrupt change due to the second throughput test is clearly visible, as well as a gradual change of amplitude and phase over the whole period. Note the cut-off regions in the area of the overlap set to one, as specified in the text.

Figure 39 demonstrates the consistent removal of the ice layer-like etalon frequencies from the WLS spectra over the whole reference period except for the overlap regions. In contrast, small-scale structures (which for earthshine reference data could resemble atmospheric absorption structures) and broad scale changes (like the spectrally-dependent instrument throughput degradation) are not removed.

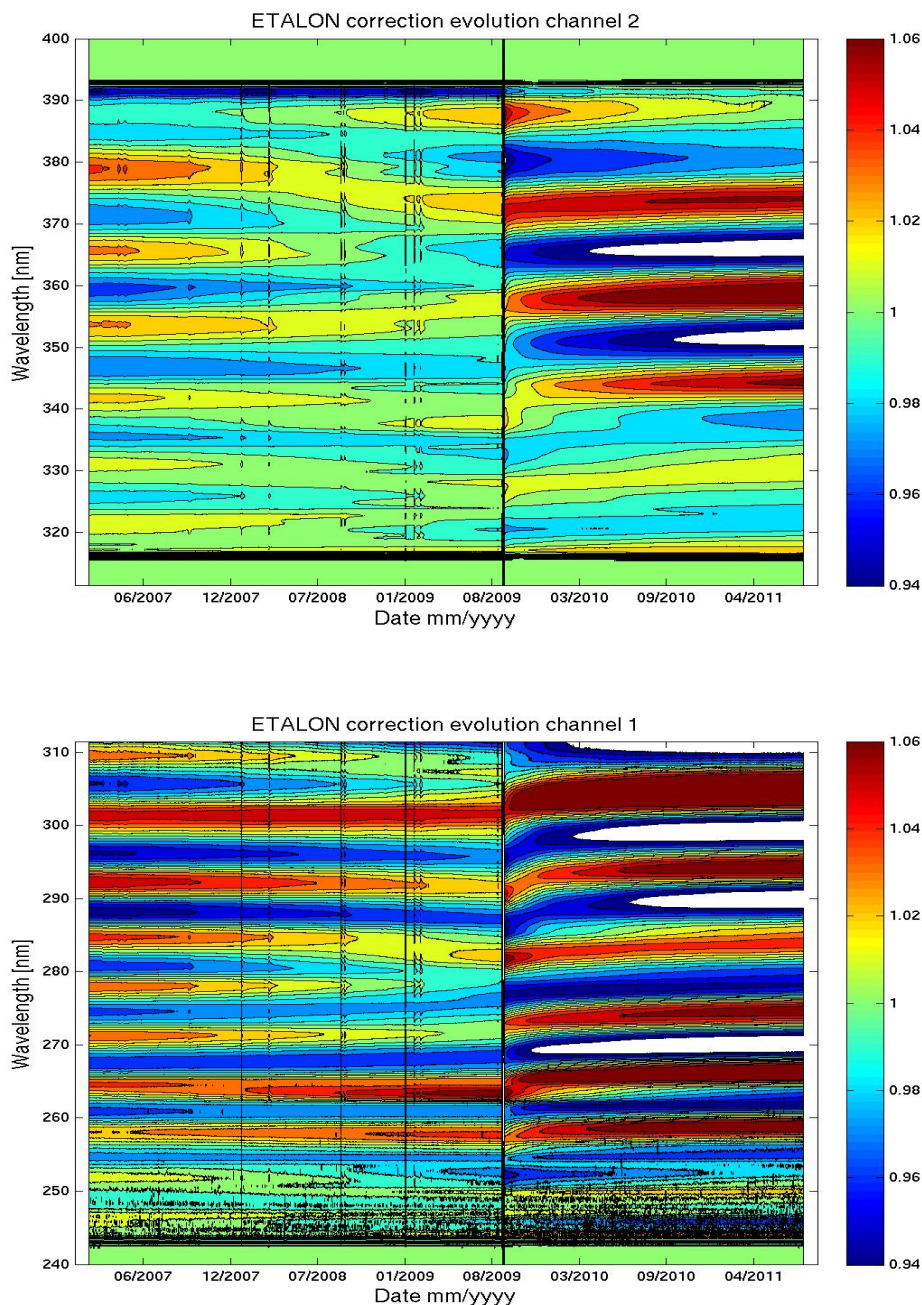


Figure 38: Typical etalon correction derived from daily WLS measurement over the reference period in channel 1 (lower panel) and 2 (upper panel).

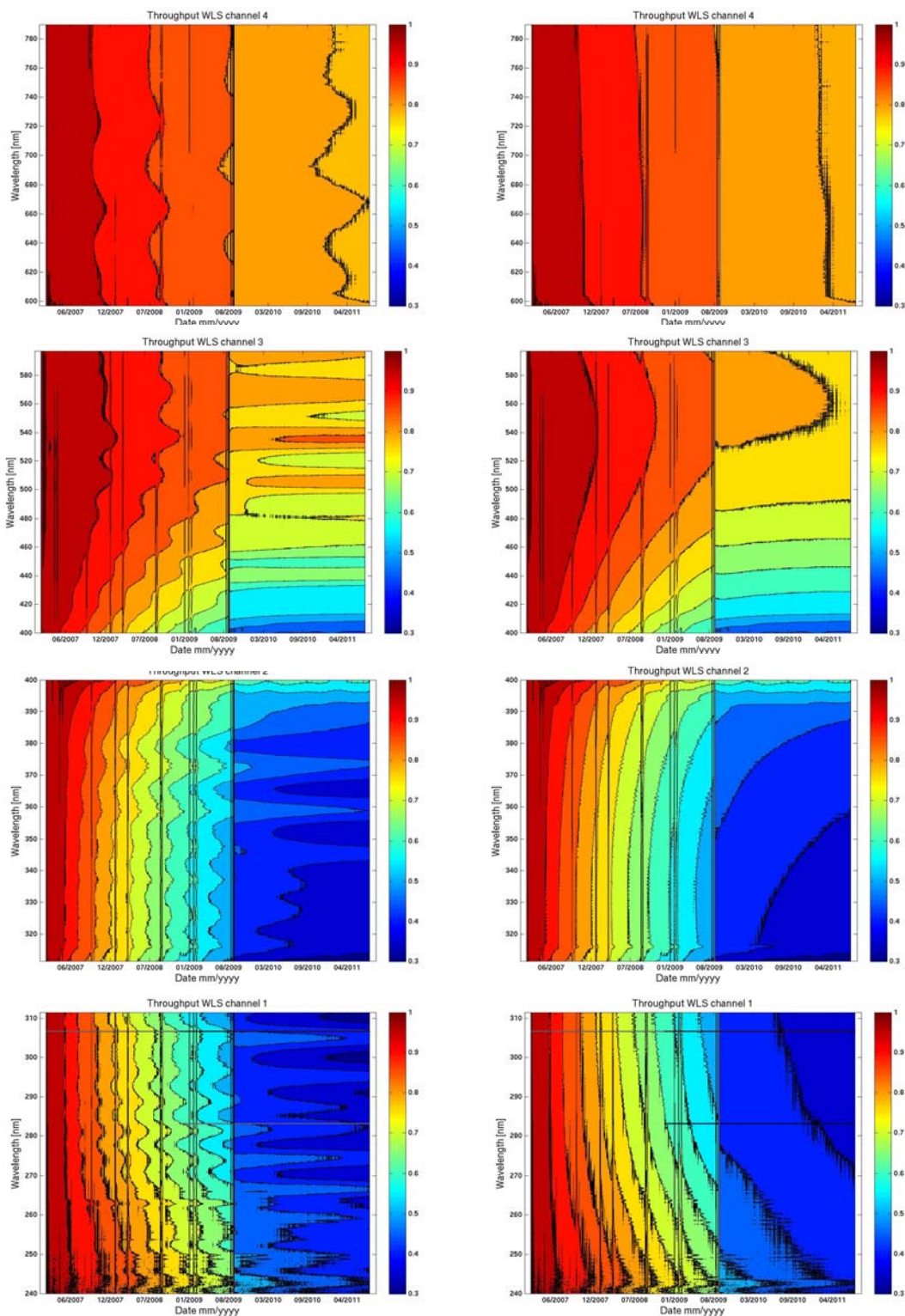


Figure 39: Relative change of the WLS spectrum with respect to the beginning of the reference period (February 2007). The left column shows main channel 1 to 4 (in rows, bottom to top) results not corrected with the derived etalon signature. The right column shows the same but with the etalon correction applied.

## 7.5 Instrument polarisation correction (Stokes Fractions) (A2.21, A3.10)

Main channel radiance quality is sensitive to the degree of polarisation of the incoming light because of the polarisation sensitivity of the optical paths. In order to correct for this effect for each earthshine measurement the corresponding eight PMD measurements from both PMD channels are used to derive the q-Stokes fraction (fraction of 90-degree linear polarised light) together with a theoretical estimate of the u-Stokes fraction (fraction of 45-degree polarised light) to which the instrument is less sensitive (though the latter cannot be neglected). The quality of this correction depends predominantly on the quality of the derived q-Stokes fraction and the instrument calibration key-data provided prior to launch.

In recent years, q-Stokes fractions are also used more frequently directly for retrievals of atmospheric parameters sensitive to the state of polarisation of scatter light (like for aerosol and cloud parameters).

### 7.5.1 Monitoring Stokes Fractions for Special Earth Viewing Geometries

The Stokes fraction  $q$  depends on the degree of linear polarisation  $P$  and the polarisation angle with respect to the reference plane  $\chi$  in the form  $q = P \cdot \cos 2\chi$ . Assuming that the polarisation angle at all wavelengths is similar to its single scattering value,  $\chi_{ss}$ , then  $q = 0$  when  $\cos(2\chi_{ss}) = 0$  independent of the degree of linear polarisation,  $P$ , and regardless of the actual atmospheric scene observed.

Therefore, specific locations can be found, taking into account the illumination geometry, where the Stokes fraction  $q$  of the light reflected by the earth's atmosphere is exactly zero.

The level 0-to-1b processor used for G2RP-R2 is applying an online correction to all derived Stokes fractions making use of special geometry conditions [AD2]. Examining the corrected Stokes fractions for these conditions should therefore lead to very small deviations (smaller than 0.02) from zero over the whole time period and serves as a check for the overall consistency of the polarisation correction.

In Figure 40, Stokes fractions for all 15 PMD bands averaged over the full reference period for G2RP-R2 are shown. The deviation from zero is very small, as expected. This is also partly due to the applied averaging over time.

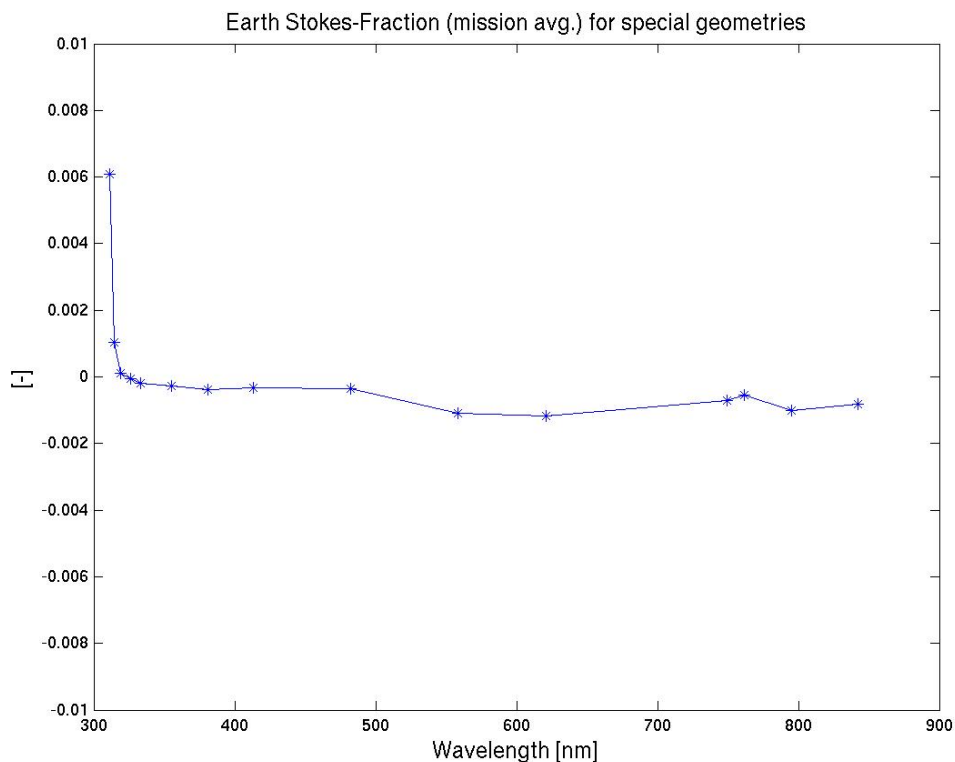


Figure 40: Stokes fractions calculated for special earth viewing geometries averaged over the full reference period for G2RP-R2 January 2011.

Figure 41 to Figure 43 show the time series of daily-averaged Stokes fractions for special geometries for all 15 PMD bands and over the full reference period. Also, here it is expected that the Stokes fractions are significantly smaller than 0.02. The seasonal cycle is due to changing solar geometry and viewing angle under which the measurement for  $q_{ss} > 0$  has been taken over the year.

The step in the time series visible for PMD band 1 and 2 occurs at 11 March 2008 with the upload of the new PMD band definitions version 3.1 (see Section Main instrument and platform events). Before this time the co-registration of PMD bands was not optimal and in particular for PMD 1 and 2. Since the ratio of both PMD band signals is the essential quantity in the calculation of the Stokes fraction value, the quality of the latter is expected to be systematically decreased before the switch to PMD band settings version 3.1 with the largest impact for band 1 and 2 (see [RD13]). The correction scheme for Stokes fractions as introduced with PPF 4.3 and which has been used unchanged in G2RP-R2 is also not tailored for PMD band settings version 1.0 (launch settings) as applied before March 2008. This should be improved for future reprocessing campaigns. Overall, the results indicate a very high quality of the Stokes-fraction for special geometry with values very close to zero for PMD 3-15 and for PMD 1 and 2 after 11 March 2008. Before March 2008, PMD 1 and 2 show systematic offsets of 0.02 and 0.004, both are still significantly smaller than the original target level of 0.05.

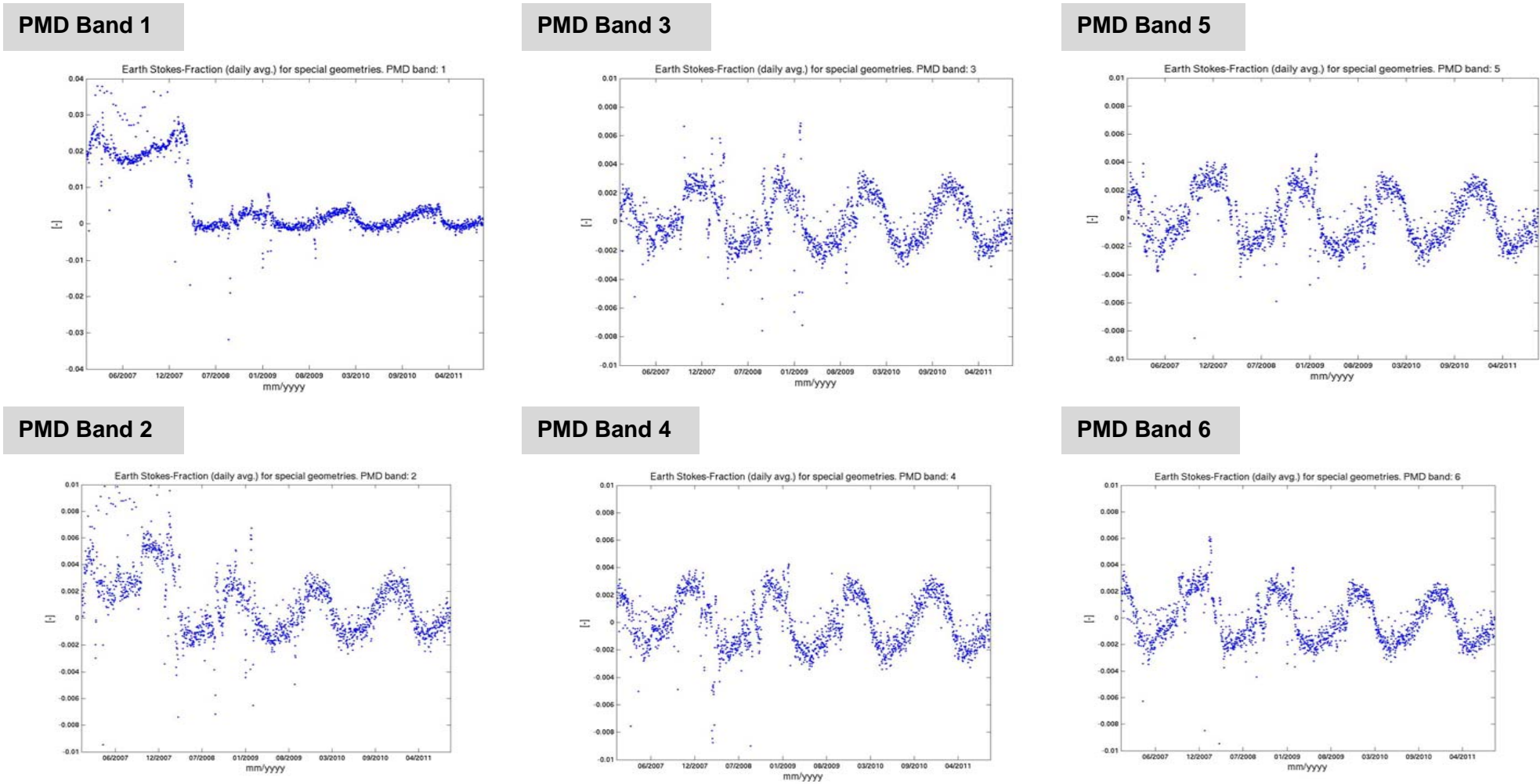
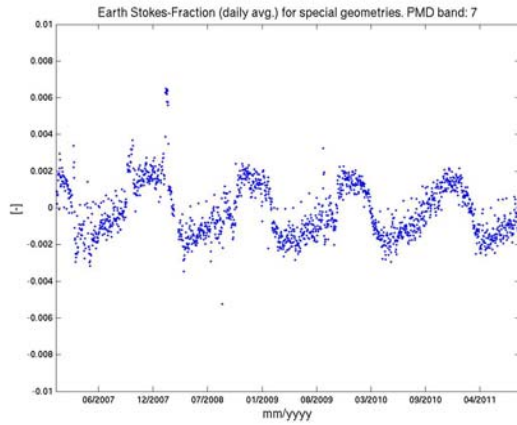
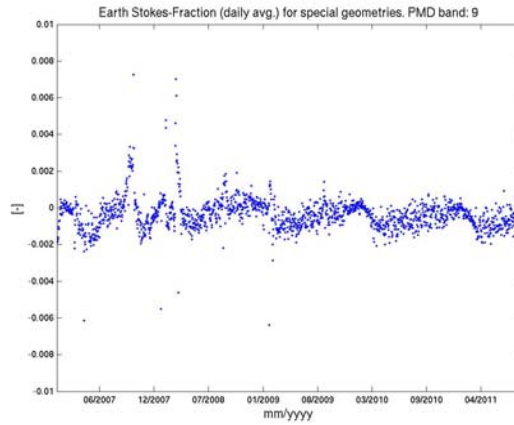


Figure 41: Stokes fractions calculated for special Earth-viewing geometries over the full reference period and per PMD bands 1-6 for G2RP-R2 January 2011.

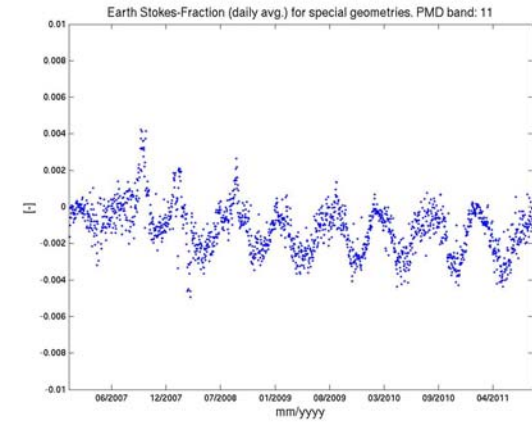
**PMD Band 7**



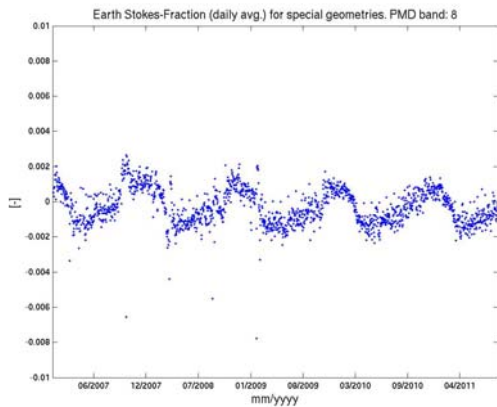
**PMD Band 9**



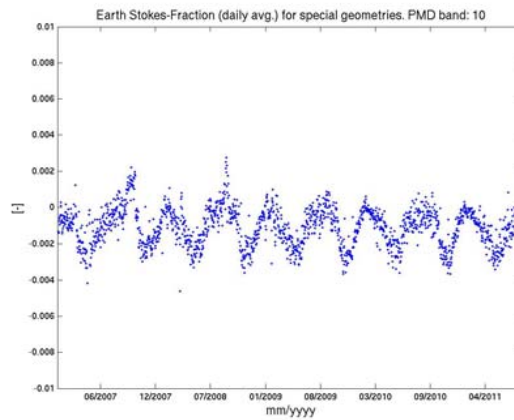
**PMD Band 11**



**PMD Band 8**



**PMD Band 10**



**PMD Band 12**

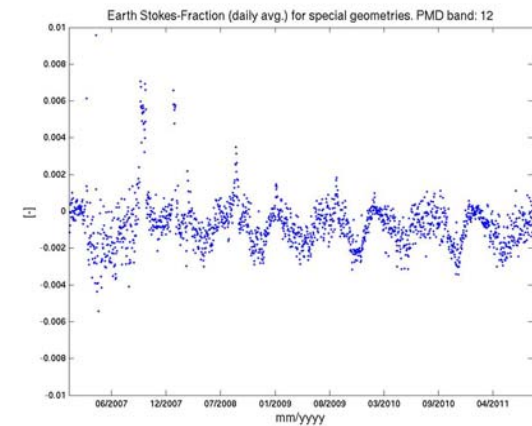
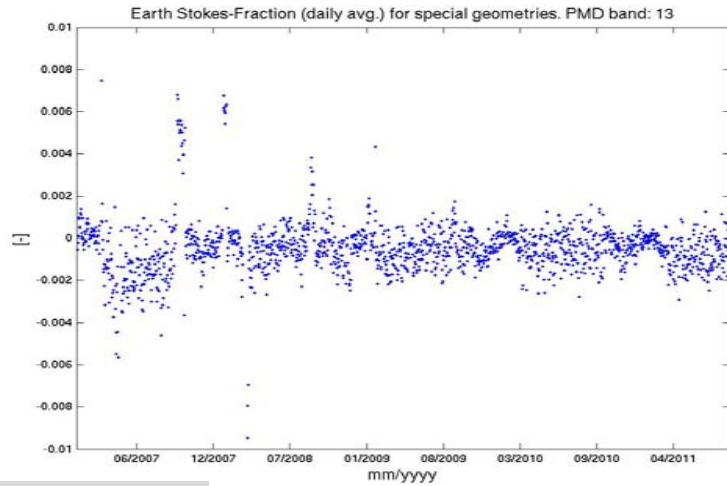
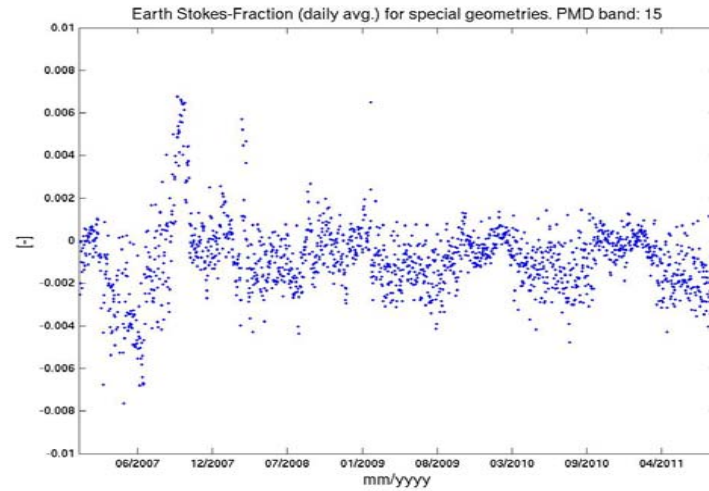


Figure 42: Stokes fractions calculated for special Earth-viewing geometries over the full reference period and per PMD bands 7-12 for G2RP-R2 January 2011.

**PMD Band 13**



**PMD Band 15**



**PMD Band 14**

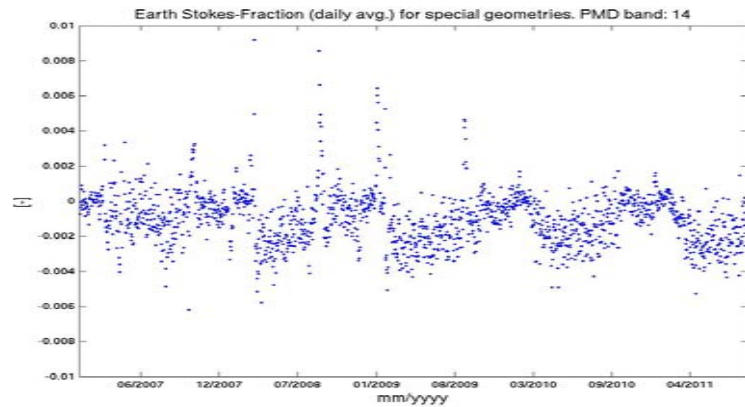


Figure 43: Stokes fractions calculated for special Earth-viewing geometries over the full reference period and per PMD bands 13-15 for G2RP-R2 January 2011.

**7.5.2 Monitor Stokes Fractions for Earthshine Scanning Measurements – Limiting Atmosphere approach**

In order to monitor and validate the measured GOME-2 Stokes fractions for conditions other than those described in Section 7.5.1 above, a more general approach is needed. The approach to be used is based on a statistical analysis developed by SRON under contract to ESA. It can be shown that the general behaviour of the Stokes fraction,  $q$ , along the orbit is primarily determined by molecular (Rayleigh) scattering, in particular over dark ocean surfaces, and that variability in  $q$  is caused by the presence of clouds and aerosols. It is observed that the measured polarisation values are always clearly between extreme limiting values. These limiting values lie between the Rayleigh single scattering values and  $q = 0$ . Furthermore, for a large number of measurements the measured polarisation values are influenced by largely cloudy scenes which depolarise the light leading to a measured Stokes fraction of  $q = 0$ . The assumption, upon which the generalised validation of  $q$  is based, is that the minimum Stokes fractions observed are representative of a limiting atmosphere with minimum depolarisation, i.e. a combination of minimum ground-albedo and minimum aerosol loading. In the case of little or no instrument degradation these limiting values will be constant in time and can be used as an empirical validation method for the long-term in-flight monitoring of polarisation measurements. Figure 44 to Figure 48 show Stokes fractions calculated from earthshine scanning measurements with respect to the single scattering Stokes fractions (diagonal line) and  $q = 0$ . Red points lie inside the physically reasonable range while blue points lie outside the physically reasonable range.

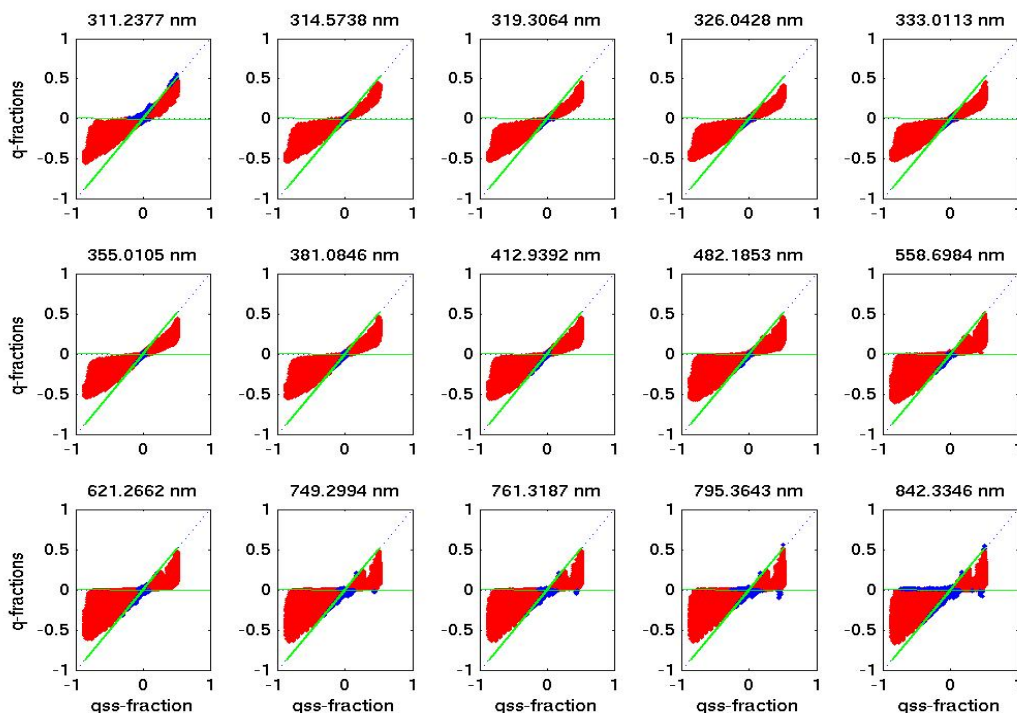


Figure 44: Limiting atmosphere plot for earthshine  $q$ -Stokes fractions and for all PMD bands. The data is derived from one orbit on 31 July 2007.

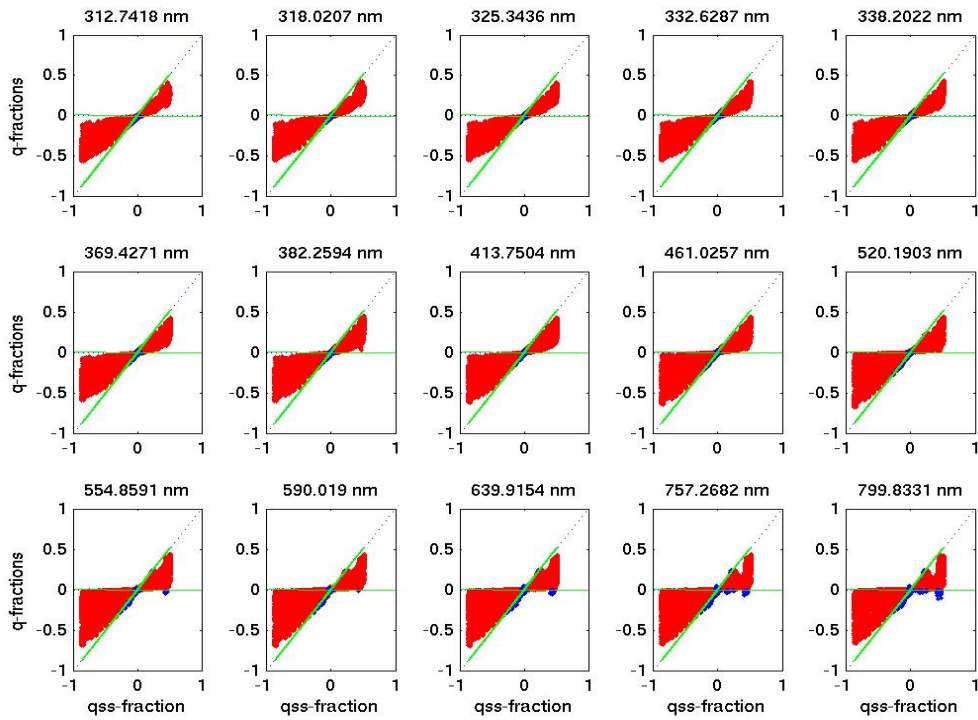


Figure 45: Limiting atmosphere plot for earthshine q-Stokes fractions and for all PMD bands. The data is derived from one orbit on 31 July 2008

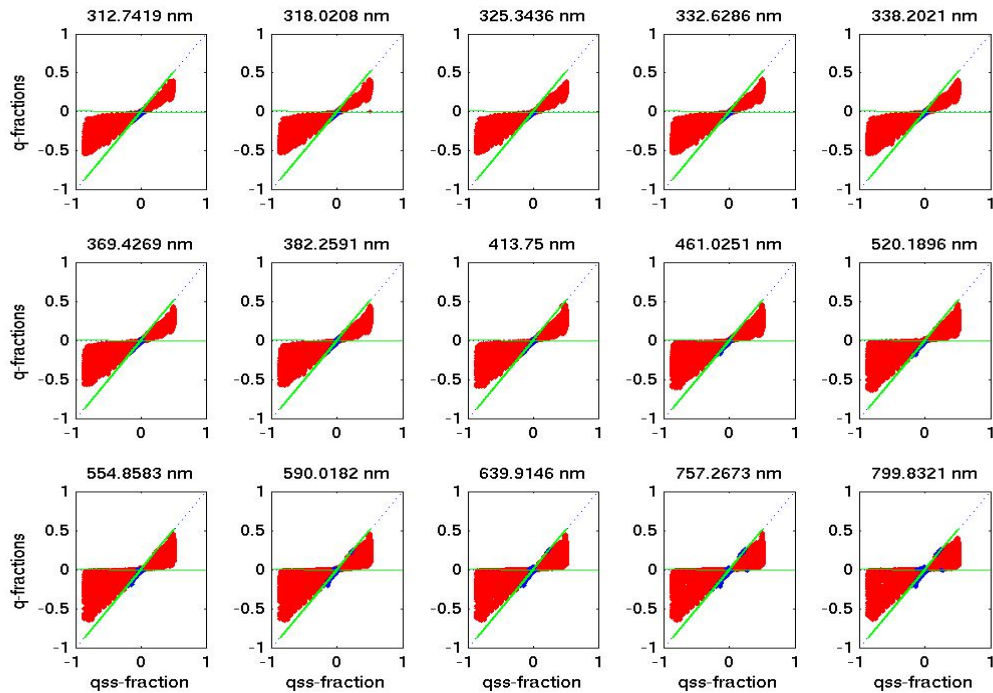


Figure 46: Limiting atmosphere plot for earthshine q-Stokes fractions and for all PMD bands. The data is derived from one orbit on 31 July 2009.

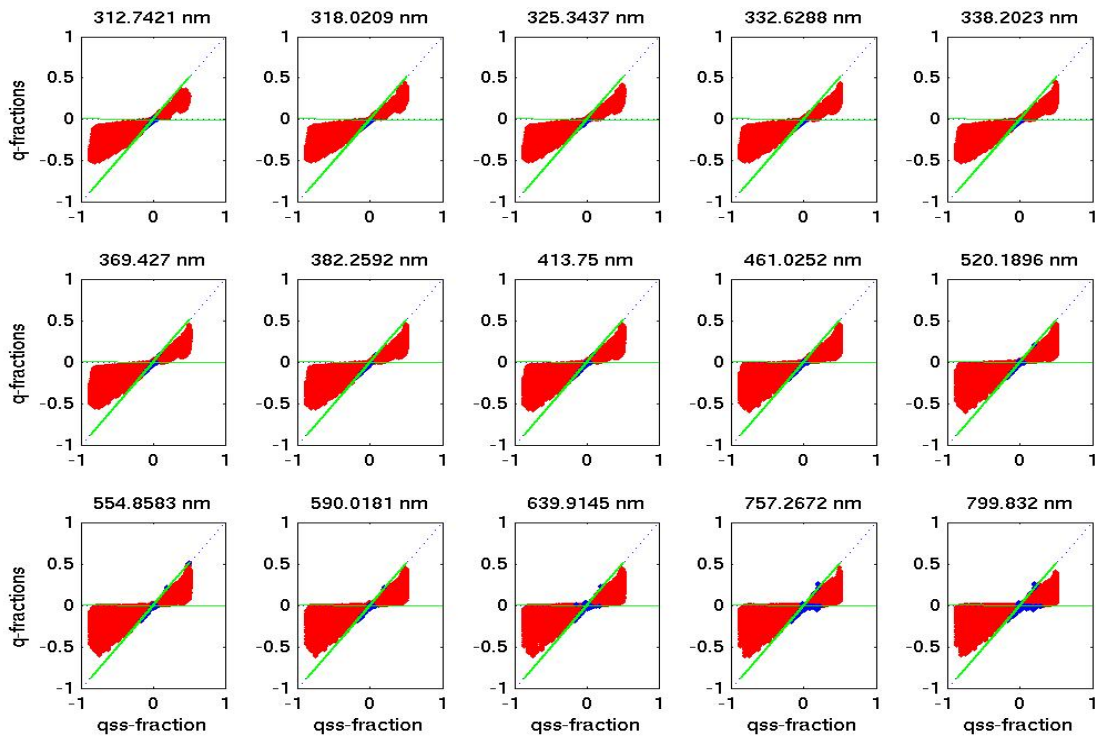


Figure 47: Limiting atmosphere plot for earthshine q-Stokes fractions and for all PMD bands. The data is derived from one orbit on 31 July 2010.

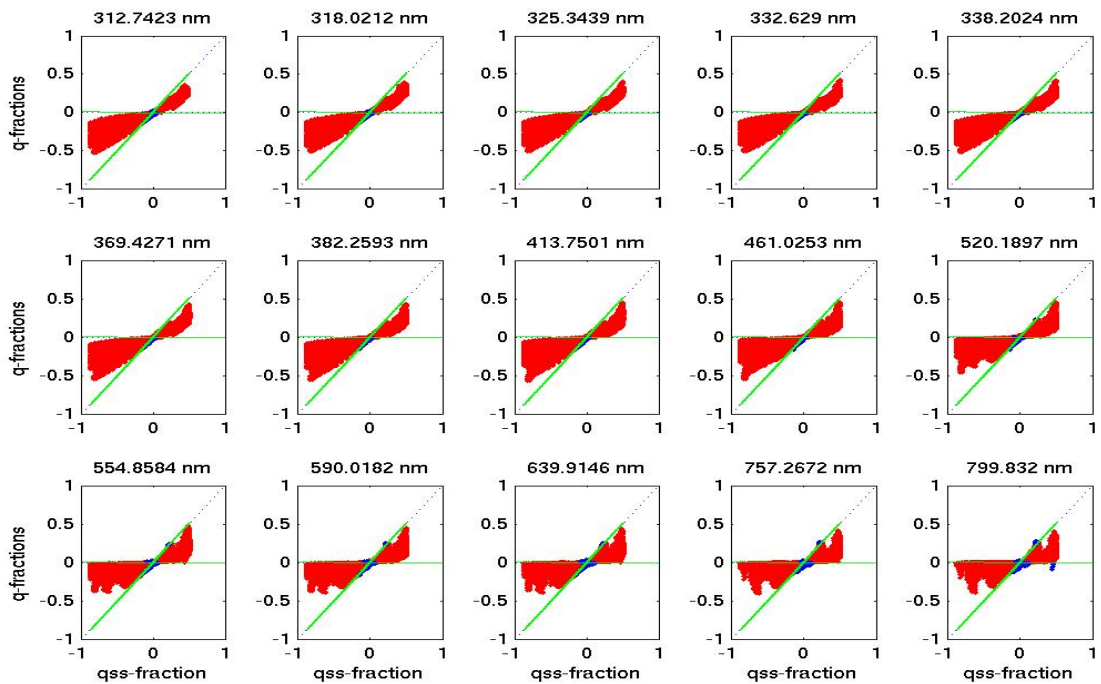


Figure 48: Limiting atmosphere plot for earthshine q-Stokes fractions and for all PMD bands. The data is derived from one orbit on 31 July 2011.

The Limiting Atmosphere plots for q-Stokes fraction values are derived for all PMD band values and for one orbit per year (15 panels in Figure 44 to Figure 48). Note that the results for 31 July 2007 in Figure 44 are results derived before the change of the on-board PMD band settings and all other results are derived for a period thereafter.

### *Analysis*

We can conclude that that quality of Stokes fractions for G2RP-R2 is very stable over the reference period and improves with the introduction of PMD band settings Version 3.1. This is demonstrated for both tests using Stokes fractions for special geometries, as well as examining the “limiting atmosphere” conditions.

## **7.6 Instrument diffuser performance (A2.20, A3.12)**

### *7.6.1 Description*

The optical path from the earthshine port (earthshine observation modes) to the detectors is predominantly similar to the light path followed by the solar irradiance measurements, and the on-board calibration measurements taken once per day, or during the monthly calibration sequence. However, a few additional optical elements do exist in the optical path and before the calibration measurement light path joins the earthshine optical path at the scan mirror (pointing under a specific angle to the calibration unit). Specifically, the solar irradiance reference measurements taken once per day are focused on a solar diffuser (SD) before it passes through the calibration unit (CU) and arrives at the scan-mirror. For a detailed schematic lay-out, see Figure 1. Since for most of the level-2 retrievals the ratio of an actual earthshine measurement  $I$  and the solar reference spectra  $I_0$  (reflectance) is used, it is assumed in any retrieval using reflectancies  $R=I/I_0$  that the influence of the CU and the solar diffuser is calibrated out by the level 0-to-1b processor. The latter is, however, only successful under the assumption that the optical components do not change during the lifetime of the mission.

### *7.6.2 Analysis*

The throughput performance of the solar diffuser is critical for this assumption because of its exposure to direct sunlight. A dedicated monitoring of the diffuser performance is therefore carried out once per month using the on-board spectral line source (SLS). During this measurement sequence, measurements over the diffuser using the SLS are carried out (at long-integration times because of the low light levels received from the diffuser) and compared with the nominal SLS measurements without the diffuser in the path. This ratio is then monitored over the lifetime of the mission.

Unfortunately, while in orbit, the SLS is not stable during one diffuser measurements with integration times as long as 288 seconds ([RD12] and references therein). This has subsequently also been confirmed by retrospective analysis of the on-ground SLS calibration campaign measurements [RD17]. As a consequence, the SLS over-diffuser signals are also not stable from monthly measurement to measurement sequence. The interpretation of the results of the long-term performance of the solar diffuser can therefore only be indicative of the latter’s contribution to the long-term changes observed in the reflectance  $R$ .

### 7.6.3 Interpretation

Figure 49 shows the ratio of SLS over solar diffuser measurements to nominal SLS signals (without diffuser in the light path) normalised to the beginning of the reference period. In case of diffuser degradation, we would expect this ratio to decrease from 1.0. The large scatter, due to the instability of the diffuser measurements, is clearly visible. At wavelength of 290 nm and 335 nm (blue and green curve), an onset of degradation might already be visible, but the trend is not significant due to the large error on the derived ratio values.

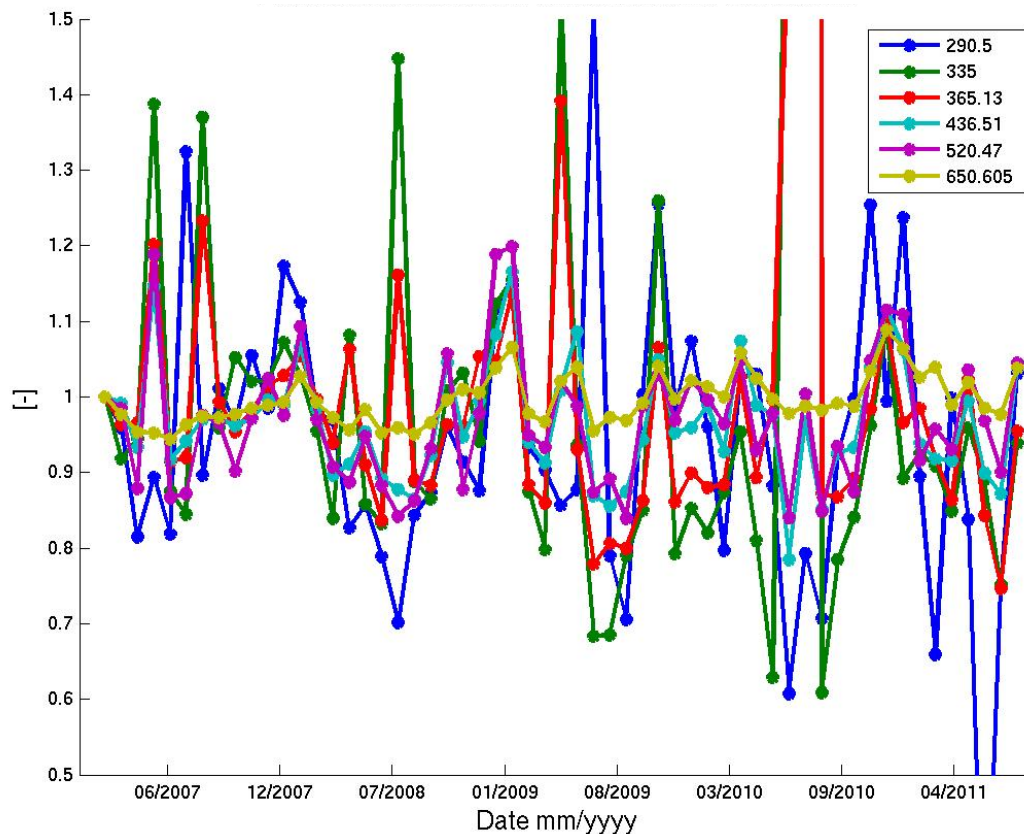


Figure 49: Ratio of SLS over solar diffuser to the nominal SLS signals normalised to the beginning of the reference period. The large variability is due to the unstable SLS signal during long integration times (for diffuser measurements). Different lines show the results for measurements at different wavelength intervals as indicated in the axis definitions.

## **7.7 Level 1B data record consistency and long-term signal variation for sun and earthshine radiances (A3.11, A3.12)**

The long-term consistency of the level-1b dataset is compromised by short, medium, and long-term changes at processor and at instrument level, most notably the instrument throughput. The impact on the consistency of the dataset due to changes in the level 0-to-1 processor quality is essentially removed by the reprocessing activity itself. However, short to long-term changes at instrument level due to instrument anomalies and instrument degradation can only be mitigated by soft-correction which has to be based on evaluation of a consistent dataset. The production of this consistent dataset is the main purpose of this reprocessing activity.

Short to long-term changes in instrument throughput may affect the geophysical parameter retrieval quality predominantly in two ways:

- In a case where the sensitivity (signal-to-noise) limit required for a specific accurate retrieval of geo-physical parameters, is reached.
- In a case where the differences in throughput degradation for different optical paths (in particular the earthshine optical path as compared to the solar optical path) alters the derived reflectivity values.

*Note:* Under hypothetical conditions where the solar path throughput and the earthshine throughput would degrade in exactly the same way, the level-2 retrievals would not be affected by throughput degradation or a changing instrument, except in case one above.

In the following analysis, we first examine the consistency of the solar mean reference dataset and the earthshine dataset individually. Then, we derive from both analyses the long-term differential degradation effect on reflectivity. Note that the main purpose of this validation is to evaluate the level of consistency and accuracy of the dataset including (but not compensating for) the effect of instrument changes. The correction of the latter will be part of a subsequent work on level 1b radiance correction (level 1b-to-1c processing).

### **7.7.1 Solar Measurements**

During nominal operations, a solar measurement sequence is carried out daily. From this sequence, a solar mean reference spectrum is derived for use in level-2 retrievals using reflectivity as input. Since the sun serves as a stable radiometric calibration source, these measurements can be used to monitor the instrument throughput stability. The instrument throughput degradation (defined as the relative change in the calibrated measurement of a stable input source e.g. the sun or WLS, where all components in the optical path can contribute to the degradation) is an important measure of the instrument health and the consistency of the reprocessed data records. It can be defined as the relative change in the calibrated measurement of a stable input source (e.g. the sun or WLS) where all components in the optical path can contribute to the degradation. Apart from instrument-related features, we expect to see no impact of processor or calibration-related features in the G2RP-R2 solar mean reference (SMR) spectrum time series. Figure 50 provides an overview of the SMR time series at all wavelengths for the main channels.

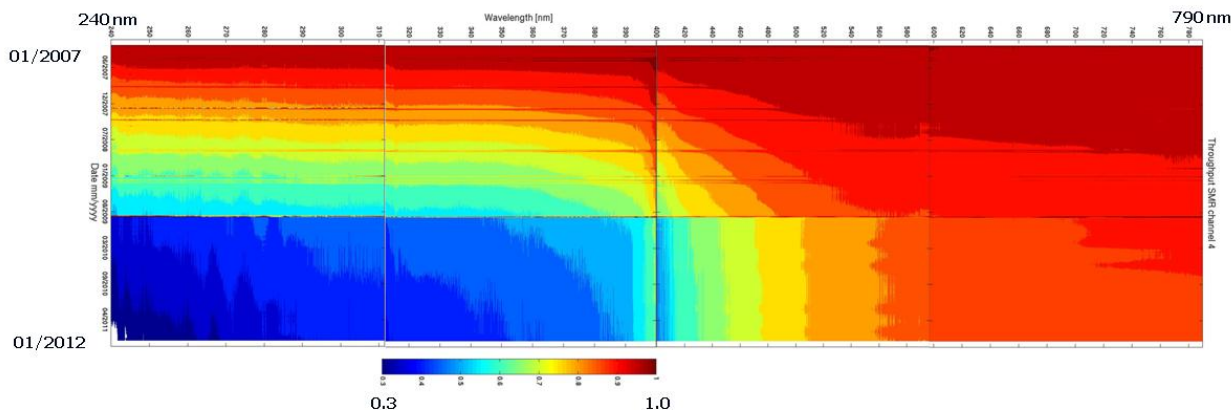


Figure 50: SMR spectra for all four main channels, for the whole reference period and normalised to January 2007.

Figure 51 shows the same criteria, but for PMD-P and PMD-S channels. For convenience, Figure 52 shows the same as Figure 51 for the main channels, but focuses on the ratio of the spectra with respect to January 2007 at three different points in time: before and after the second throughput test in September 2009, and at the end of the reference period in July 2011.

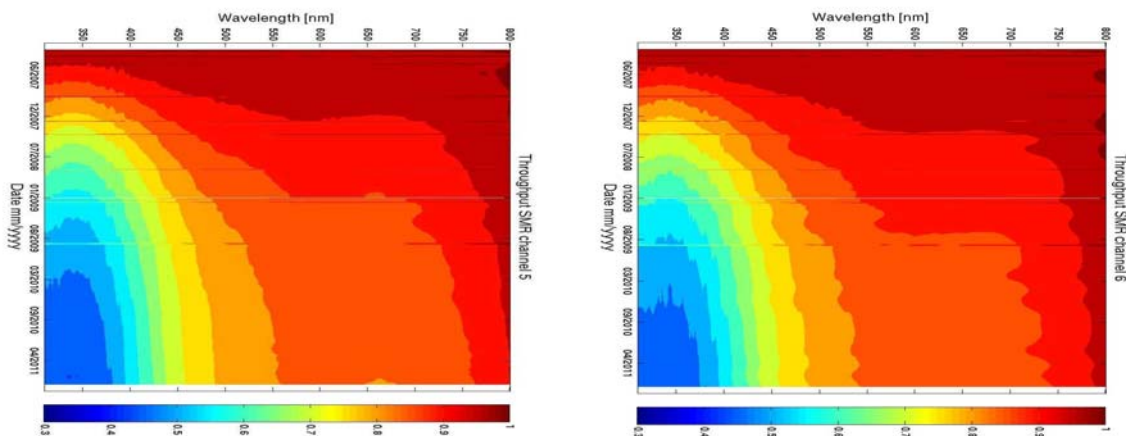


Figure 51: SMR spectra for the PMD-P (left panel) and the PMD-S channels, for the entire reference period and normalised to January 2007.

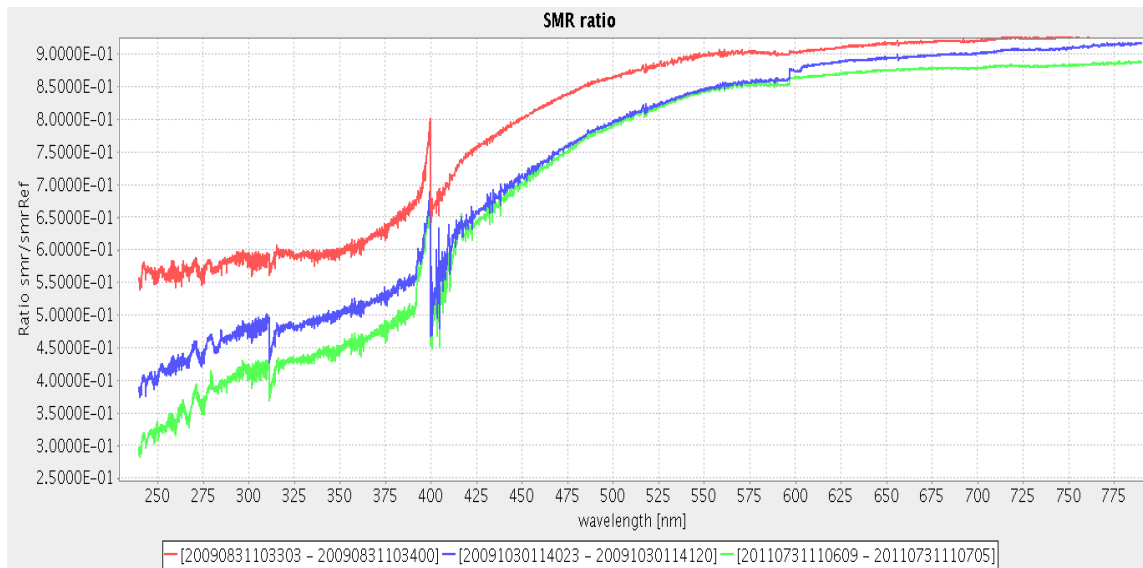


Figure 52: Solar mean reference (SMR) spectra for all four main channels normalised to January 2007. The red and the blue curve are ratios before and after the second throughput test in September 2009, respectively. The green curve is the ratio on 31 July 2011

An important quantity is the ratio of PMD-S to PMD-P, since this ratio is used in the derivation of Stokes fractions (using earthshine measurements) and therefore impacts on the accuracy of the polarisation correction of main channel data or level-2 retrievals using Stokes fractions as science data (like for aerosol properties retrievals) directly (see also Section 7.5). Since the sun is unpolarised, this ratio, in principle, should be 1.0 and should not change over the lifetime of the mission provided that both channels degraded or changed in exactly the same way. The 3D time series of the solar PMD-S to PMD-P ratio as shown in Figure 53, therefore, a measure as to what extent deficiencies in the on-ground calibration and the differential degradation or in changes between the channels need to be accounted for both in-flight and in-time to provide accurate Stokes fractions. For the reprocessed dataset, as before, the observed variation in this time series is expected to be only instrument related.

### 7.7.2 Solar Measurements for PMD and main channels at individual wavelength

Before the second throughput test in September 2009 (see Section 5.2), both PMD channels were degrading differently than the main channel signals (larger degradation initially but an earlier onset of levelling off); however, after the throughput test the degradation rate is broadly similar for both PMD and main channels. This is apparent when comparing the reprocessed normalised PMD and main channel signals at various wavelength over the full spectrum as shown in Figure 54 through Figure 60. Note that in Channels 1 and 2, the degradation rate is still not zero but close to what is expected as the contribution of the degradation of the scan-mirror. The scan mirror is known to degrade (especially in the UV) during an extended time period (at least seven years) until the process might be reversed due to effects of “hole-filling” by deposits on the mirror. In contrast, the degradation rate in Channel 3 is now close to zero after the second throughput test and continues relatively unaffected by the test in channel 4 (with first signs of levelling off), where the impact of degradation on the signals, however, has been quite small.

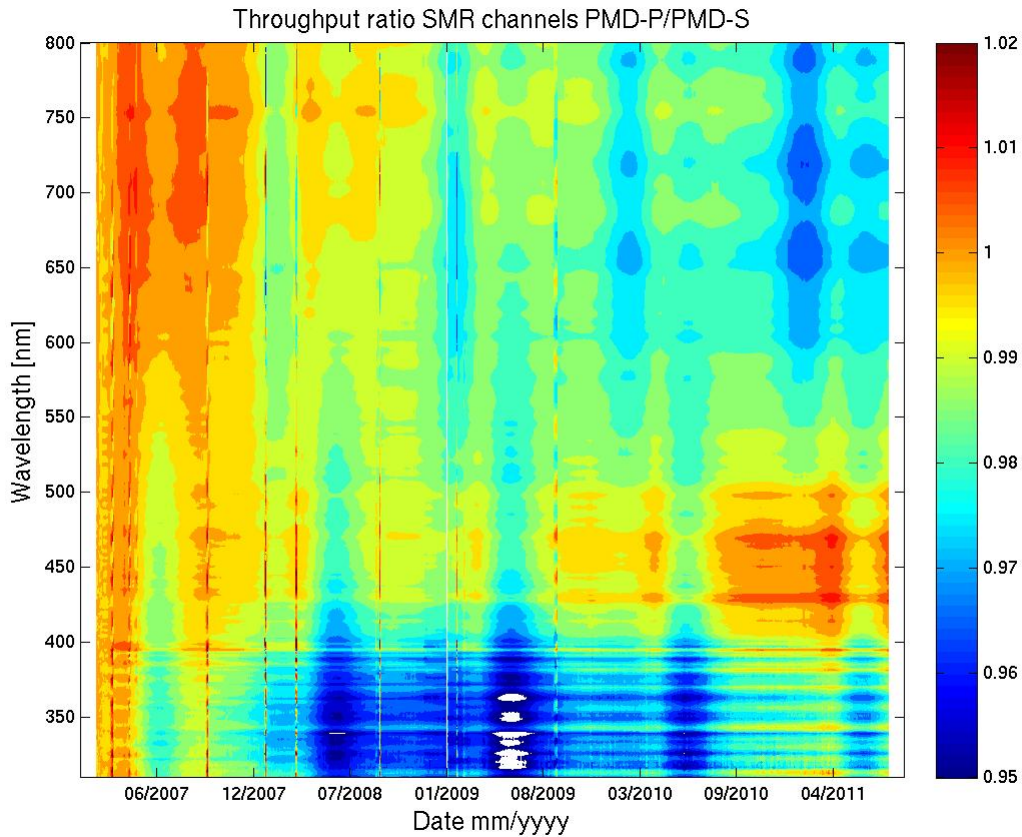


Figure 53: Solar mean reference (SMR) spectra for the PMD-P to S ratio, for the whole reference period and normalised to January 2007.

The difference between the degradation of SMR main and PMD channels (ratio) is important for the impact of degradation on the quality of the polarisation correction of main channel data. Due to this differential degradation, and in order to account for the effect of the PMD-P to PMD-S variations in time, an online Stokes fraction correction has been introduced which corrects for this effect along with the systematic deficiencies of instrument key-data (see also Section 7.5). This on-line correction is the first correction addressing instrument degradation implemented in the level 0-to-1 processing, but focuses only on long-term Stokes fraction degradation. This is then to be complemented by correcting the calibrated main channel radiances in a level 1B-to-C correction step (see Section 1.1).

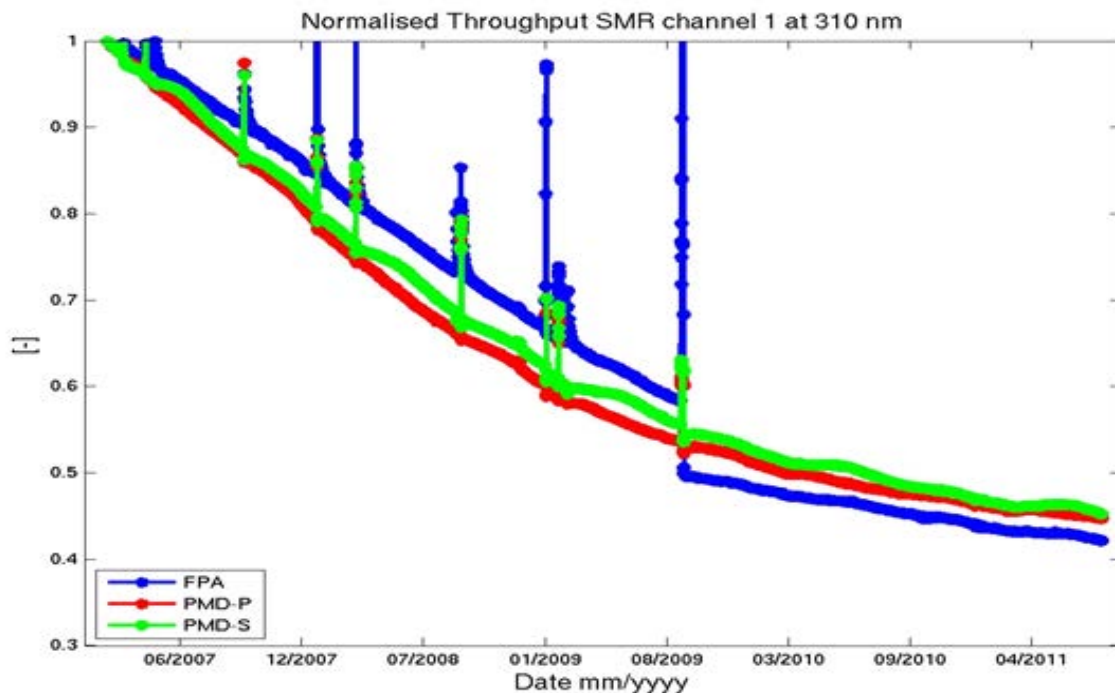


Figure 54: SMR signals normalised to February 2007 at 310 nm in channel 1 for both main channel (blue curve) and PMD-P and PMD-S signals (red and green curve)

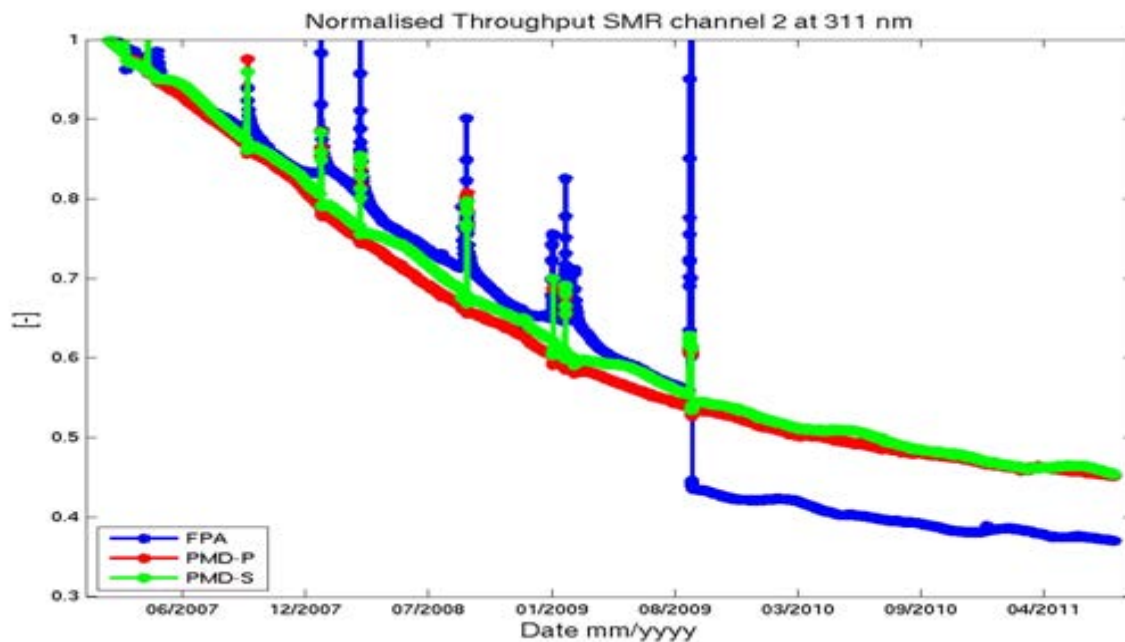


Figure 55: SMR signals normalised to February 2007 at 311 nm in Channel 2 for both main channel (blue curve) and PMD-P and PMD-S signals (red and green curve)

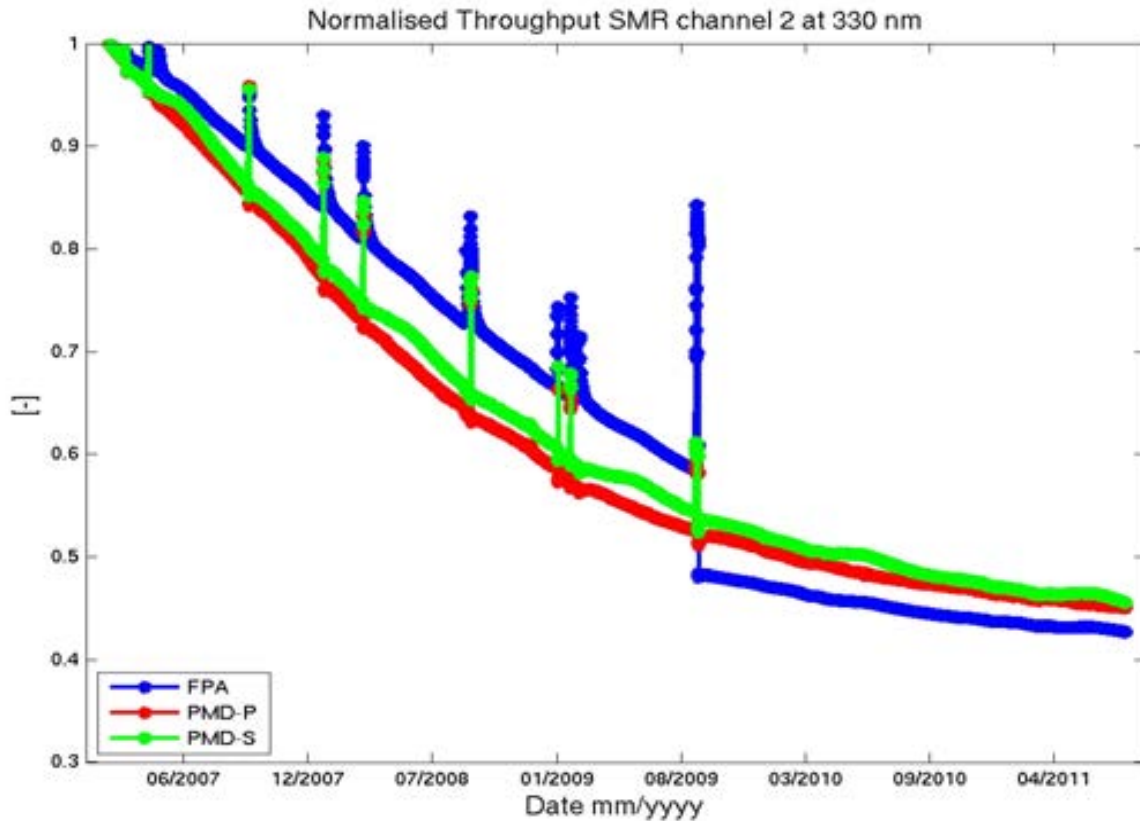


Figure 56: SMR signals normalised to February 2007 at 330 nm in channel 2 for both main channel (blue curve) and PMD-P and PMD-S signals (red and green curve)

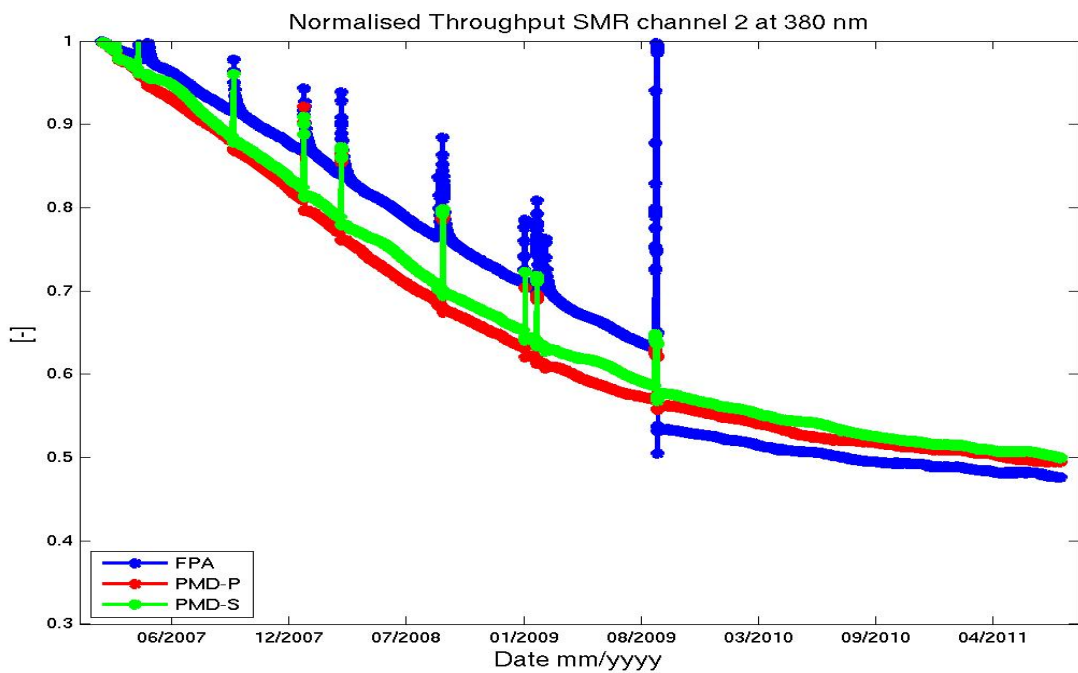


Figure 57: SMR signals normalised to February 2007 at 380 nm in channel 2 for both main channel (blue curve) and PMD-P and PMD-S signals (red and green curve)

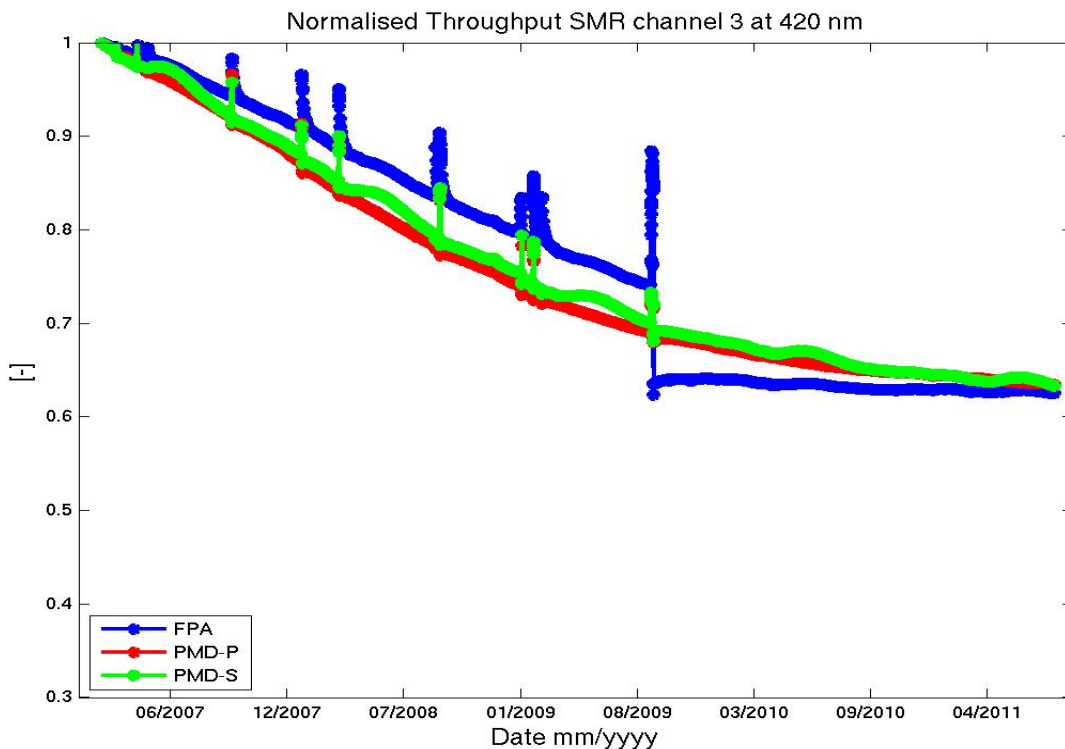


Figure 58: SMR signals normalised to February 2007 at 420 nm in channel 3 for both main channel (blue curve) and PMD-P and PMD-S signals (red and green curve)

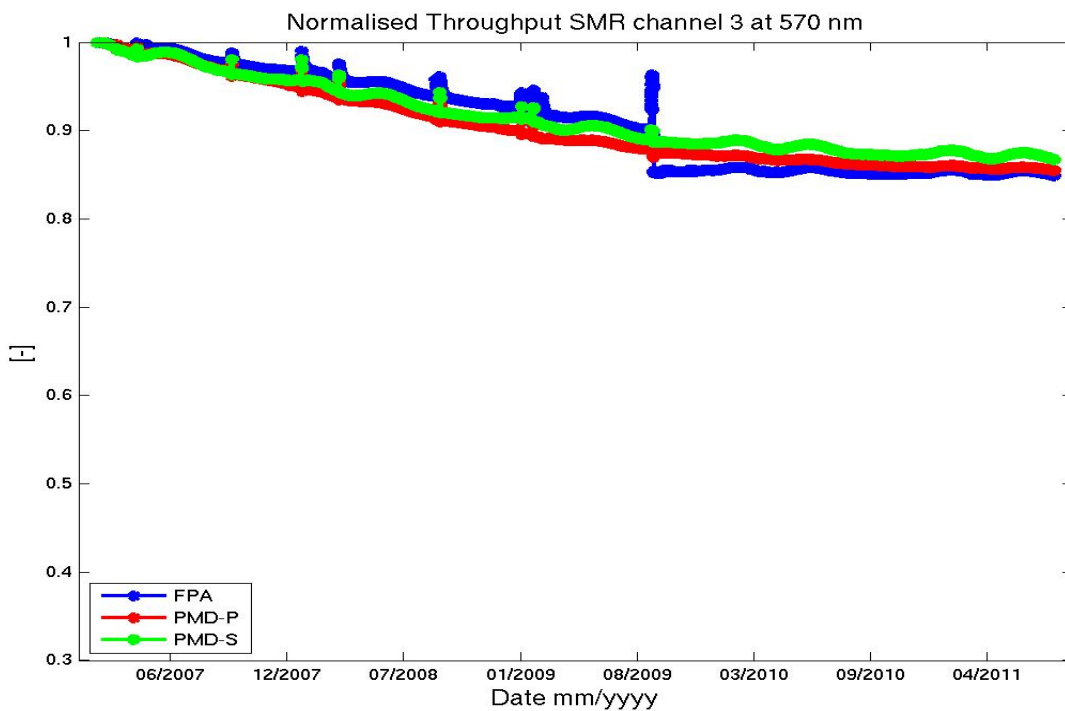


Figure 59: SMR signals normalised to February 2007 at 570 nm in channel 3 for both main channel (blue curve) and PMD-P and PMD-S signals (red and green curve)

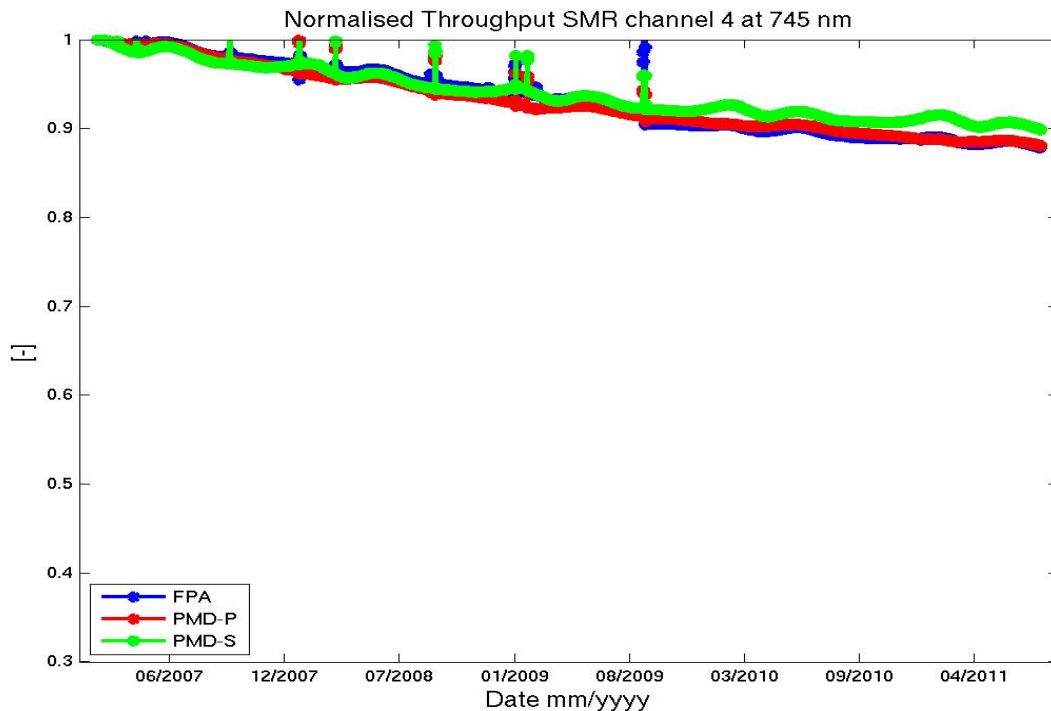


Figure 60: SMR signals normalised to February 2007 at 745 nm in channel 4 for both main channel (blue curve) and PMD-P and PMD-S signals (red and green curve)

### 7.7.3 Earthshine long-term degradation

Because the solar light path and the light path of the earthshine measurements are not exactly the same, one cannot just assume that the impact on degradation, changes in calibration, and processor changes are the same for both signals. The solar light path through the instrument is different by its way from the solar port through the calibration unit involves the diffuser (see Section 7.6) until reaching the scan mirror. Also, the incident angle on the scan mirror—having different effects on the measured radiances depending on residual polarisation from the calibration unit (solar path) or the state of the polarisation of earthshine data needs to be considered (see Figure 1). Whereas the incident angle on the scan mirror is fixed for the solar measurements, it varies from -45 to +45 degrees scanning from east to west for earthshine measurements. Scan position number 16 at +18.5 degrees for the earthshine data is therefore comparable with the scan-mirror incident angle for the SMR measurements and will, therefore, play a more pronounced role in what follows. It is expected that there are differences observed in the rate of degradation for various earthshine viewing angles.

#### 7.7.3.1 Consideration on reflectivity degradation

If we assume zero degradation of the calibration unit and the diffuser, the solar path signals and the earthshine signals should degrade in exactly the same way for scanner angle +18.5 degrees. In this case, the degradation of the most important quantity for level 2 products, reflectivity (i.e. the ratio of earthshine to sunshine data), is zero. However, since it is expected that there is an increasing scan mirror-induced difference in degradation towards the UV, there is a residual “differential degradation” in reflectivity expected depending on the scan-mirror position.

### 7.7.3.2 *Results for earthshine degradation for G2RP-R2*

The monitoring of long-term earthshine signals is complicated by the large amount of data to be processed, but even more so by the influence of a constantly-changing atmosphere, as well as constantly-changing surface properties. Both of these can be expected to change with the season as well as, potentially, from year to year. For the routine monitoring of earthshine data (both NRT and reprocessed), we therefore evaluate the data only from measurements over certain regions which are known to provide relatively stable conditions during the year and from year to year in order to minimize the effect of seasonality, pollution events and climatological changes. Figure 61 shows some “stable” target regions of choice. From these regions, we will focus on the Sahara, this being the most stable target with least interference of clouds, i.e. best statistics, only under cloud-free conditions.

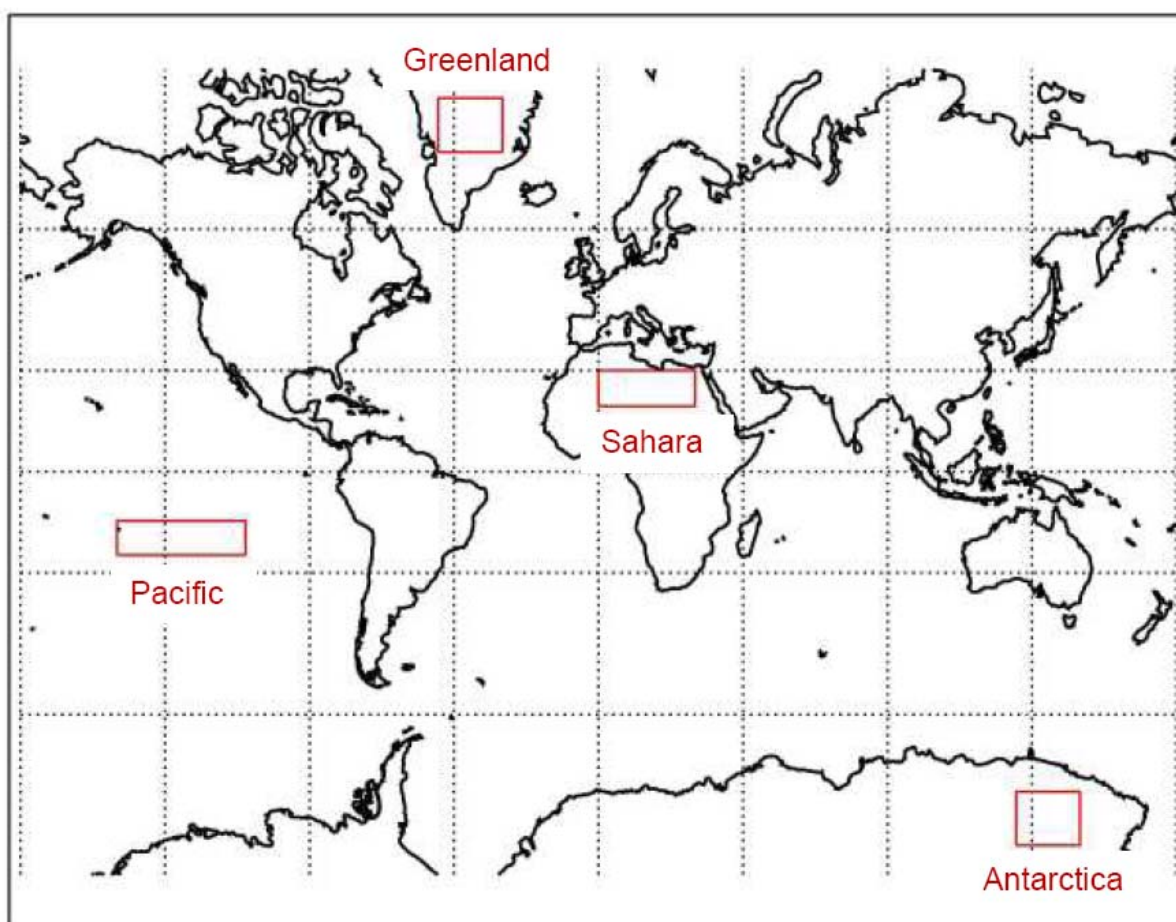


Figure 61: “Stable” target areas used for the routine NRT monitoring as well as the evaluation of reprocessed earthshine data. For the evaluation of G2RP-R2 we consider only the Sahara area, which provides the most stable situation and best statistics (most clear-sky cases).

Below, Figure 62 shows the normalised earthshine signals for every second scanner position (coloured lines) at 310 nm for Channel 1. Overlaid for reference is the normalised solar mean measurement reference signal with a comparable incident angle on the scan-mirror for scanner position number 16 of the forward scan part. Due to the influence of the seasonal cycle, all time series (including the solar-mean reference time series) are normalised to the mean of the year 2007 (instead of the mean of February 2007, as before). This is important since the observed degradation signal is very sensitive to the normalisation point. Even though we are artificially lowering the reference point here (since the continuous degradation was already very strong during the year 2007) for the purpose of evaluating the overall reflectivity degradation, we are interested only in the relative changes in time. The absolute difference in throughput degradation between launch and the mean of January 2007 is not taken into account and needs to be evaluated in a separate study involving instrument key-data accuracy. Since changing day-to-day atmospheric conditions introduce a significant amount of variations, we provide smoothed curves instead in Figure 63 to Figure 69 and for various wavelengths. The smoothing is kept very moderate by applying a 3-days running mean.

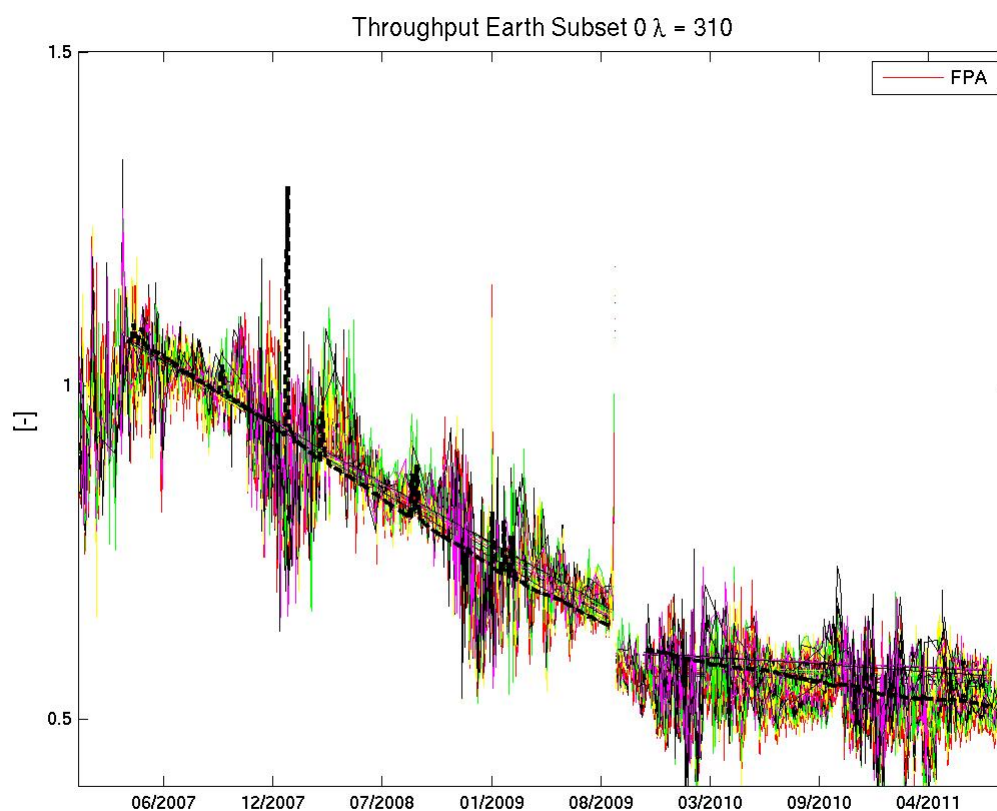


Figure 62: Earthshine signals normalised to the mean of 2007 at 310 nm in Channel 1 and for every second scanner position (coloured curves). The SMR normalised signal, a dashed black line, is provided as a reference.

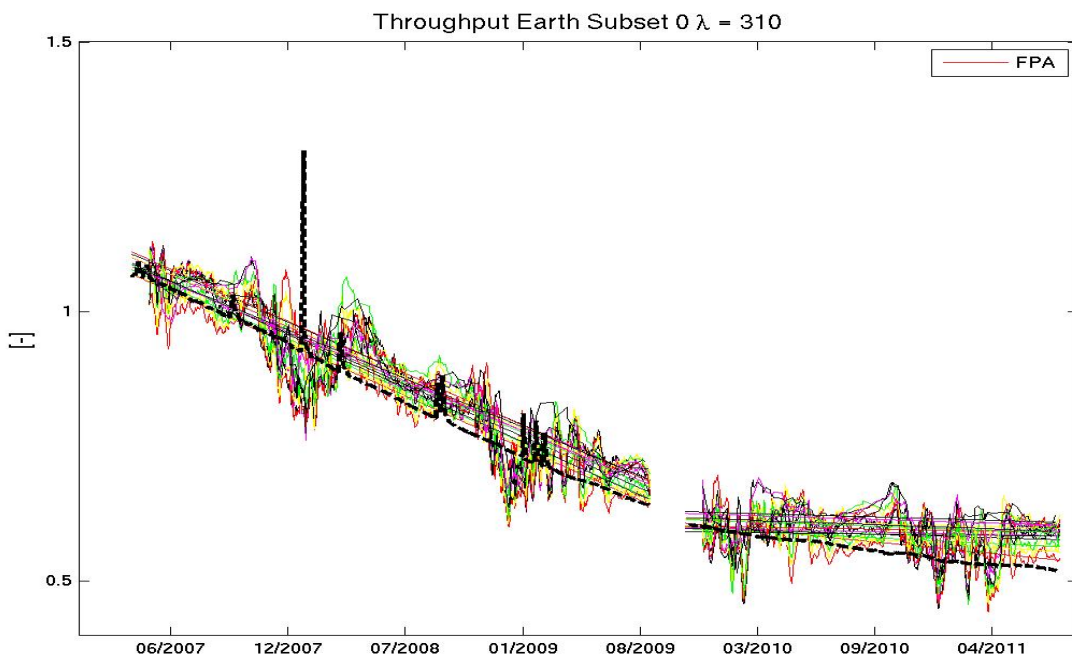


Figure 63: Earthshine signals normalised to the mean of 2007 at 310 nm in Channel 1 and for every second scanner position (coloured curves). The SMR normalised signal, a dashed black line, is provided as a reference. A 3-day moving average is applied for smoothing.

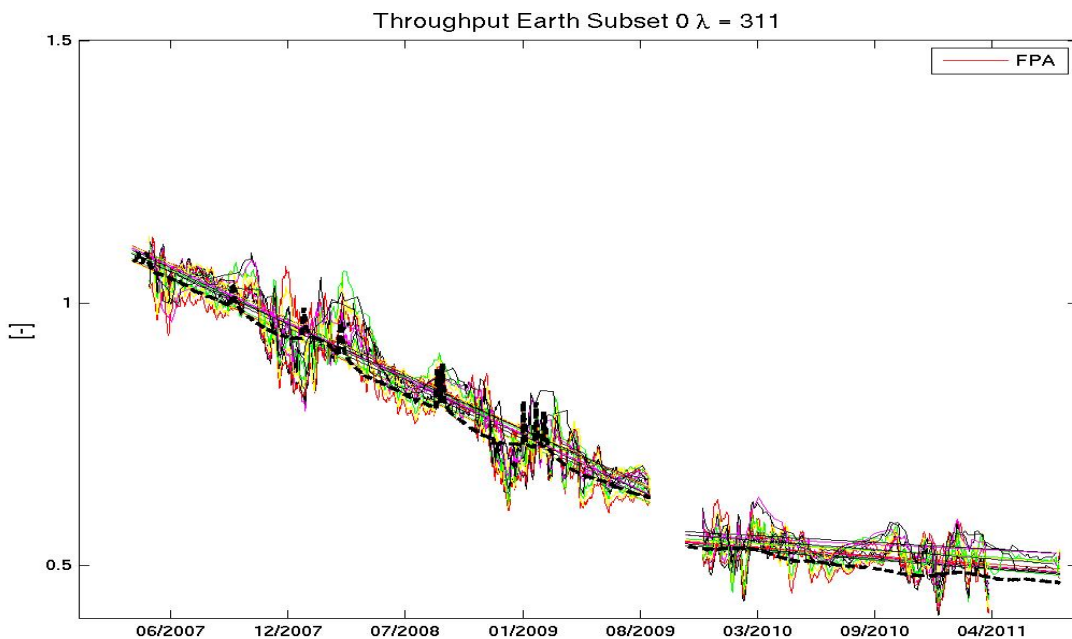


Figure 64: Temporally smoothed earthshine signals normalised to the mean of 2007 at 311 nm in Channel 2 and for every second scanner position (coloured curves). The SMR normalised signal, a dashed black line, is provided as a reference.

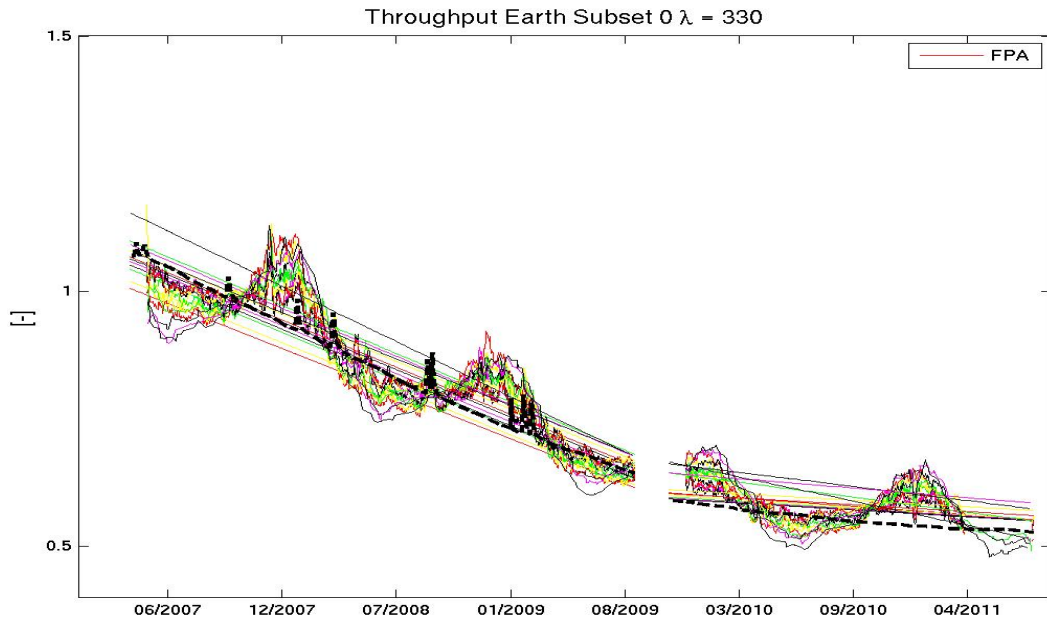


Figure 65: Temporally smoothed earthshine signals normalised to the mean of 2007 at 330 nm in Channel 2 and for every second scanner position (coloured curves). The SMR normalised signal, a dashed black line, is provided as a reference.

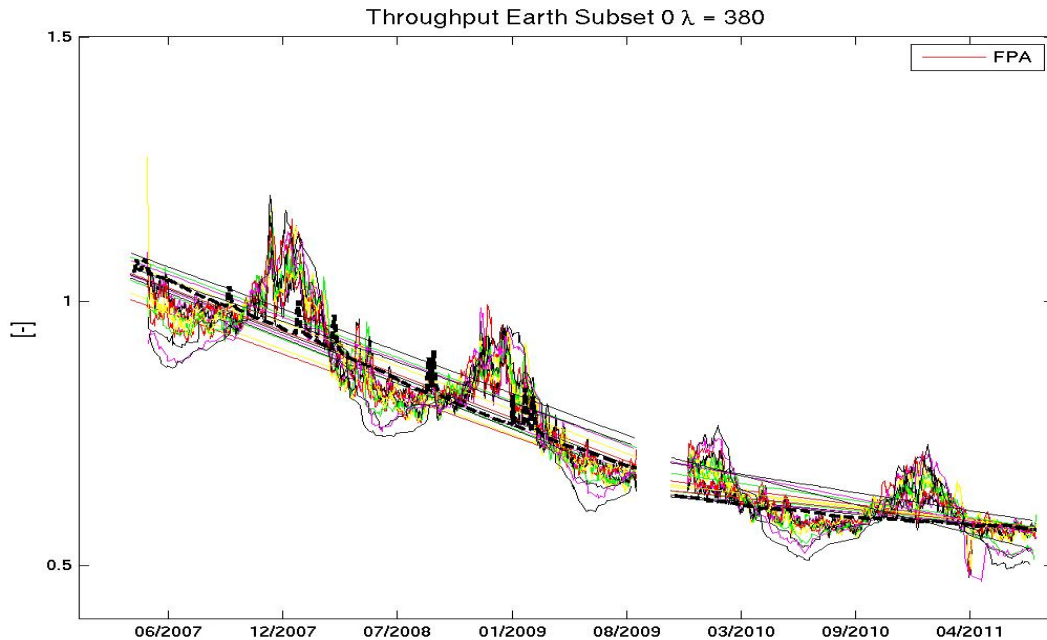


Figure 66: Temporally smoothed earthshine signals normalised to the mean of 2007 at 380 nm in Channel 2 and for every second scanner position (coloured curves). The SMR normalised signal, a dashed black line, is provided as a reference.

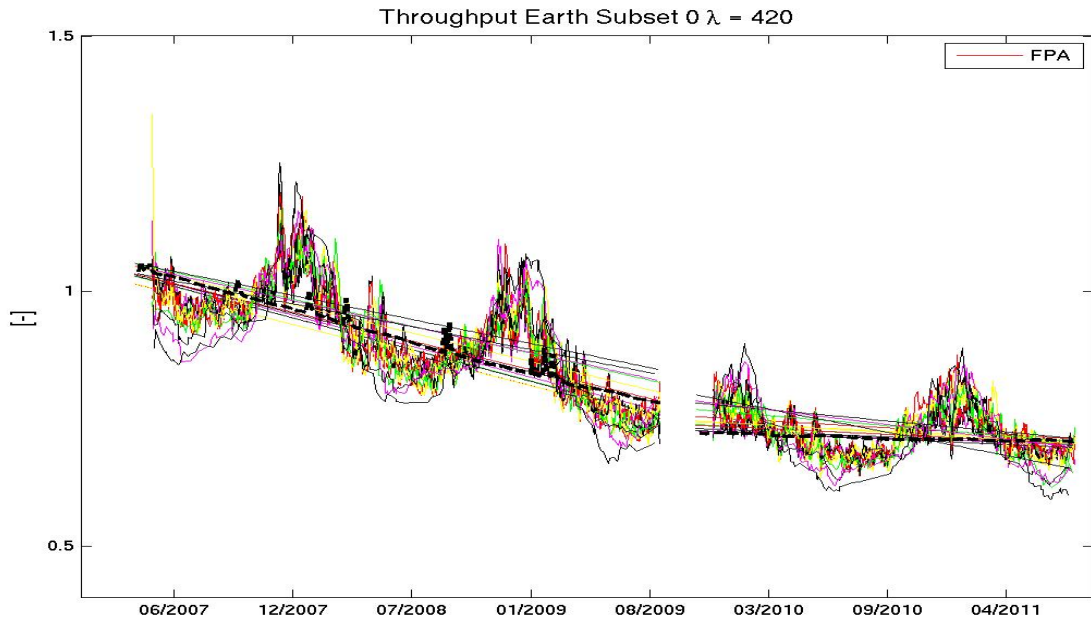


Figure 67: Temporally-smoothed earthshine signals normalised to the mean of 2007 at 420 nm in Channel 3 and for every second scanner position (coloured curves). The SMR normalised signal, a dashed black line, is provided as a reference.

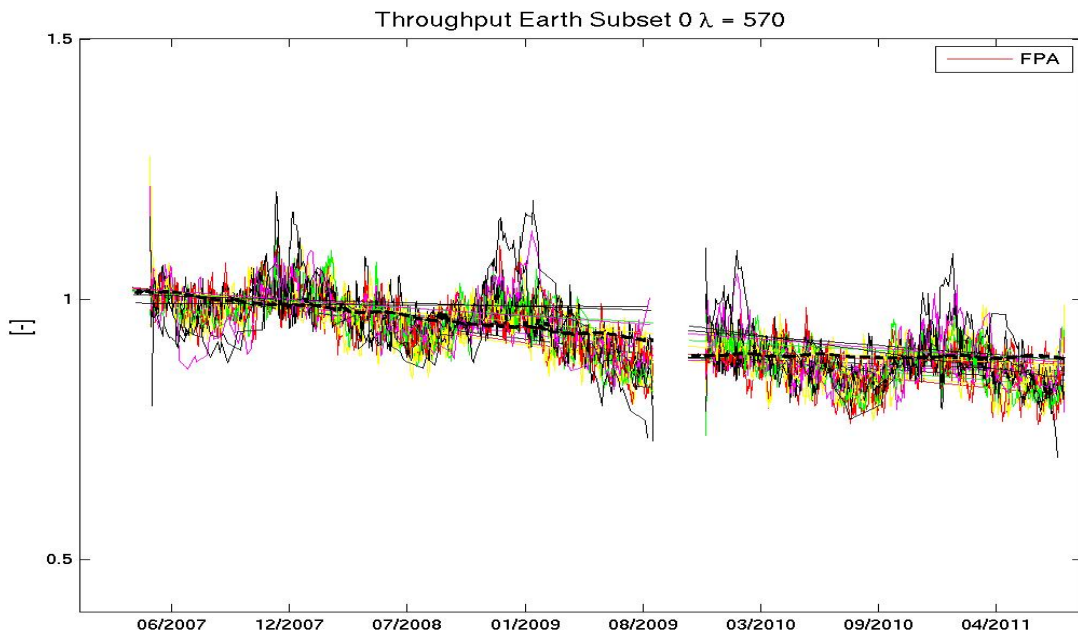


Figure 68: Temporally smoothed earthshine signals normalised to the mean of 2007 at 570 nm in Channel 3 and for every second scanner position (coloured curves). The SMR normalised signal, a dashed black line, is provided as a reference.

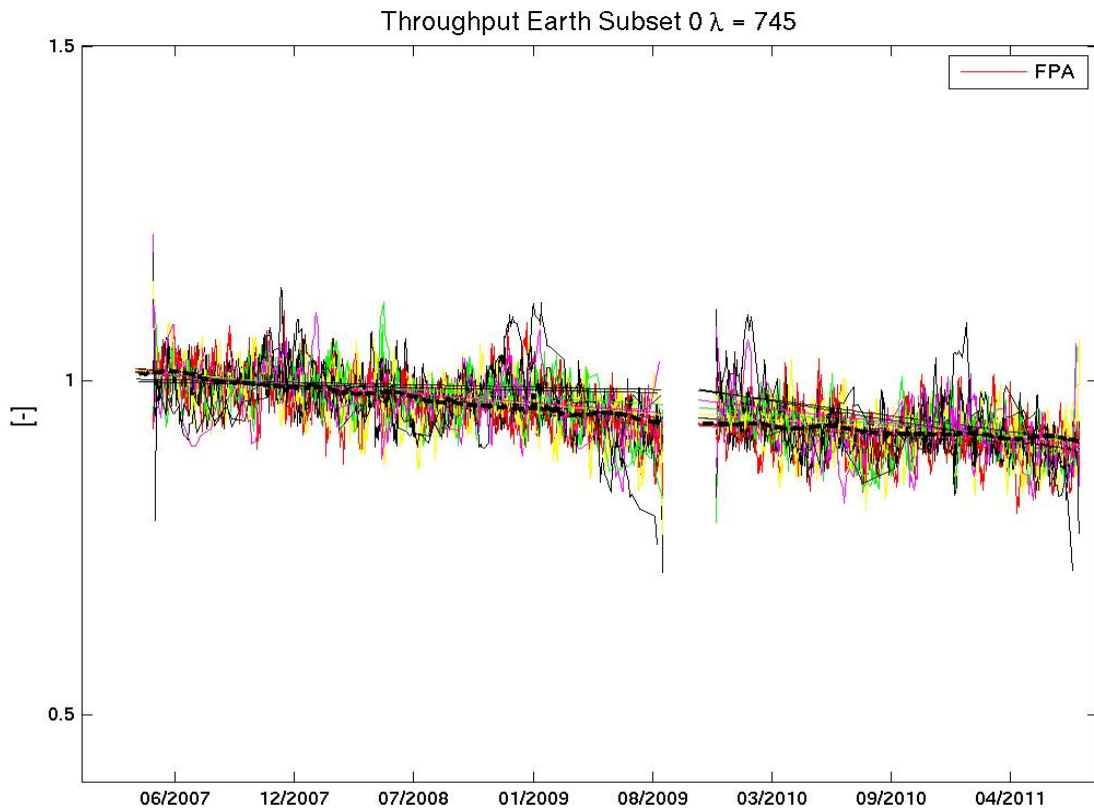


Figure 69: Temporally smoothed earthshine signals normalised to the mean of 2007 at 745 nm in Channel 4 and for every second scanner position (coloured curves). The SMR normalised signal, a dashed black line, is provided as a reference.

The impact of the seasonal cycle is most pronounced in spectral regions dominated by single-scattering in the mid-to-lower troposphere. It is less noticeable in wavelengths observing the higher troposphere or lower stratosphere or in signals dominated by the surface, as, for example, at 745 nm in Figure 69 above.

Figure 70 to Figure 72 show the earthshine signal degradation (in percentage) over the period before the second throughput test (Period 1: January 2007 to September 2009) and after the test (Period 2: September 2009 to January 2012). Degradation rates are evaluated at every second scan-angle position using a linear robust-fit (giving less weight to outliers). The error is evaluated as the  $2\sigma$  error of the fit and relies therefore only the measurement statistics and does not include any systematic effects. Especially for the period before the second throughput test, we do not expect that the signals are degrading linearly over the whole period (see Section 7.7.1 on the degradation of SMR signals). However, the “real” degradation is not a simple function of second or higher (or exponential order) and using different orders or functional dependencies will potentially increase systematic errors introduced considering the large degrees of freedom due to seasonal and other atmospheric and surface signals not removed. The derived earthshine signal degradation rates can therefore be only indicative of the real (functional) dependence of the observed degradation rates and we need to leave it to the post-reprocessing exercise of deriving a 3D degradation matrix for GOME-2 / Metop-A (see Section 1.1 on the purpose and scope of the G2RP-R2 campaign) in order to evaluate these rates per wavelength in greater detail and with higher accuracy.

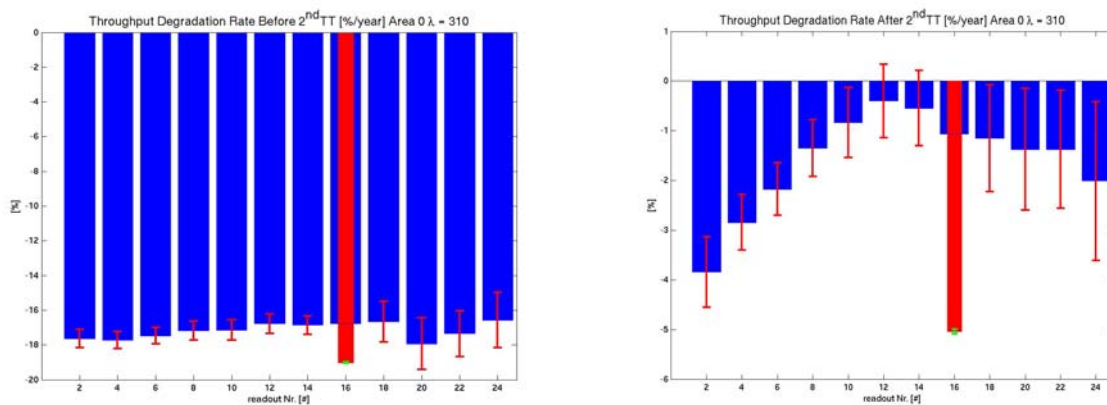
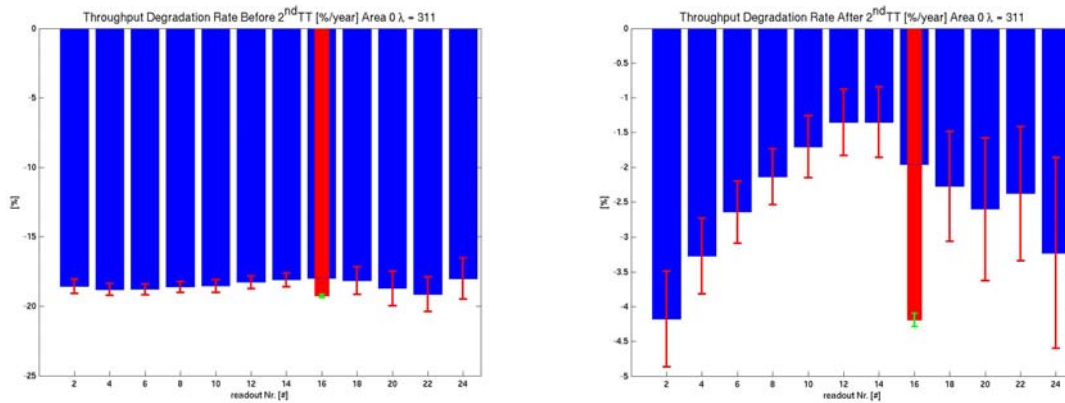
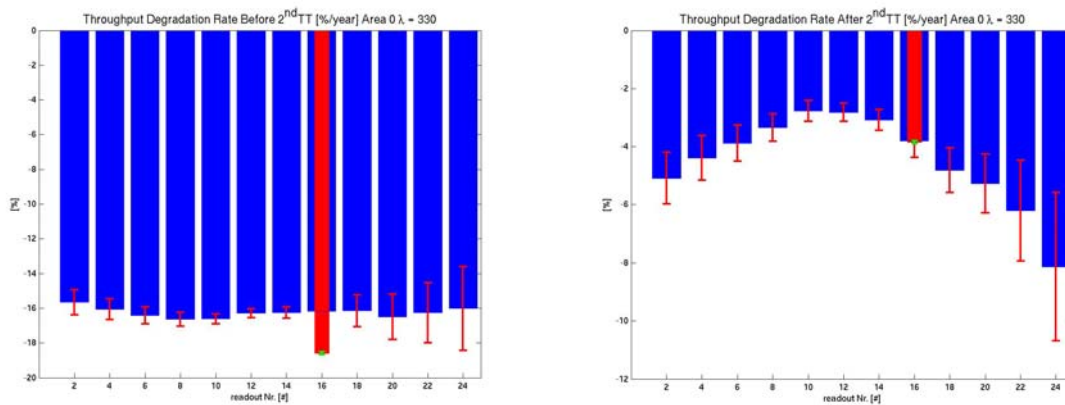


Figure 70: Earthshine signal degradation rate per year for the period before the second throughput test (left panel) and after the throughput test (right panel) at 310 nm (channel 1). The plots also show the corresponding degradation rate of SMR at scanner position 16. See text for detailed explanation.

### 311 nm (Channel 2)



### 330 nm (Channel 2)



### 380 nm (Channel 2)

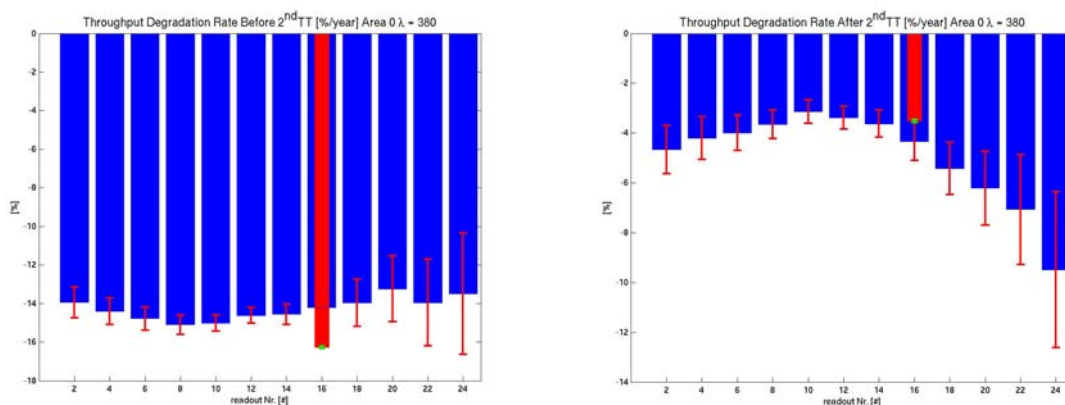
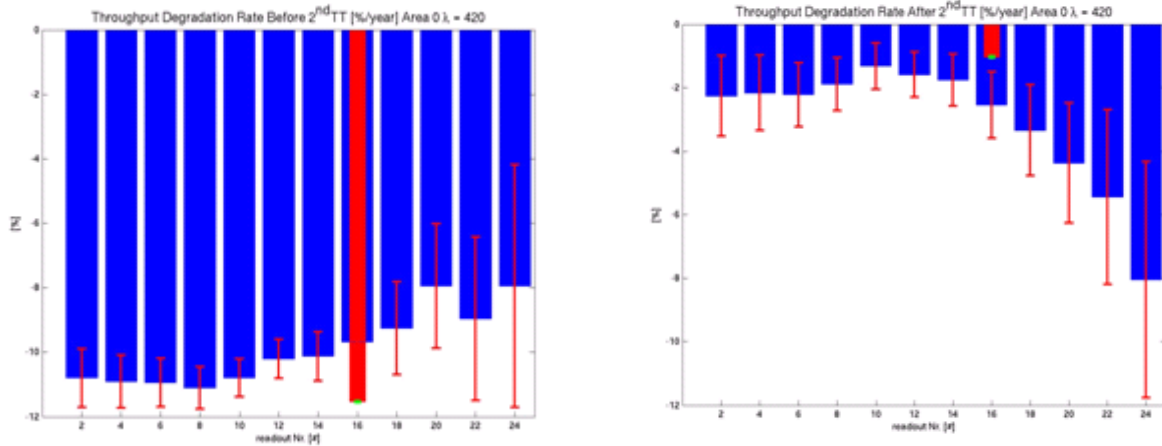
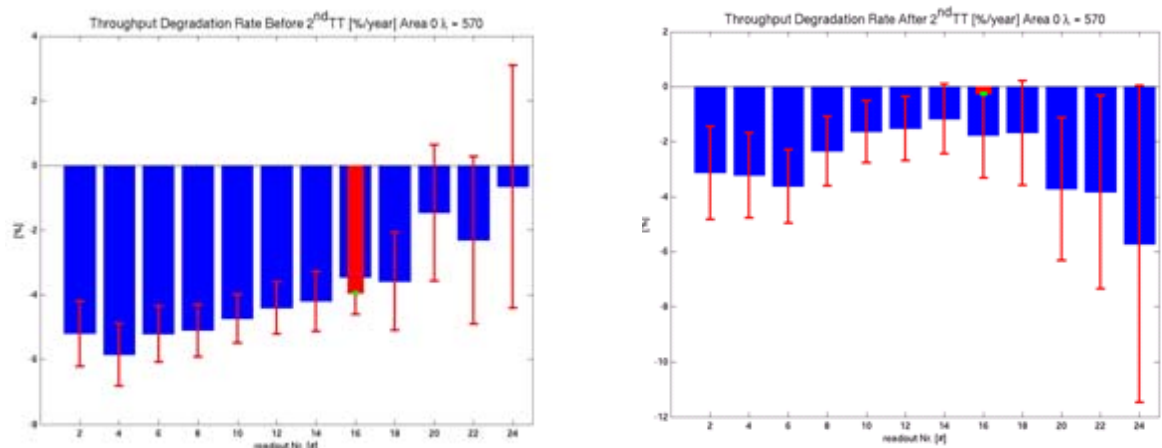


Figure 71: Earthshine signal degradation rate per year for the period before the second throughput test (left panel) and after the throughput test (right panel) at 311, 330, and 380 nm (channel 2). The plots also show the corresponding degradation rate of SMR at scanner position 16. See text for detailed explanation.

420 nm (Channel 3)



570 nm (Channel 3)



745 nm (Channel 4)

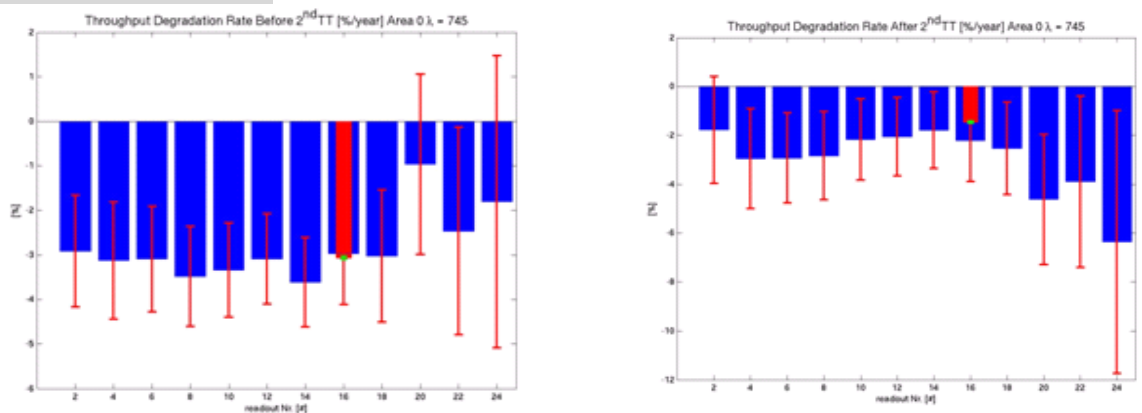


Figure 72: Earthshine signal degradation rate per year for the period before the second throughput test (left panel) and after the throughput test (right panel) at 420 and 570 nm (Channel 3) and 745 nm (Channel 4). The plots also show the corresponding degradation rate of SMR at scanner position 16. See text for detailed explanation.

The scan-angle related differences in the degradation rate of the signal are also different before and after the throughput test. Before the test, it is on the order of 1-2 %, whereas after the test, the differences are more on the order of 2-4% (note the different y-axis scales). The figures also indicate the degradation rates of the solar reference mean signal (red bar) at the corresponding scanner angle position (read-out 16; see before). Any difference between the SMR degradation rate and any of the earthshine degradation rates will consequently lead to a non-zero degradation rate in reflectivity as will be discussed in the next section.

#### 7.7.4 Results for reflectivity degradation from G2RP-R2

Before the second throughput test in September 2009 and for all observed wavelengths, the SMR had been degrading in, broadly speaking, the same way as the earthshine path for G2RP-R2, with some variation for different scanner angles. After the test, we observe some substantial differential degradation at 310 nm (Channel 1), which we expect to see in an increase in the reflectivity degradation rate from before to after the throughput test. Generally speaking, the trending analysis of earthshine monitoring data suggests larger signatures of differential degradation (and therefore larger degradation in reflectivity) for the period after the second throughput test, despite significantly lower degradation rates of the individual earthshine and sunshine measurement time-series.

Figure 73 to Figure 74 show the reflectivity degradation in percentage over the period before the second throughput test (Period 1) and after the test (Period 2). Degradation rates have been evaluated in the same way as for the earthshine signal degradation in the previous section at every second scan-angle position. Note that for zero differential degradation of the earthshine signal and the solar signal the reflectivity degradation at position 16 should be also zero (see previous section), whereas for the other positions different degradation patterns introduced by different light incident angle position on the scan mirror then provide a dominant contribution to the observed reflectivity degradation rate. Non-zero reflectivity degradation rates at position 16, in contrast, indicate a differential degradation contribution from the solar measurement path, which, in addition to the earthshine path, includes the calibration unit and/or the diffuser (see Figure 3).

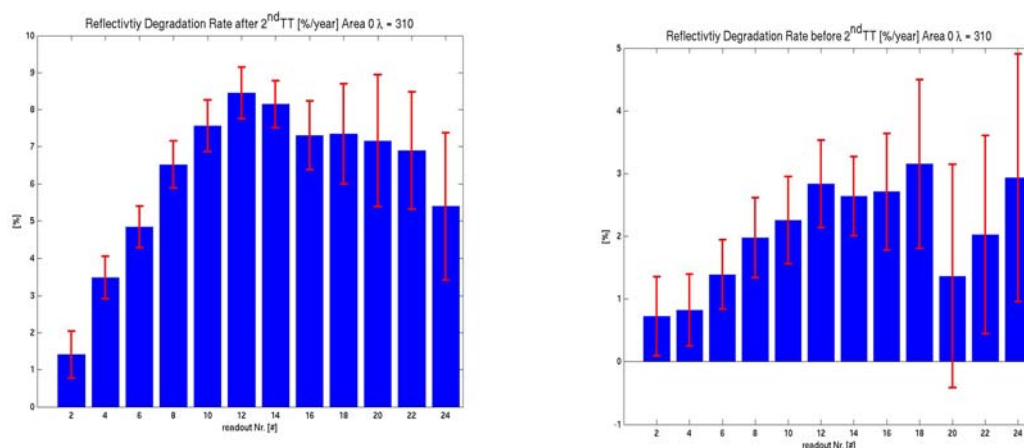
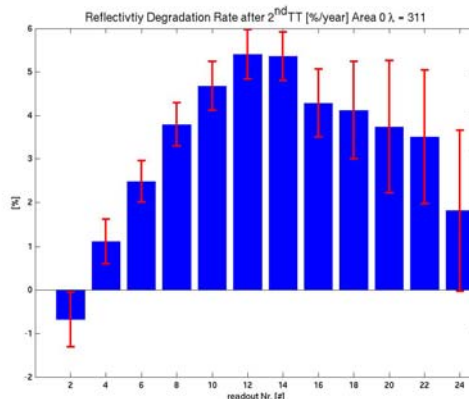
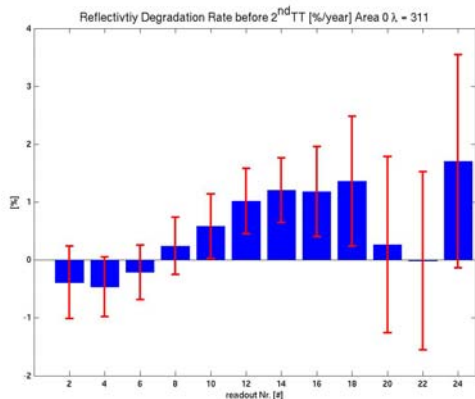
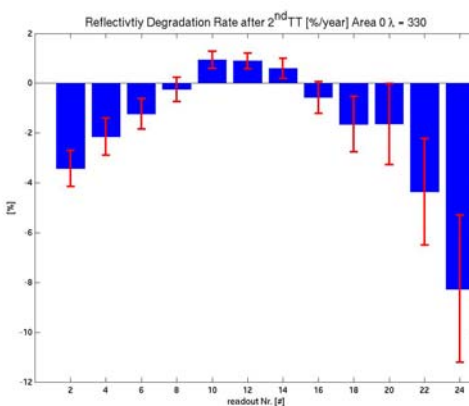
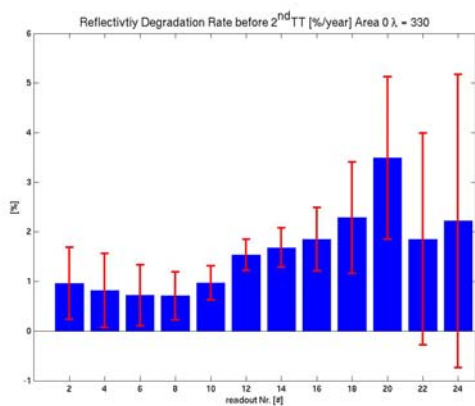


Figure 73: GOME-2/Metop-A reflectivity degradation rate per year for the period before the second throughput test (left panel) and after test (right panel) at 310 nm (Channel 1).

### 311 nm (Channel 2)



### 330 nm (Channel 2)



### 380 nm (Channel 2)

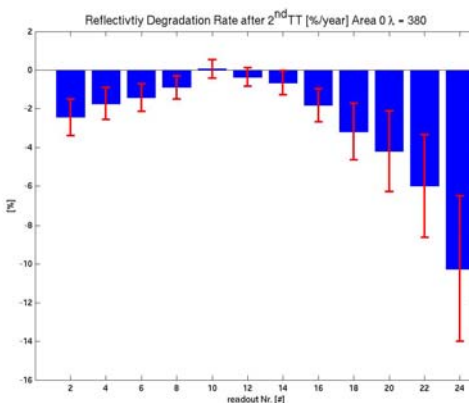
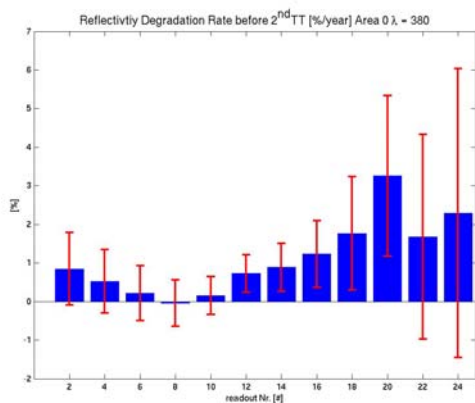
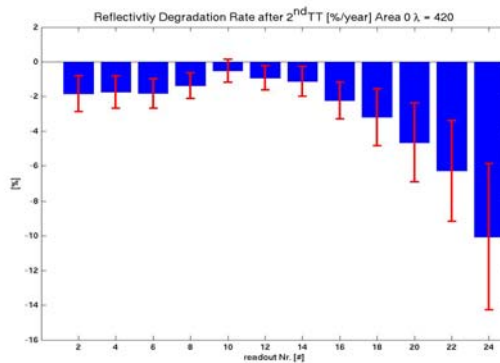
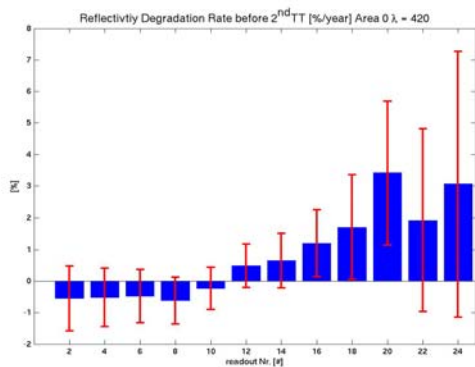
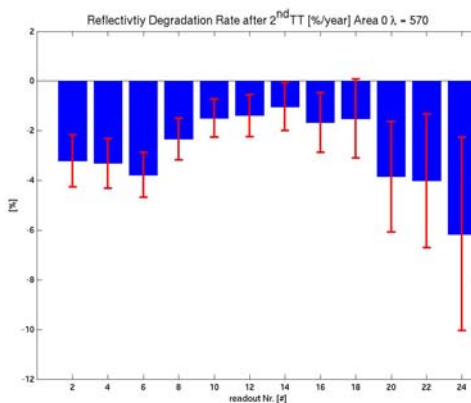
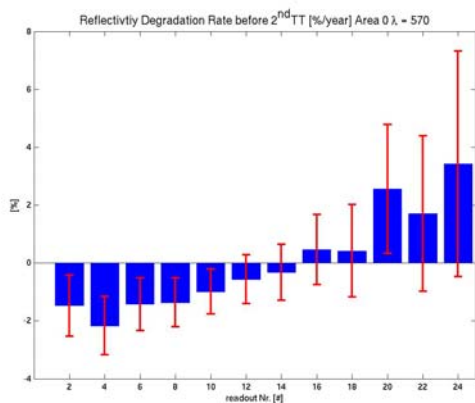


Figure 74: GOME-2/Metop-A reflectivity degradation rate per year for the period before the second throughput test (left panel) and after the test (right panel) at 311, 330 and 380 nm (Channel 2).

### 420 nm (Channel 3)



### 570 nm (Channel 3)



### 745 nm (Channel 4)

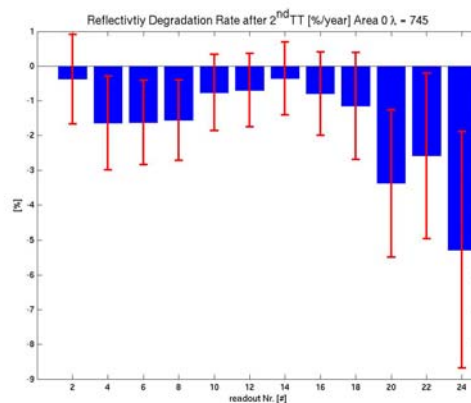
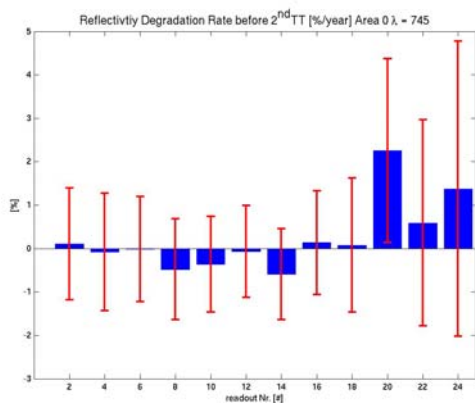


Figure 75: GOME-2/Metop-A reflectivity degradation rate per year for the period before the second throughput test (left panel) and after the test (right panel) at 420 and 570 nm (Channel 2) and 745 nm (Channel 4).

Generally, reflectivity degradation rates per year are in the order of 1-2% per year (2-4% at 310 nm in channel 1) before the second throughput test and indeed slightly larger, 2-4% per year (4-8% at 310 nm in channel 1), after the second throughput test. Notably, the scan-angle dependency of reflectivity degradation rates is larger after the test than before.

The differences between throughput degradation rates per optical path and reflectivity degradation rates (“differential degradation”) before and after the second throughput test has implications on the interpretation of level-2 degradation signals. While it has been found that the rate on the noise increase on the retrieved values and the rate of the increase of fit residuals slowed down after the second throughput test (decreased throughput degradation rates), this does not necessarily need to be the case for the rate of increase of the systematic biases of the retrieved values, which is likely more affected by the degradation rates of reflectivity values (see also [RD19]).

#### **7.7.5 Degradation signatures from G2RP-R2 for band 1a (Channel 1)**

Band 1a of channel 1 (from 240 nm to 307 nm before 10 December 2008, and from 240 nm to 283 nm thereafter) provides measurements within the reference areas (Sahara and Pacific) taken at 1.5 seconds integration time. This means that the forward scan consists of only three measurements (40 x 320 km). In the following section, we summarise the results for the degradation signatures for the wavelengths 260 nm and 280 nm in a similar fashion than in the previous sub-sections, except that the dataserie are not smoothed. For this wavelength region, the day-to-day variations are smaller because they contain predominantly information from the stratosphere.

Figure 76 to Figure 77 show the earthshine signal degradation for 260 nm and 280 nm relative to the year 2007, overlaid with the corresponding SMR signal degradation. A significant difference in the degradation rate between earthshine and SMR is already visible from these plots and confirmed by the throughput degradation rates evaluated before and after the second throughput test for both wavelengths in Figure 78 and Figure 79.

Note that the west-side viewing angles (scanner position 3) are based on considerably weaker statistics, and have therefore larger error bars than nadir and east-viewing results. This is due to the geographic position of the reference area box and the 29-day repeat cycle favouring nadir and west-viewing geometries.

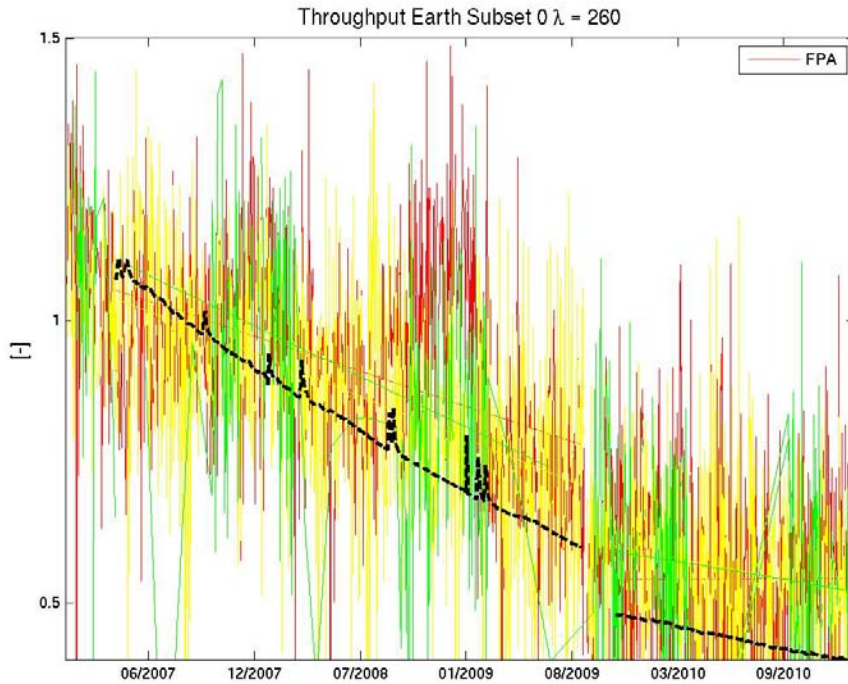


Figure 76: Earthshine signals normalised to the mean of 2007 at 260 nm in channel 1 (band 1a) and for all three forward scanner positions (coloured lines: red, yellow and green). The SMR normalised signal, a dashed black line, is provided as a reference.

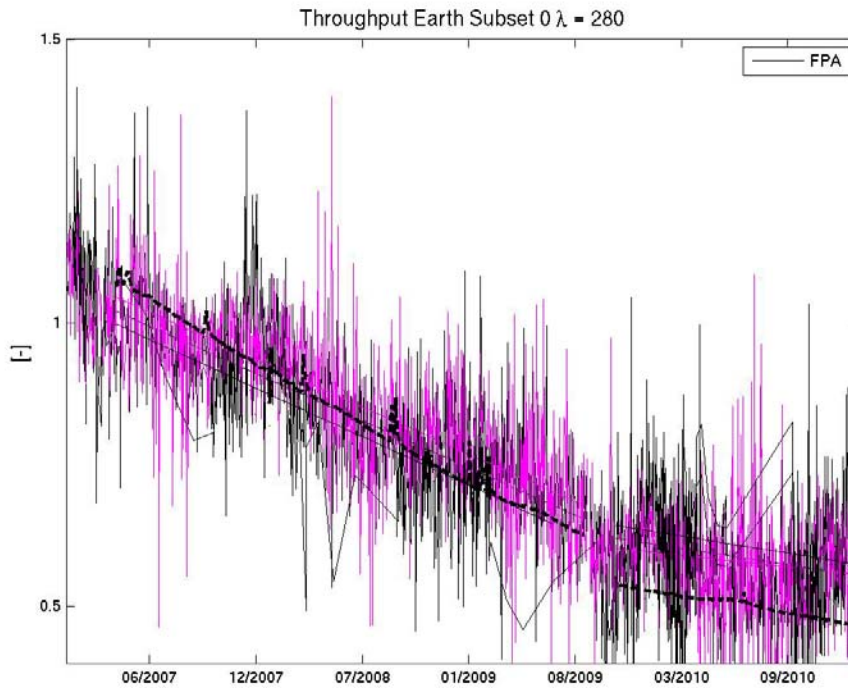
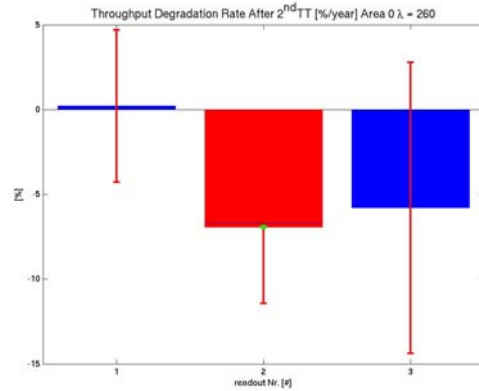
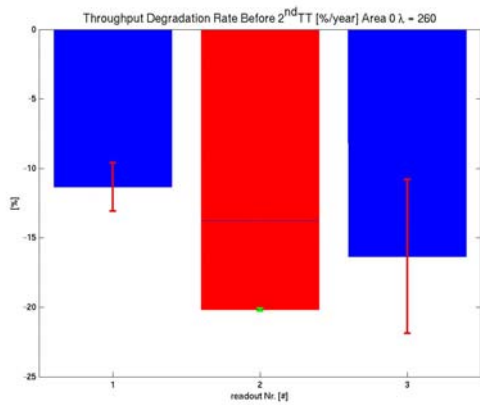


Figure 77: Earthshine signals normalised to the mean of 2007 at 280 nm in channel 1 (band 1a) and for all three forward scanner positions (coloured curves). The SMR normalised signal, a dashed black line, is provided as a reference.

**260 nm (Channel 1, Band 1A)**



**280 nm (Channel 1, Band 1A)**

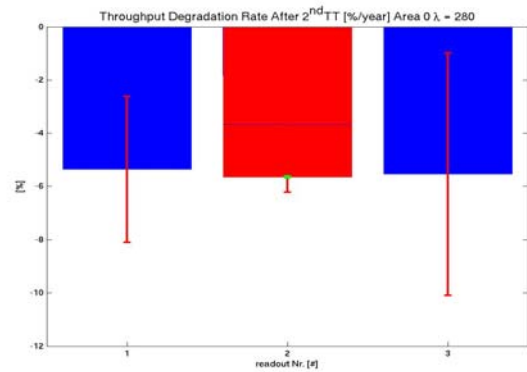
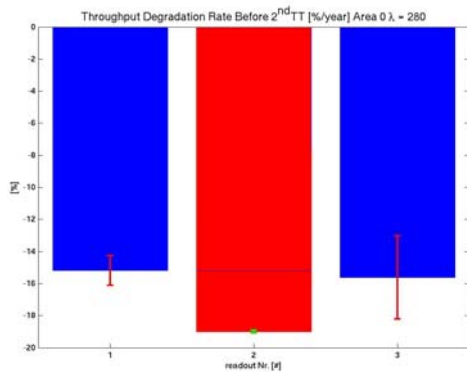
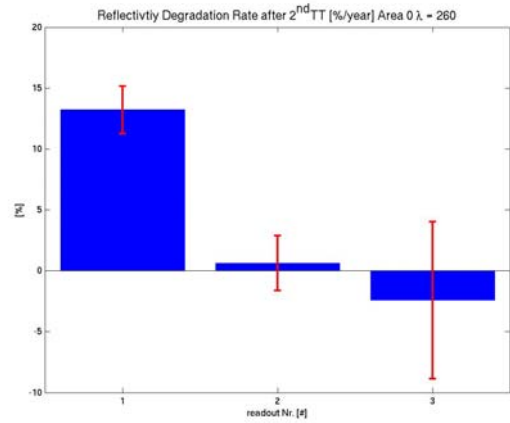
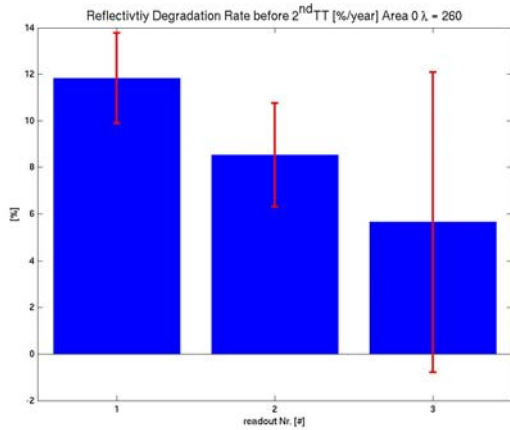


Figure 78: Earthshine signal degradation rate per year for the period before the second throughput test (left panel) and after the throughput test (right panel) at 260 and 280 nm (channel 1; band 1a). The plots also show the corresponding degradation rate of SMR at forward scan position 2 (for details see text).

### 260 nm (Channel 1, Band 1A)



### 280 nm (Channel 1, Band 1A)

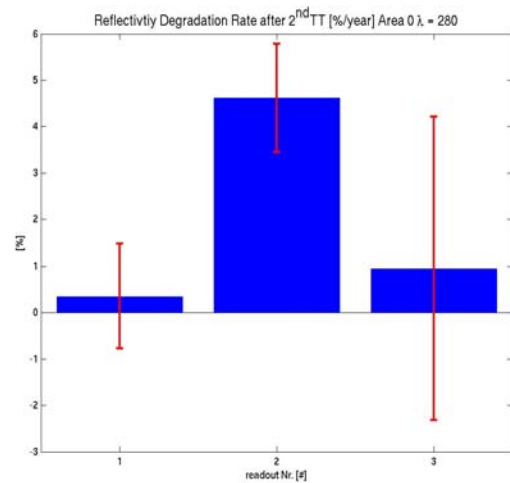
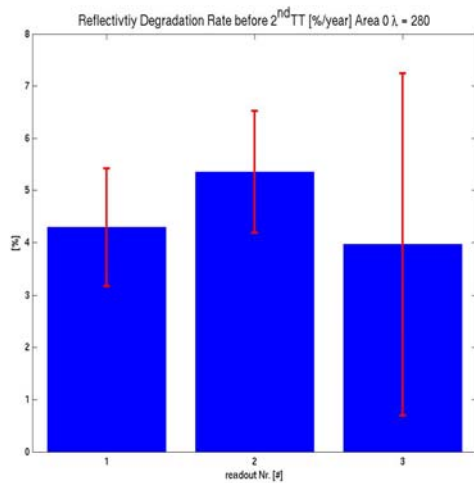


Figure 79: GOME-2 / Metop-A reflectivity degradation rate per year for the period before the second throughput test (left panel) and after the throughput test (right panel) at 260 nm and 280 nm (Channel 1; Band 1a).

## **7.8 Differences with Respect to the Extended G2RP-R1 (January 2007 to January 2011; PPF 4.0)**

The main differences and improvements concerning product quality and homogeneity of time-series with respect to the previously reprocessed dataset G2RP-R1 (January 2007 until January 2009) and the subsequently available NRT data, covering processor version 4.0 to 5.3 is expected to originate from the improvement of the quality of the polarisation correction for main channel data and the improvement on the usage of additional and improved key-datasets especially for PMD signals (see Section 5.3). The latter improves not only the quality of the derived Stokes fractions from PMD (see Section 7.5) but also the calibrated level 1b radiances for both PMD-P and PMD-S, which are more and more frequently used directly for level 2 retrievals.

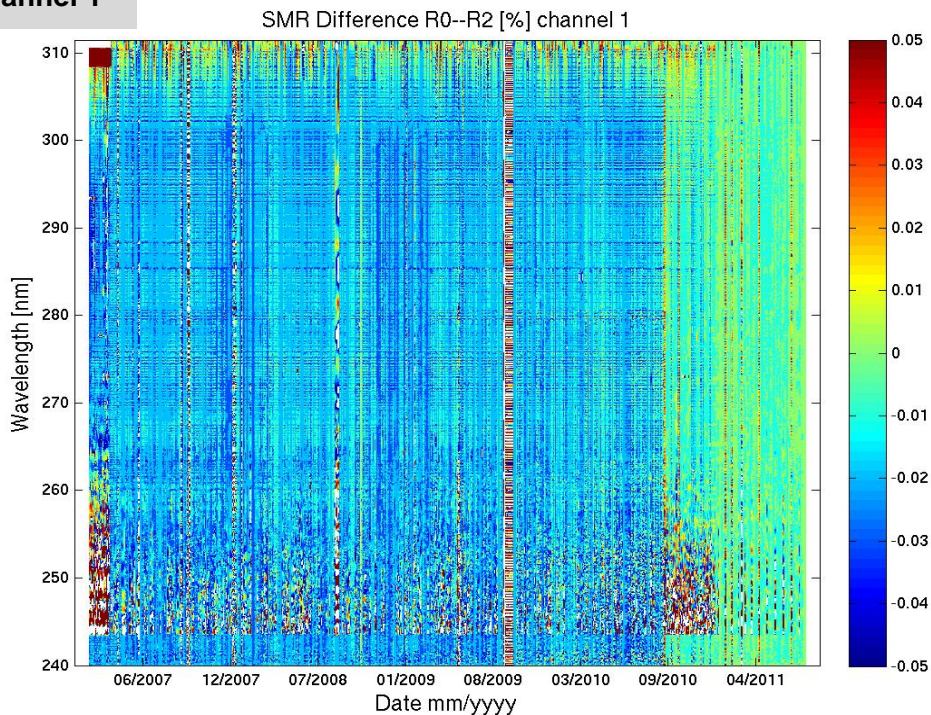
In the following section, we compare some of the key-parameters as derived in the previous sections for G2RP-R2, affecting level 1b data quality and time-series homogeneity, with a focus on the major changes between PPF version 4.0 and 5.3. Besides the original G2RP-R1 dataset, an extended time series of data derived from processor version 4.0 does exist offline at EUMETSAT that covers the period January 2007–January 2011. In the following we will use this extended time-series for the comparisons between R1 and R2.

### ***7.8.1 Homogeneity with respect to NRT: differences for the solar path***

We compare time-series of SMR spectra for the reference period, covering processor version 3 to 5, with the near-real time dataset (R0) in order to identify the impact of the reprocessing on instrument events and changing processor versions.

Generally, the differences are small and vary between 0.05 % in Channels 1, 2 and 4 and 0.1 % in channel 3 before January 2008 (Figure 80 and Figure 81). Differences on the order of 0.5 % to 2 % are visible before early 2008 for both PMD channels Figure 82. All differences approach zero (0) towards the introduction of processor version 5.3 in January 2012, which confirms a gradual improvement in product quality due to processing upgrades over time. The largest improvements in SMR quality are seen with the introduction of the usage of the full spectral grids internally to the processing in channel 3 and the completely revised PMD spectral calibration scheme in channel 5 and 6 (PMD-P and PMD-S) in January 2008 (PPF 3.8). Instrument events, like the second throughput test in September 2009 are visible as vertical stripes but do not show any sustained effect in the difference between NRT and R2. The sudden improvement in September 2010 in all channels is due to the improvement of the fixed Mueller Matrix Elements angle-grid linked to PPF update to 4.5.0 in September 2009. The latter had a small but non-negligible effect on the SMR spectra.

**Channel 1**



**Channel 2**

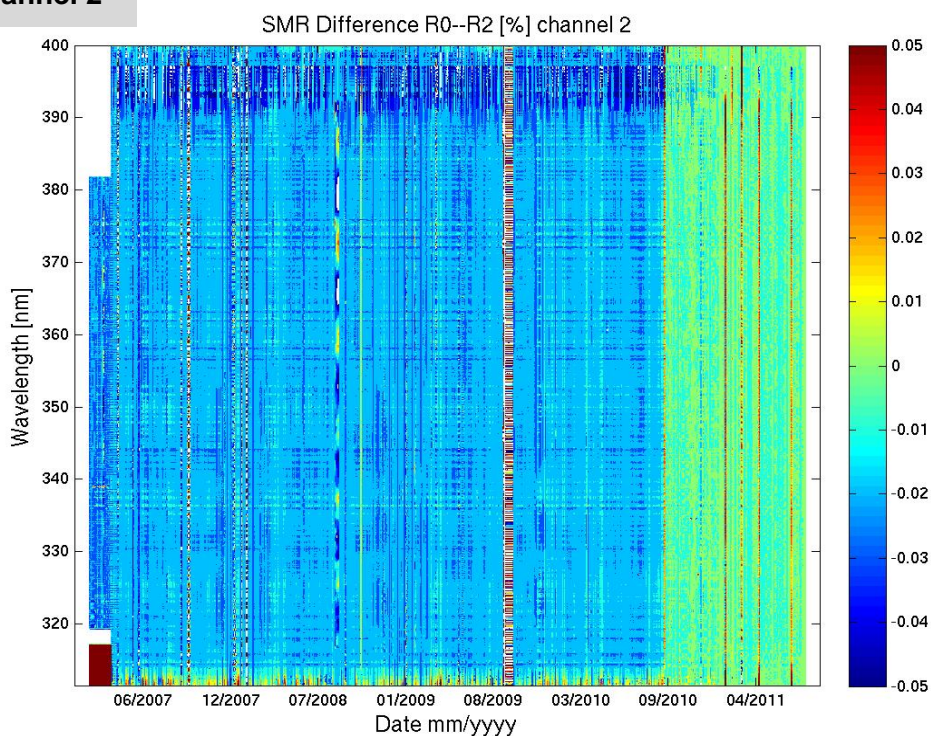
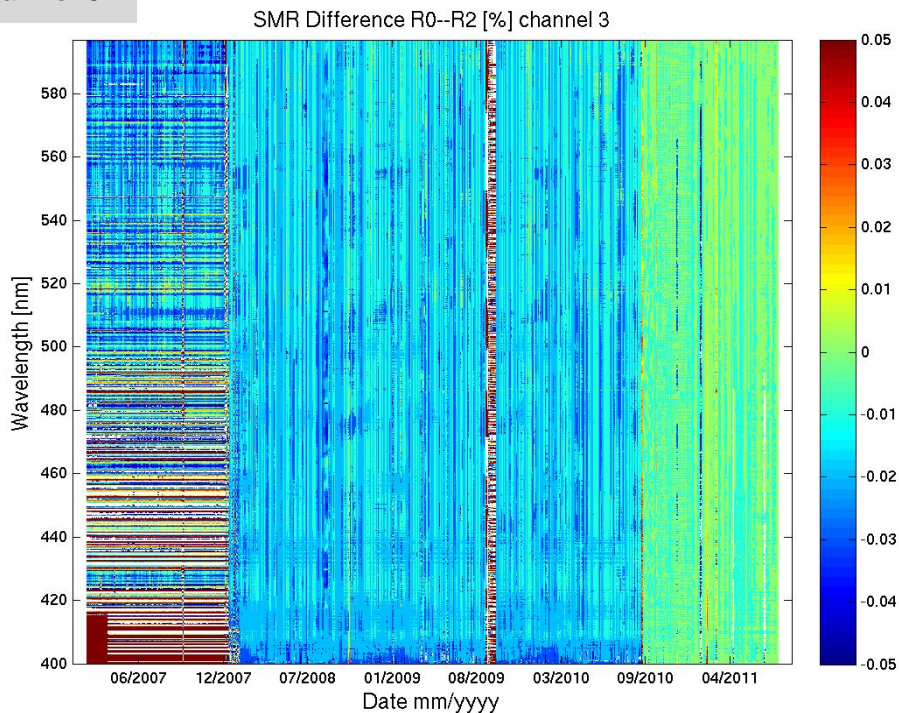


Figure 80: GOME-2/Metop-A: Difference (per cent) between solar mean reference spectra in Channels 1 and 2, derived from the near-real time (NRT) time series and the G2RP-R2 time series

**Channel 3**



**Channel 4**

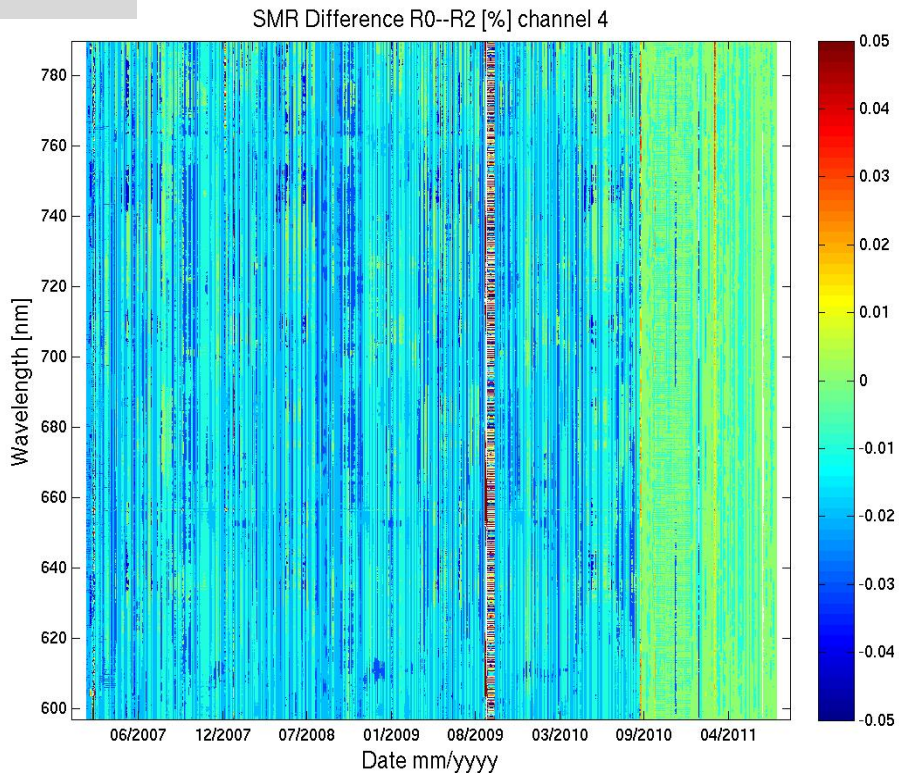
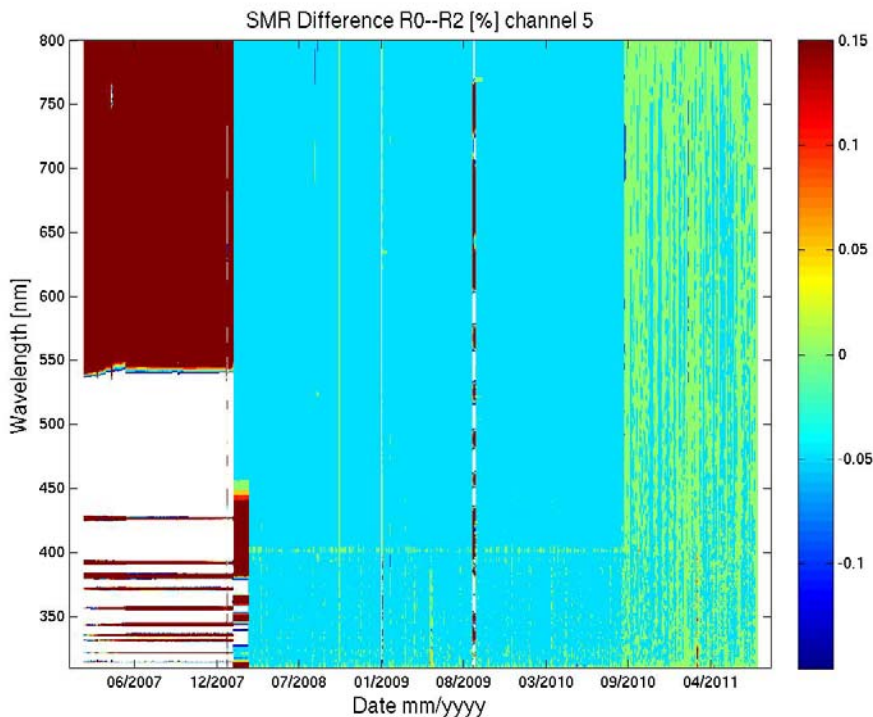


Figure 81: GOME-2/Metop-A: Difference (per cent) between solar mean reference spectra in Channels 3 and 4, derived from the NRT time series and G2RP-R2.

**Channel 5 (PMD-P)**



**Channel 6 (PMD-S)**

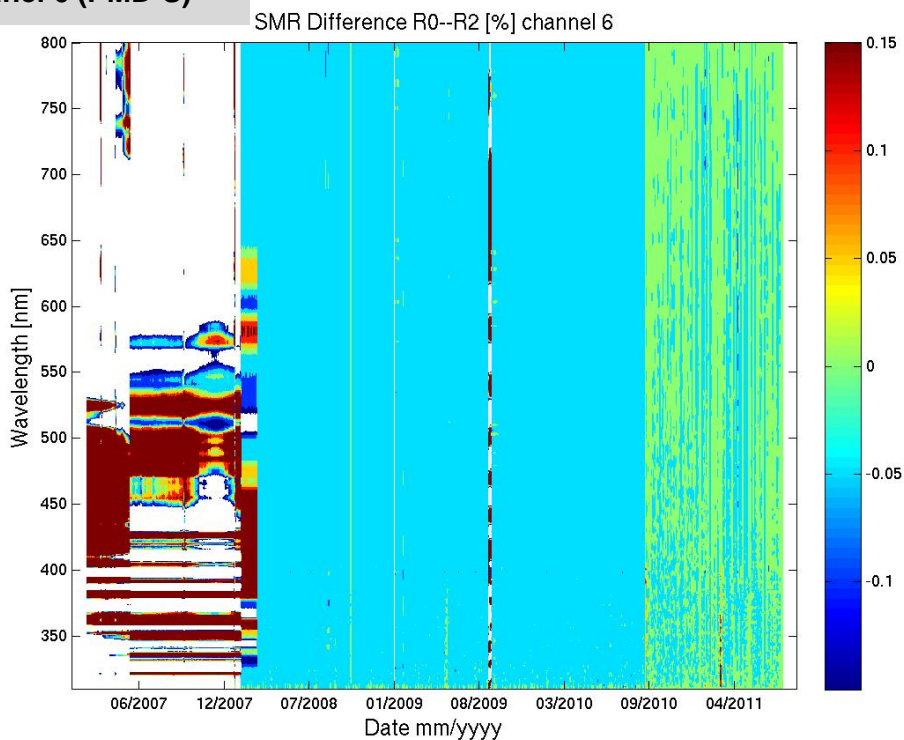


Figure 82: GOME-2/Metop-A: Difference (per cent) between solar mean reference spectra for PMD-P and S, derived from the NRT time series and G2RP-R2.

### 7.8.2 Differences with respect to R1: Earthshine path – Stokes fractions.

In the following two sub-sections, we look at the difference between the previous and extended reprocessed products from R1+ (January 2007 to January 2011) and the current R2 time series. A number of changes have been introduced between PPF version 4.0 (R1+) and the current version 5.3 (R2), which affect the quality of the derived Stokes fractions.

A major change concerning this quality has been introduced in August 2009 with PPF 4.3. Therein, we have introduced an online correction scheme for the Stokes fractions, which has proven to significantly improve the quality of the main channel polarisation correction [RD13].

Figure 83 to Figure 88 show Stokes fraction time series for both reprocessing versions for special geometries (for which  $q$  should equal 0) over the reference periods of R1+ and R2 (see also Section 7.5 for details) and for all 15 PMD bands.

#### PMD Band 1

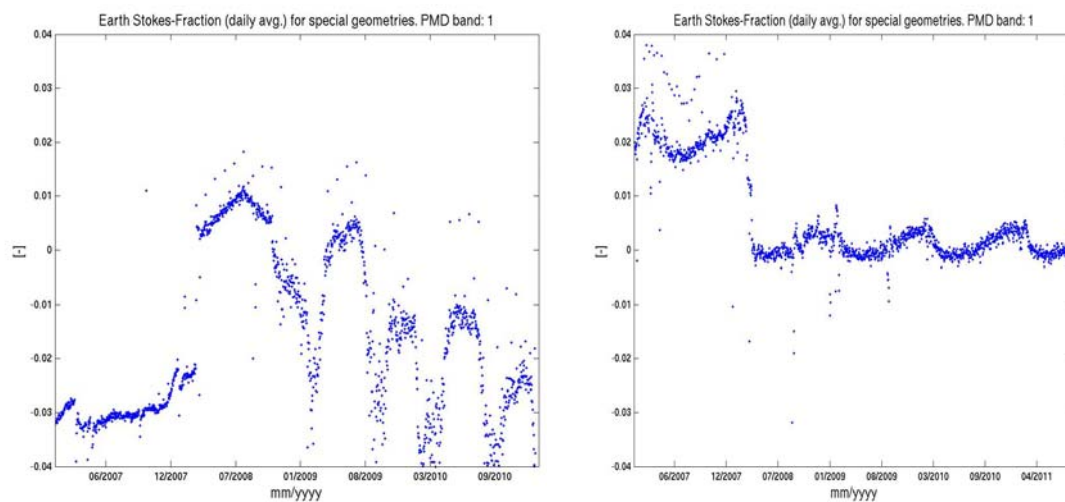
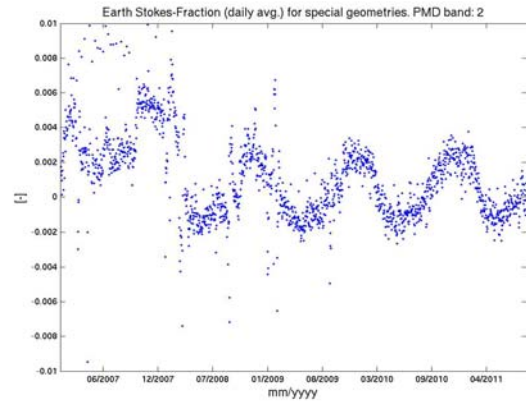
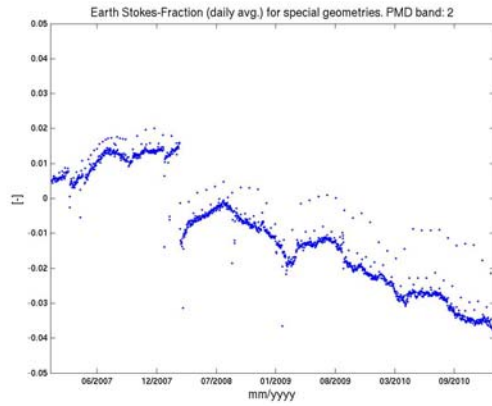
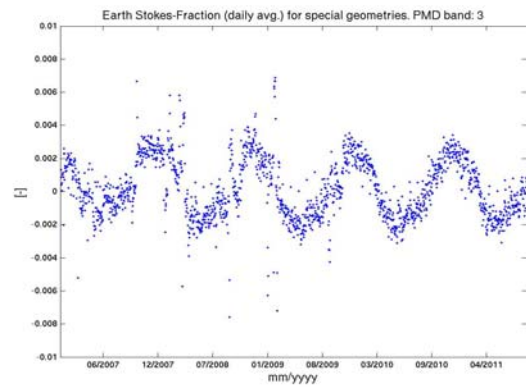
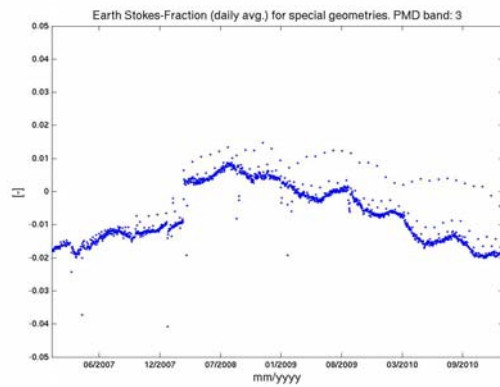


Figure 83: Stokes fractions for special geometries as for Figure 41 to Figure 43 and derived from PMD band 1. The left panel shows the time series for the extended R1+ products. The right panel shows the results for R2.

### PMD Band 2



### PMD Band 3



### PMD Band 4

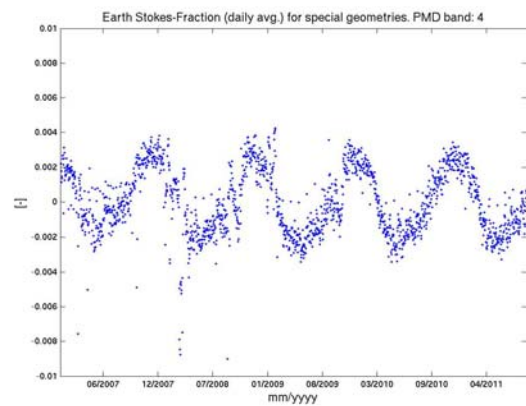
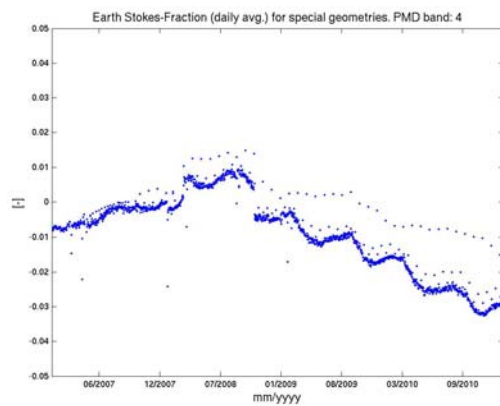
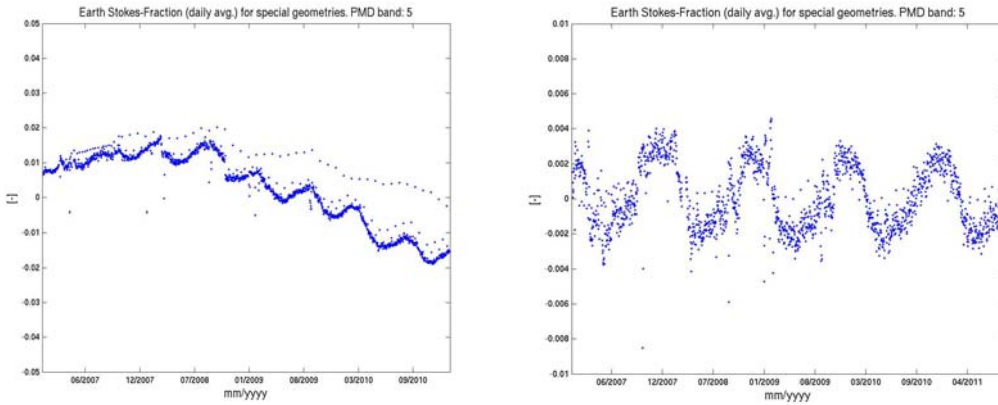
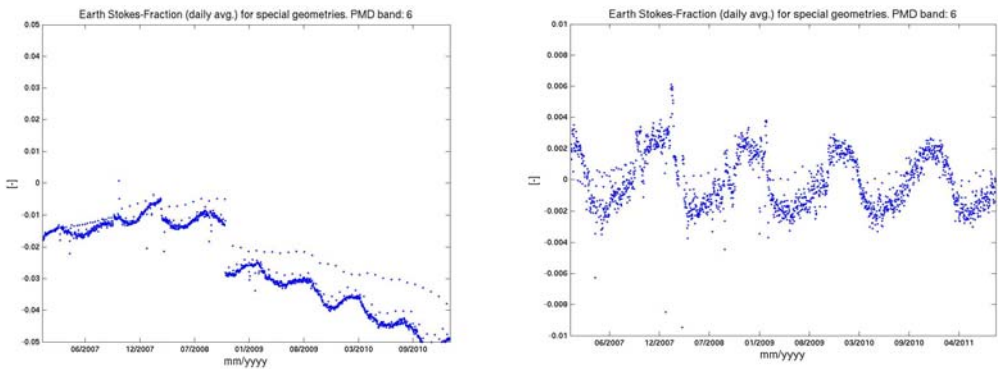


Figure 84: Stokes fractions for special geometries as for Figure 41 to Figure 43 and derived from PMD bands 2, 3, and 4. The left panel shows the time series for the extended R1+ products. The right panel shows the results for R2.

**PMD Band 5**



**PMD Band 6**



**PMD Band 7**

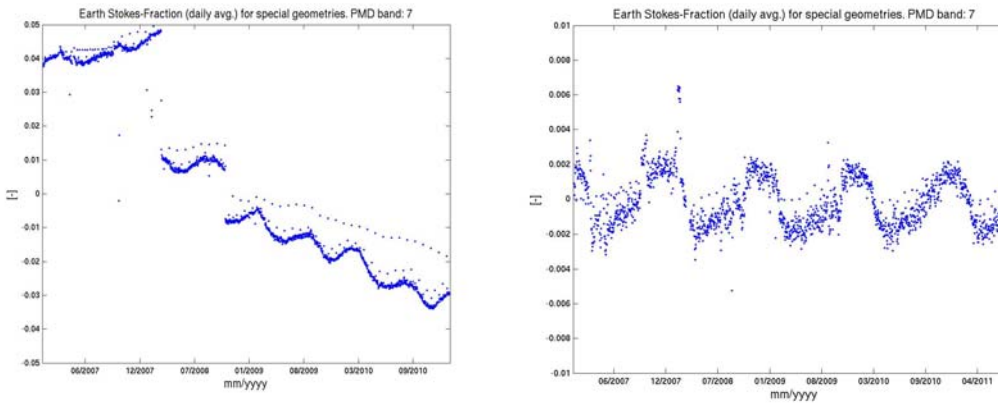
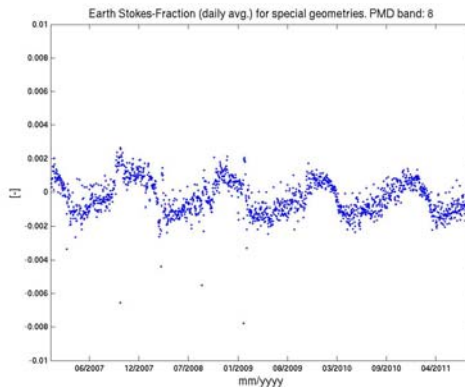
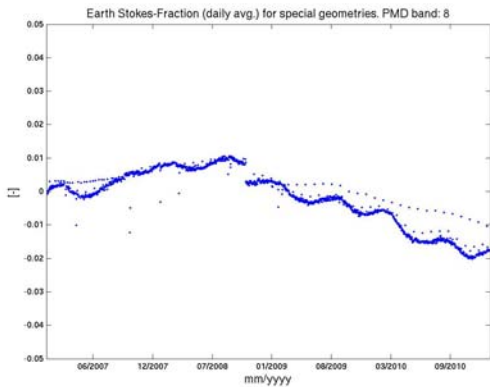
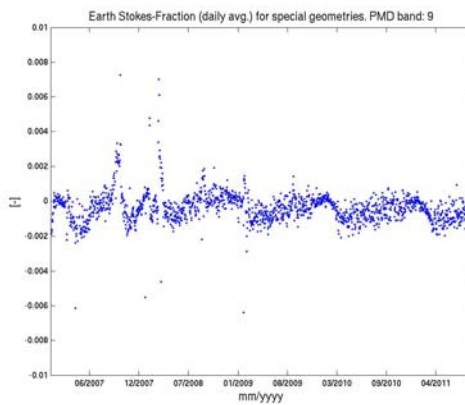
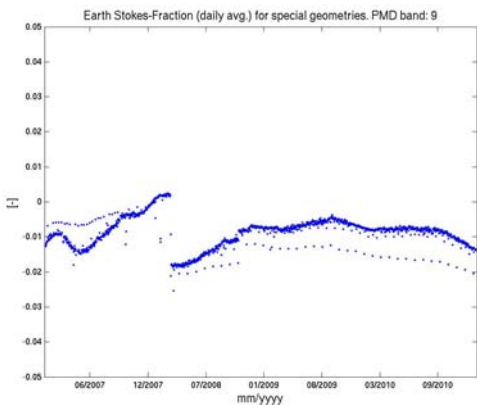


Figure 85: Stokes fractions for special geometries as for Figure 41 to Figure 43 and derived from PMD bands 5, 6, and 7. The left panel shows the time series for the extended R1+ products. The right panel shows the results for R2.

**PMD Band 8**



**PMD Band 9**



**PMD Band 10**

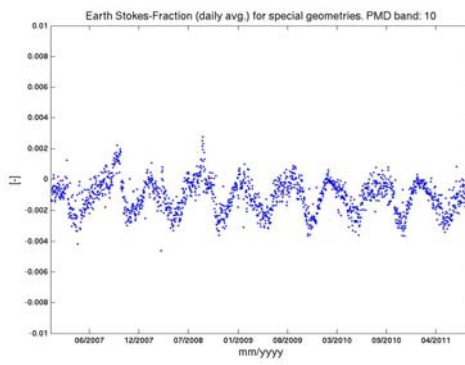
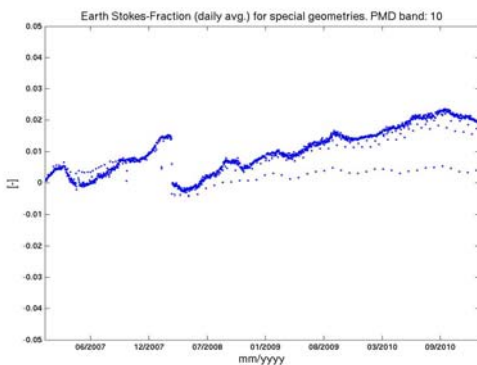
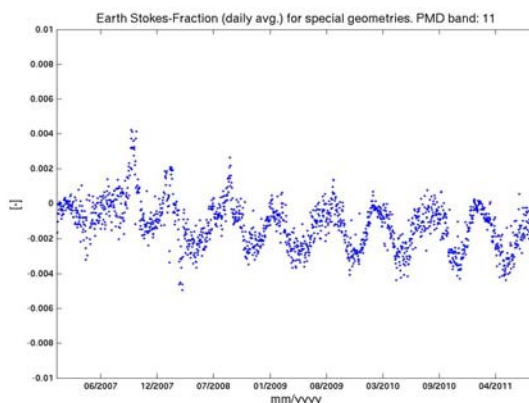
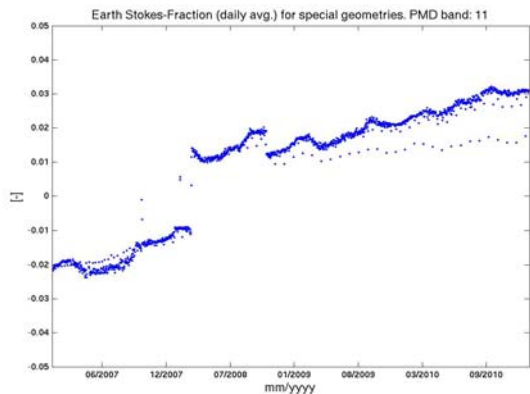
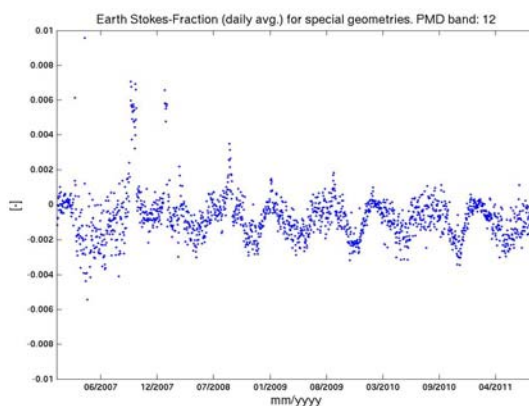
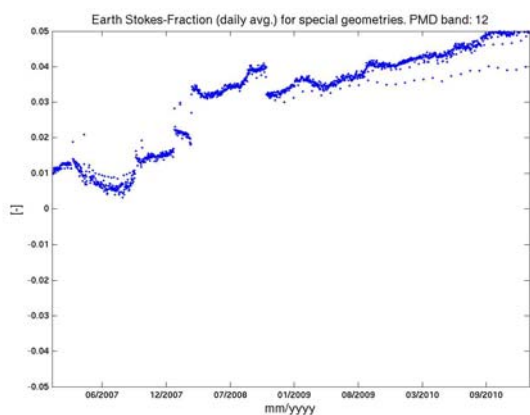


Figure 86: Stokes fractions for special geometries as for Figure 41 to Figure 43 and derived from PMD bands 8, 9, and 10. The left panel shows the time series for the extended R1+ products. The right panel shows the results for R2.

**PMD Band 11**



**PMD Band 12**



**PMD Band 13**

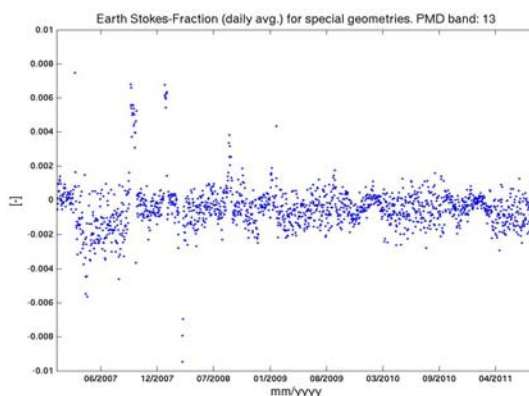
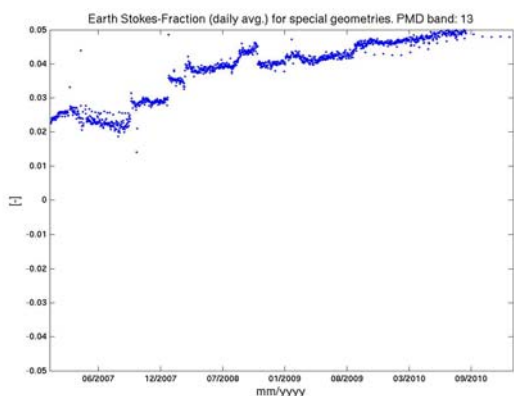
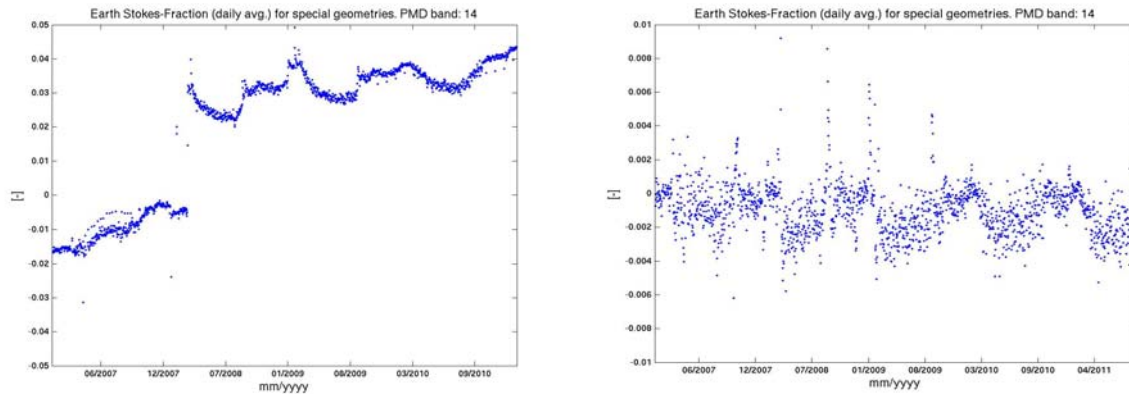


Figure 87: Stokes fractions for special geometries as for Figure 41 to Figure 43 and derived from PMD bands 11,12, and 13. The left panel shows the time series for the extended R1+ products. The right panel shows the results for R2.

**PMD Band 14**



**PMD Band 15**

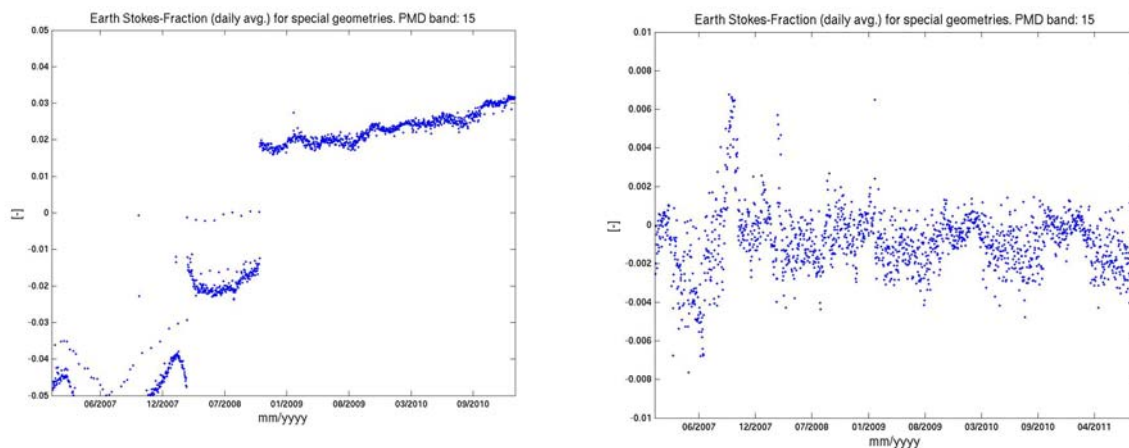


Figure 88: Stokes fractions for special geometries as for Figure 41 to Figure 43 and derived from PMD bands 14 and 15. The left panel shows the time series for the extended R1+ products. The right panel shows the results for R2.

Figure 83 to Figure 88 show that R2 significantly improves the quality of the Stokes fractions per band and over the complete reference period with respect to R1+. The largest discontinuity which is visible in both time series (though to a significantly smaller magnitude for R2) is the change in PMD band definitions introduced at the beginning of 2008 (see also Section 7.5). In addition, a second step-function is visible in the last quarter of 2008 and for some PMD bands only. Since the processor version and the configuration for processing has not changed, this must be related to a change in the instrument probably during the second upload of the on-board co-adding patch. The exact reason for this jump is, however, not understood. In contrast both of these discontinuities are not visible in the R2 dataset because the online correction of the Stokes fraction takes care of relative changes in PMD-P to PMD-S signal.

Finally, we also compare the difference of Stokes fraction for special geometries averaged over the complete time series for both R1+ and R2 in Figure 89, which again confirms the improvements of R2 with respect to R1+.

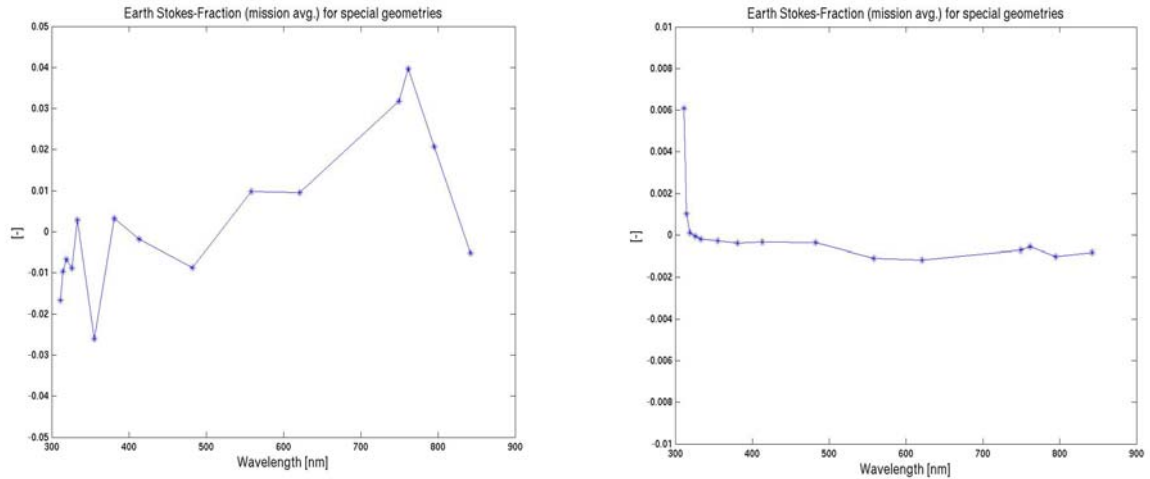


Figure 89: Stokes fractions for special geometries as for Figure 40 averaged over the complete time series, for both the extended R1+ (left panel) and R2 (right panel) products. Note difference in scale of the y-axis.

### 7.8.3 Differences with respect to R1: Earthshine Path

The improvements in the quality of the Stokes fractions and the main channel polarisation correction as well as the improvements in key-data for the absolute calibration of PMD signals is expected to have an significant effect on the calibrated level 1b earthshine signals for main channels and PMDs respectively.

Figure 90 to Figure 92 show the difference between the extended R1+ time-series from January 2007 to January 2011 and the new R2 products for the same wavelength as in Section 7.7.2, Figure 62 to Figure 69. We show smoothed spectra using a 29-days cycle moving average and compute the relative difference between the two time series R1+ and R2 in percentage of the absolute earthshine radiances at every second scanner position (left panels) and for the most extreme positions (west, nadir, east at readout 24, 12 and 2; right panels).

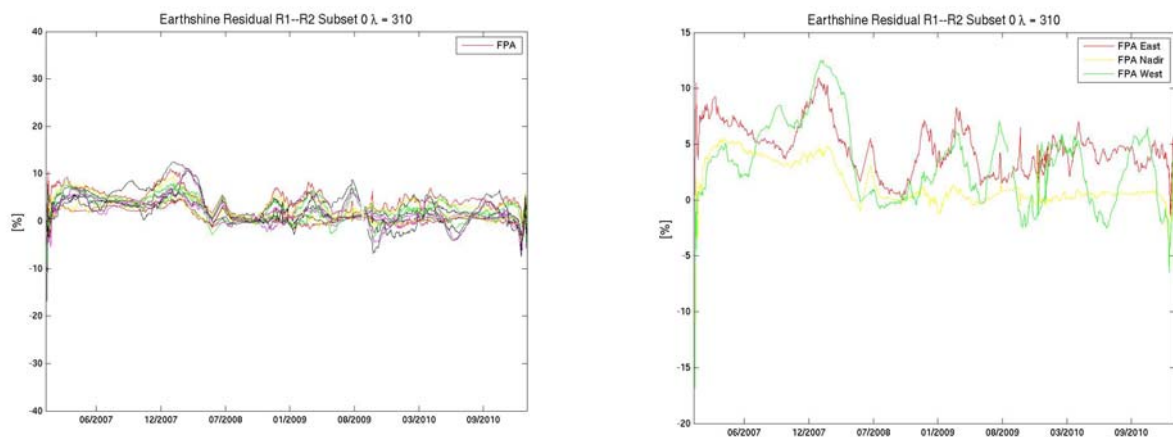
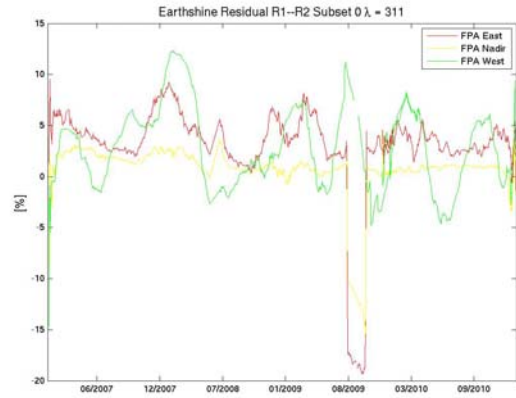
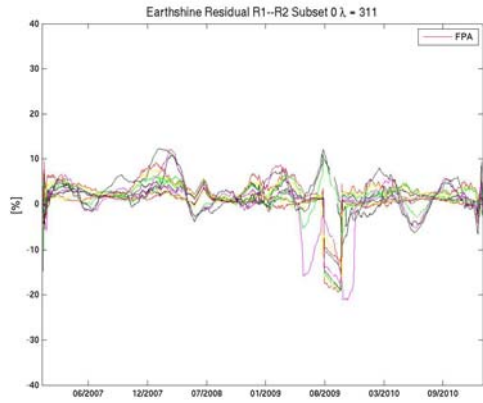
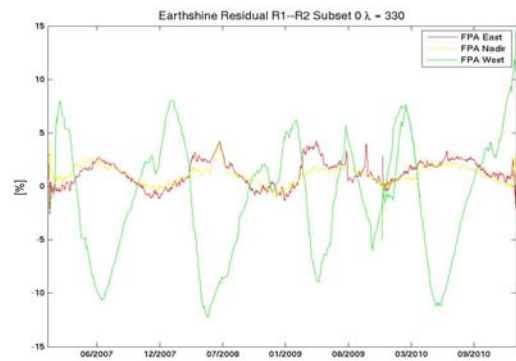
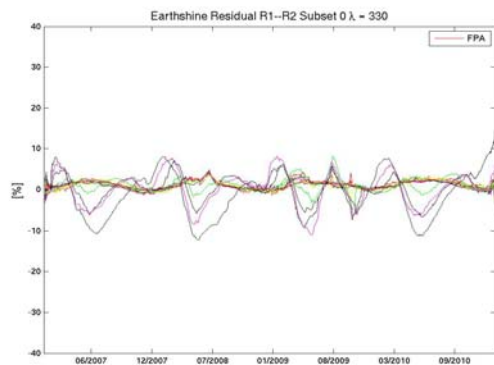


Figure 90: Percentage difference between reprocessed time-series R1+ and R2 (R1-R2) of calibrated earthshine spectra for main channels at every second scanner position (left panel) and for the most extreme positions. Data derived at a wavelength of 310 nm (Channel 1).

### 311 nm Channel 2



### 330 nm Channel 2



### 380 nm Channel 2

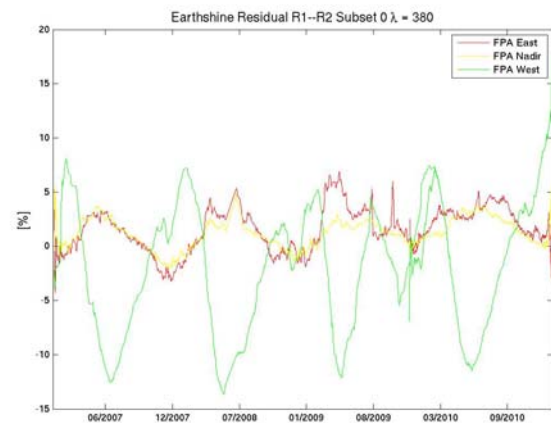
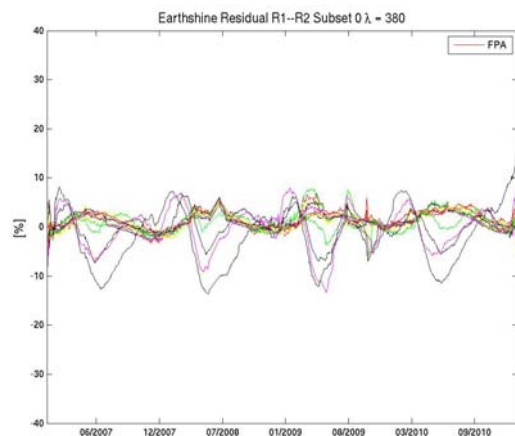
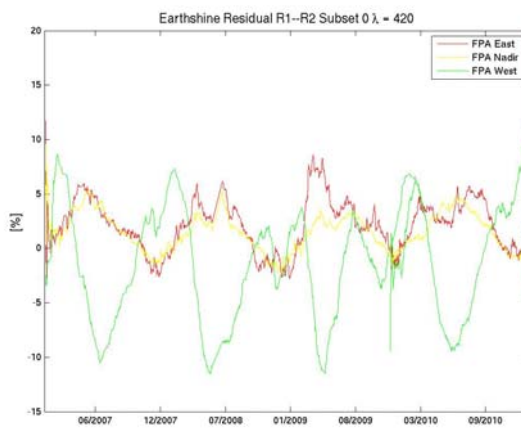
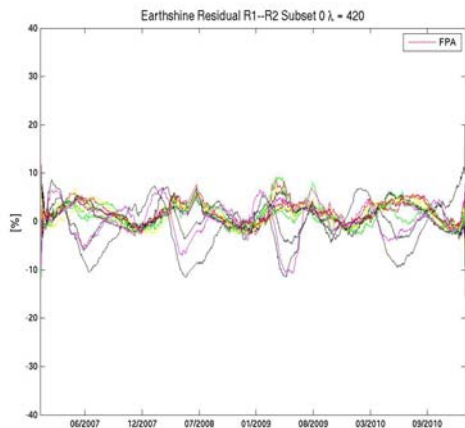
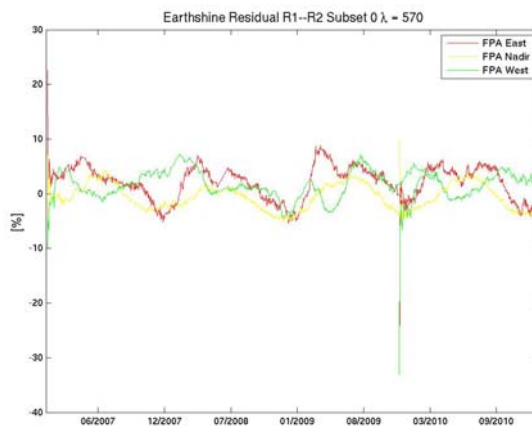
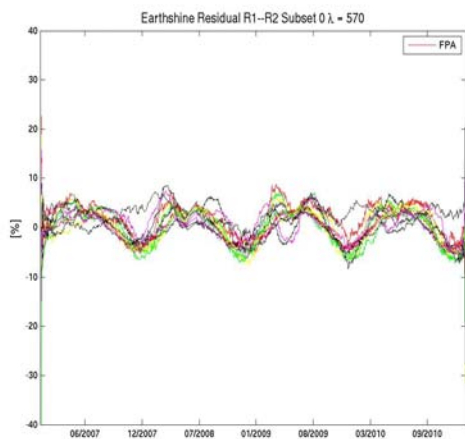


Figure 91: Percentage difference between reprocessed time-series R1+ and R2 (R1-R2) of calibrated earthshine spectra for main channels at every second scanner position (left panel) and for the most extreme positions east, nadir, and west corresponding to readout number 2, 12 and 24. Here we show data derived at wavelengths of 311, 330 and 380 nm (channel 2).

**420 nm Channel 3**



**570 nm Channel 3**



**745 nm Channel 4**

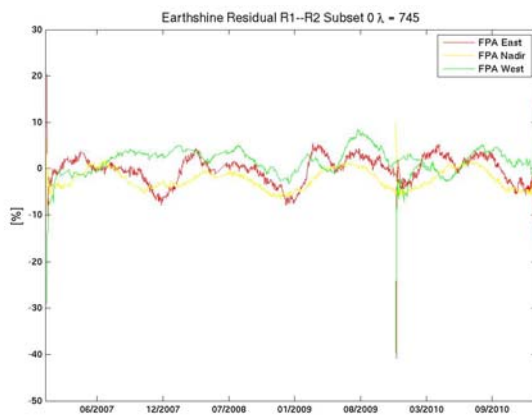
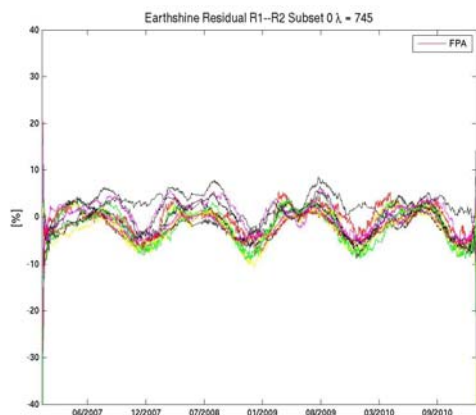


Figure 92: Percentage difference between reprocessed time-series R1+ and R2 (R1-R2) of calibrated earthshine spectra for main channels at every second scanner position (left panel) and for the most extreme positions east, nadir, and west corresponding to readout number 2, 12 and 24. Here we show data derived at wavelengths of 420, 570 and 745 nm (channel 2).

The observed differences for earthshine signals between R1+ and R2 are quite significant—ranging between 5 % and almost 15 %, depending on wavelength and viewing angles. Generally, the strength of an observed seasonal cycle in the residuals increases towards longer wavelength and for west-viewing geometries.

The largest impact of the quality of the polarisation correction from main channel on the earthshine signal and on the observed residuals is expected in the range between 300 nm to 600 nm where single-scattering in the atmosphere is the dominant kind of scattering and the degree of polarisation is therefore expected to be highest. For the Sahara case observed here, west-looking measurements coincide with small Stokes fraction values, for which the relative difference between R1+ without Stokes fraction correction and R2 with Stokes fraction correction is largest.

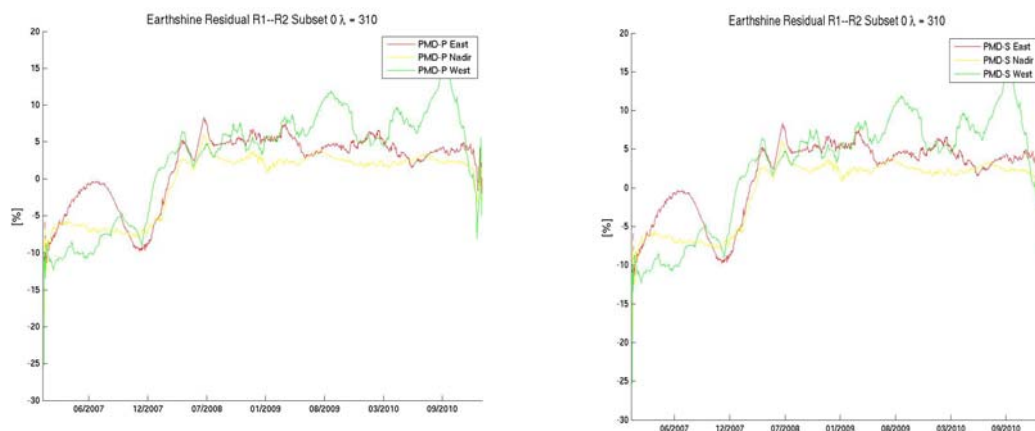
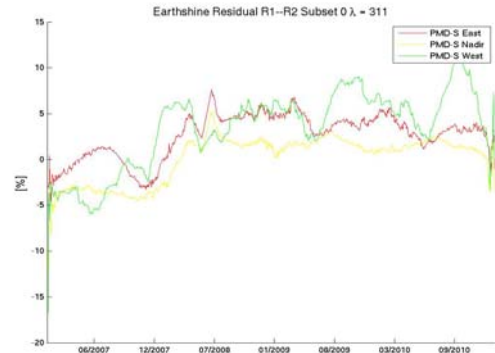
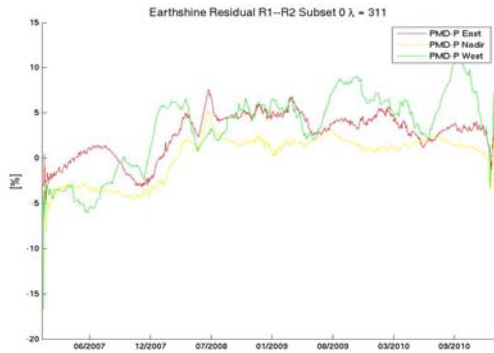
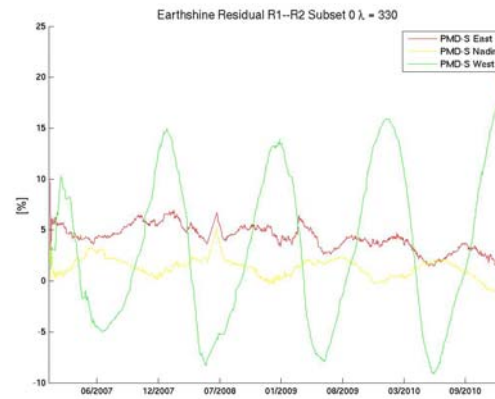
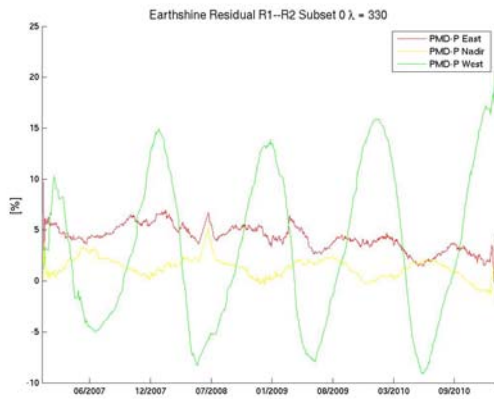


Figure 93: Percentage difference between reprocessed time-series R1+ and R2 (R1-R2) of calibrated earthshine spectra for PMD-P (left panel) and PMD-S (right panel) for the most extreme positions east, nadir, and west corresponding to readout number 2, 12 and 24 for main channels. Here we show data derived from PMD bands closest to the main channel wavelength of 310 nm.

**311 nm**



**330 nm**



**380 nm**

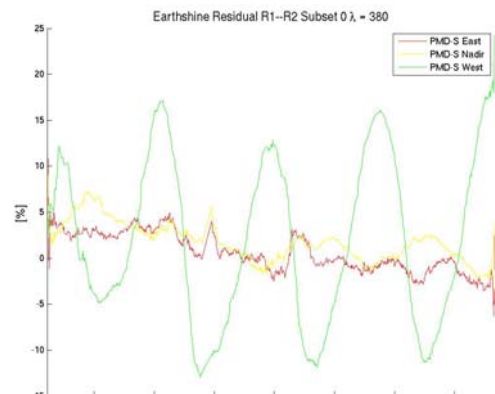
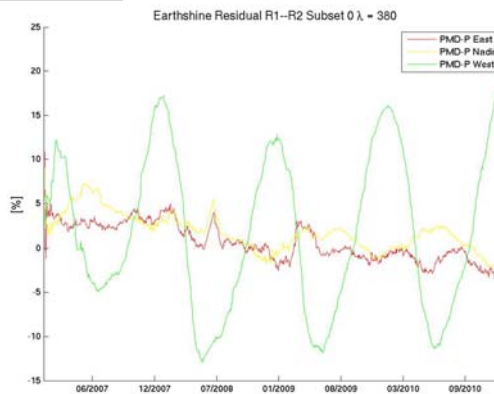
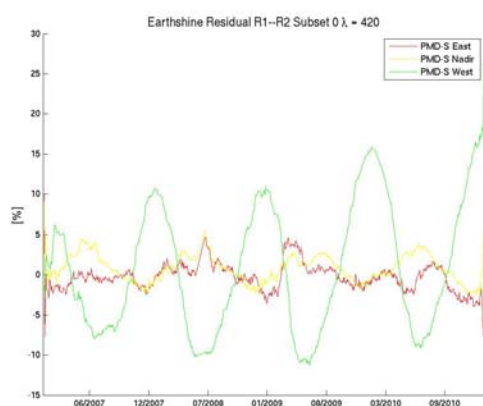
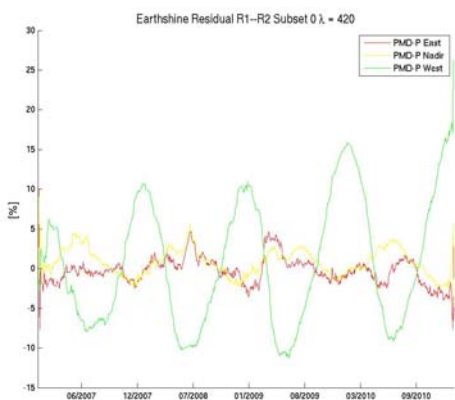
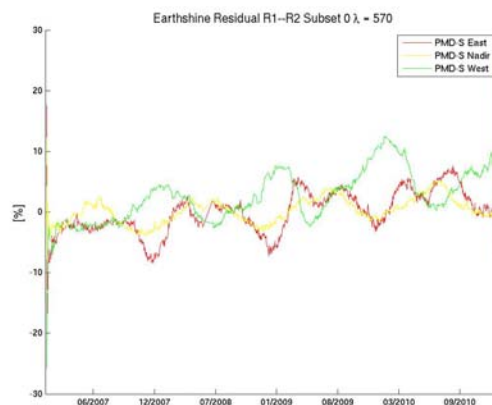
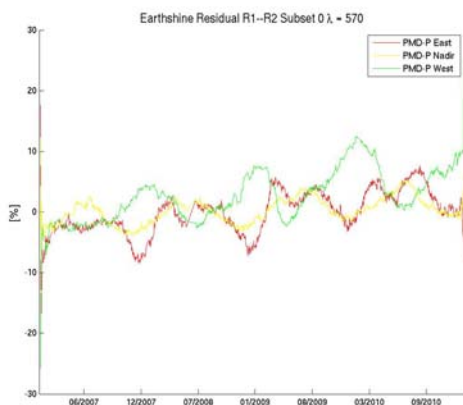


Figure 94: Percentage difference between reprocessed time-series R1+ and R2 (R1-R2) of calibrated earthshine spectra for PMD-P (left panel) and PMD-S (right panel) for the most extreme positions east, nadir, and west corresponding to readout number 2, 12 and 24 for main channels. Here we show data derived from PMD bands closest to the main channel wavelengths of 311, 330, and 380 nm.

**420 nm**



**570 nm**



**745 nm**

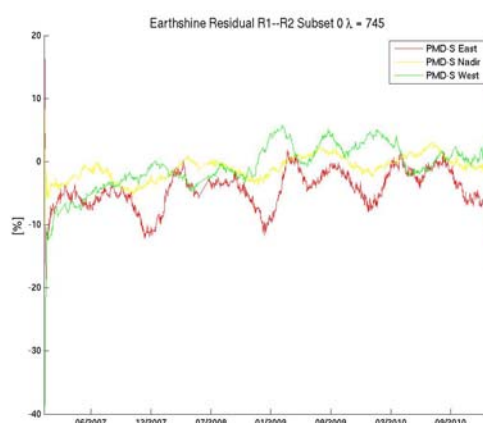
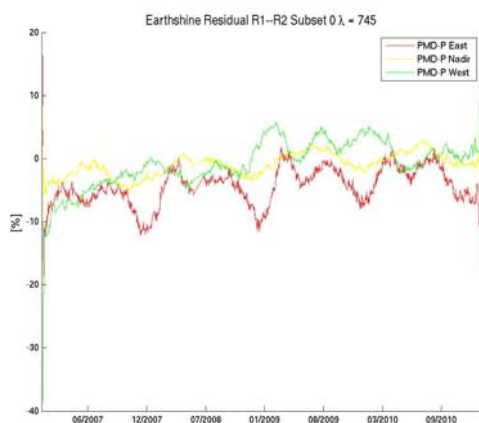


Figure 95: Percentage difference between reprocessed time-series R1+ and R2 (R1-R2) of calibrated earthshine spectra for PMD-P (left panel) and PMD-S (right panel) for the most extreme positions east, nadir, and west corresponding to readout number 2, 12 and 24 for main channels. Here we show data derived from PMD bands closest to the main channel wavelengths of 420, 570, and 745 nm.

Similar patterns as for main channels are observed for PMD-P and for PMD-S at corresponding wavelength and viewing angles and shown in Figure 92 to Figure 95. The most likely explanation for the observed residuals between R1+ and R2 for main channel earthshine signals is therefore the impact of improved PMD signals by introduction of stray light corrected key-data for the calibration of PMD signals as well as the introduction of a dedicated set of key-data for the angular dependence of the sensitivity of the PMDs to 45 degrees polarised light, introduced for PPF 4.3 and included in R2. In addition, the introduction of the online correction of Stokes fractions had a significant impact on the polarisation correction, as has been shown in the previous sections.

**7.8.4 Differences with respect to R1: Reflectivity degradation rates.**

Due to the relatively large difference observed between R1+ and R2 earthshine signals in the previous section (the impact on the solar path was, in contrast quite small; see Section 7.8.1), a significant effect on the evaluation of reflectivity degradation rates can be expected.

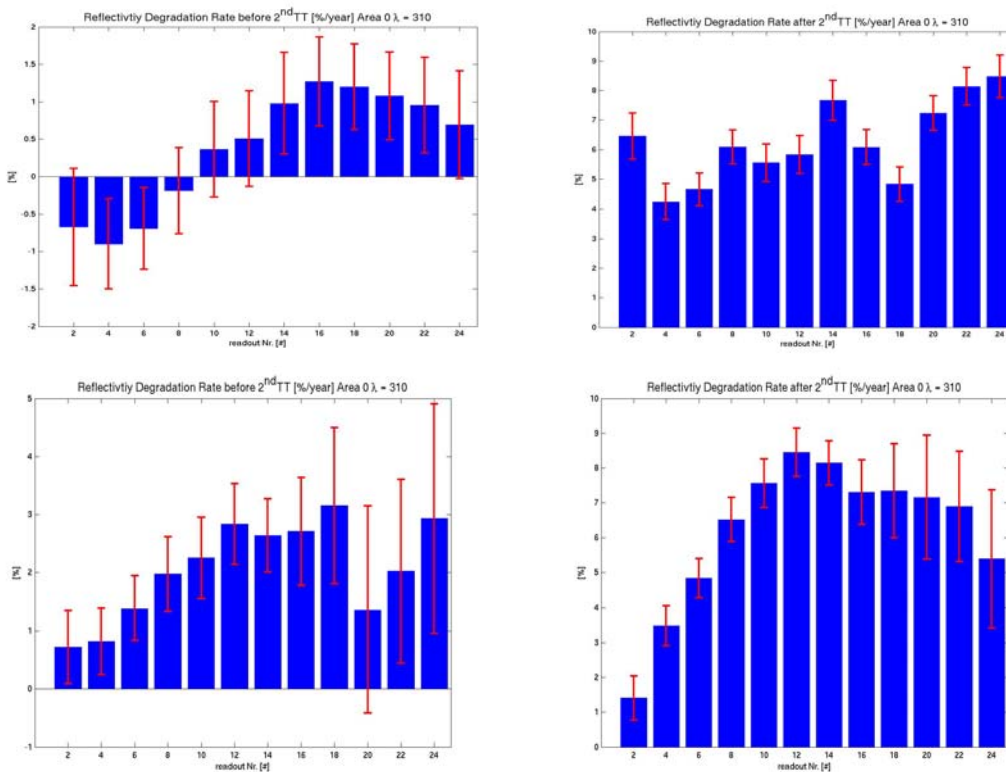


Figure 96: Reflectivity degradation rates at 310 nm (Channel 1) before (left panels) and after (right panels) the second throughput test. The top row shows yearly rates derived from R1+ and the bottom row of panels show the results from the recent R2 campaign.

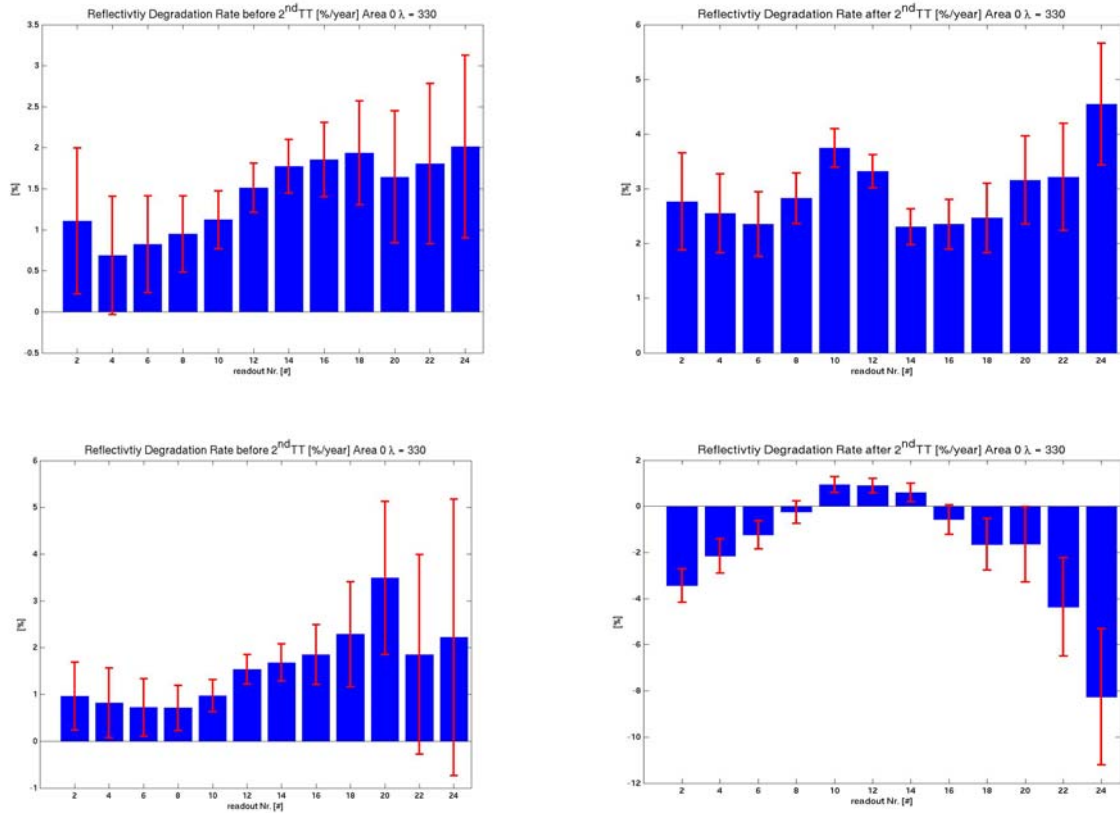


Figure 97: Reflectivity degradation rates at 330 nm (Channel 2) before (left panels) and after (right panels) the second throughput test. The top row shows yearly rates derived from R1+ and the bottom row of panels show the results from the recent R2 campaign.

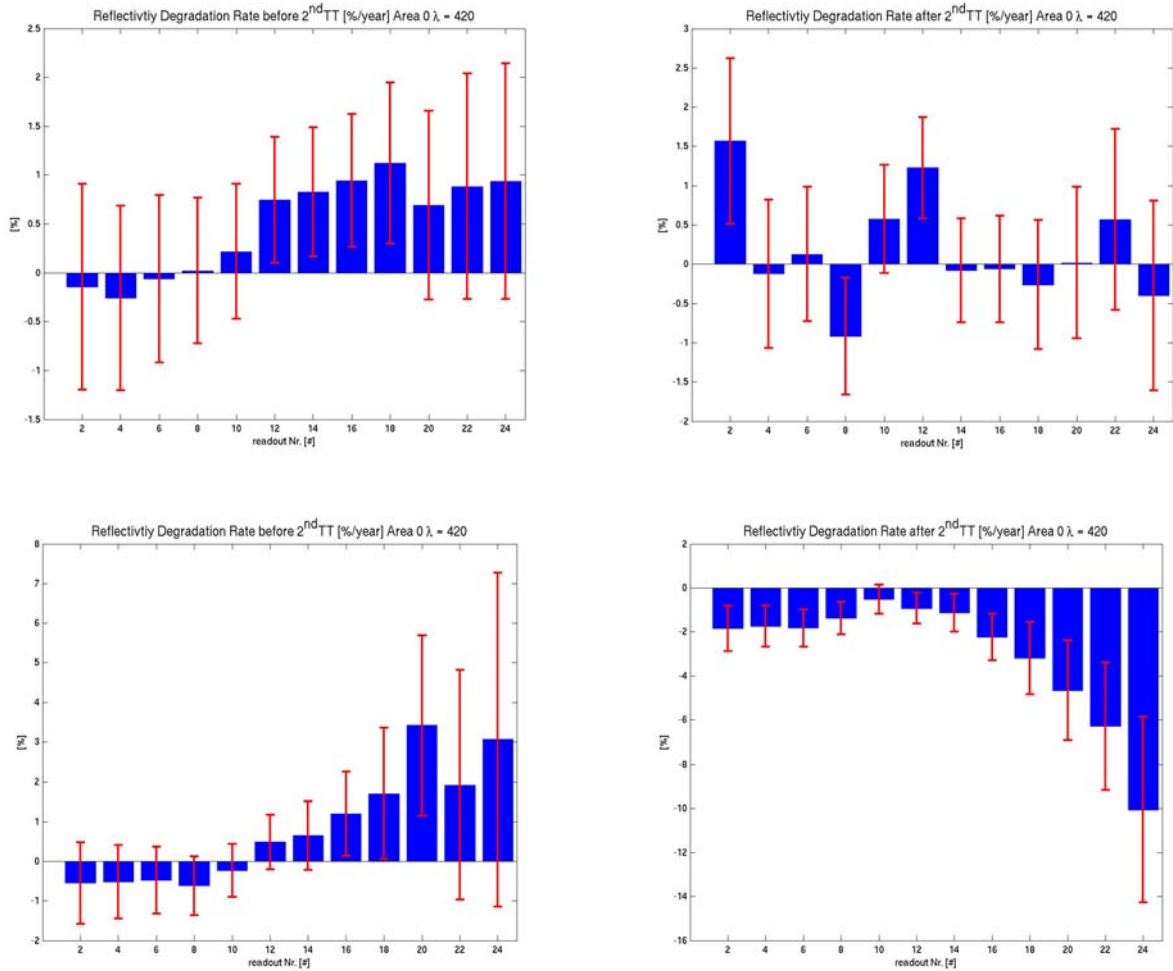


Figure 98: Reflectivity degradation rates at 420 nm (Channel 3) before (left panels) and after (right panels) the second throughput test. The top row shows yearly rates derived from R1+ and the bottom row of panels show the results from the recent R2 campaign.

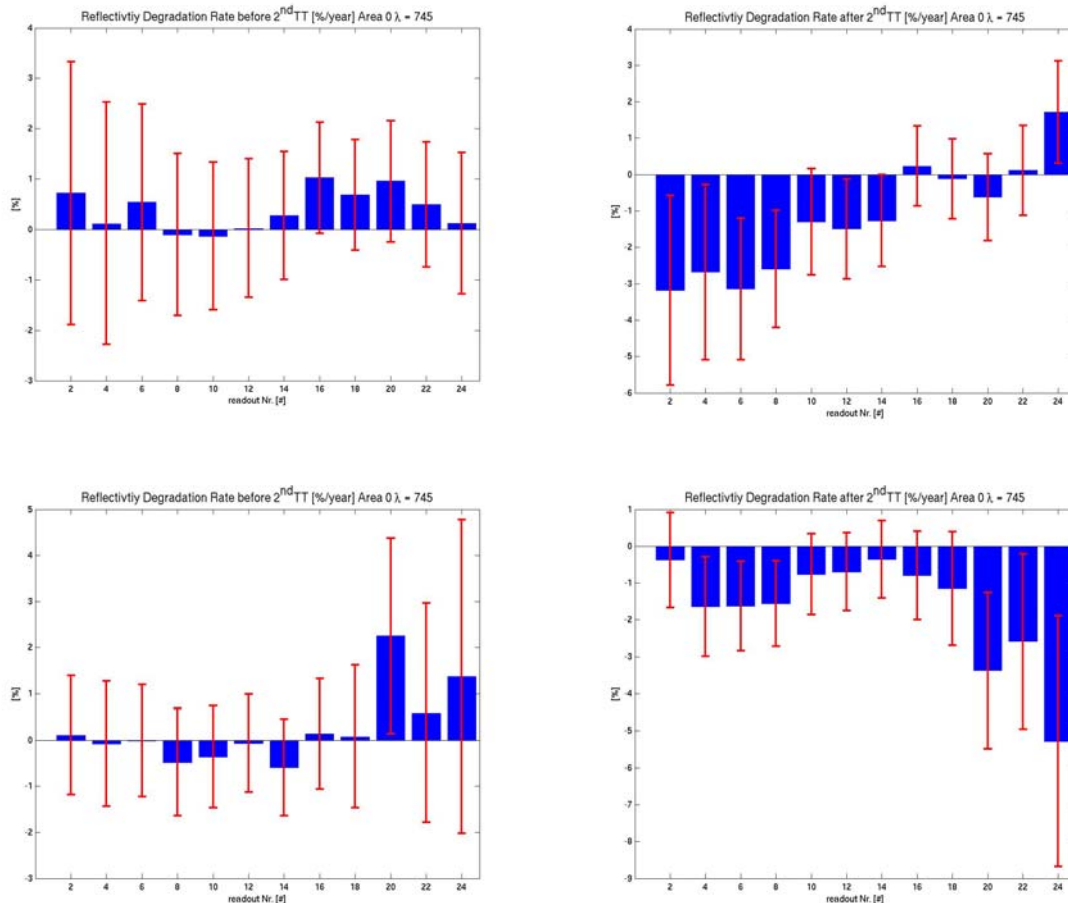


Figure 99: Reflectivity degradation rates at 745 nm (Channel 4) before (left panels) and after (right panels) the second throughput test. The top row shows yearly rates derived from R1+ and the bottom row of panels show the results from the recent R2 campaign.

Again, please note that the reflectivity degradation reflects the differential degradation between the solar and the earthshine paths. Since the differential degradation between both instrument optical paths increased after the second throughput test, the reflectivity degradation rates also increased, even though the overall throughput degradation of the individual optical paths is much smaller after the test (for details see Section 7.7.3).

The results presented in Figure 96 to Figure 99 show that for R2, the yearly degradation rates appear to change more systematically with wavelength. For R2, reflectivity-degradation both before and after the throughput test are positive for wavelengths below 330 nm. Degradation rates become smaller towards zero before the second throughput test and at wavelengths larger than 330 nm. Degradation rates become consistently negative after the second throughput test with strong viewing angle dependencies. Generally, degradation rates are larger for the west-viewing direction (high scanner position numbers) than for east-viewing directions and tend to be smallest at nadir for wavelengths larger than 330 nm.

## 8 Conclusions

### 8.1 Product Validation Summary

The target of the G2RP-R2 campaign is recalled here (see Section Purpose and Scope). The reprocessed dataset shall demonstrate the following:

- to remove any spurious effects on the level 1B data quality due to processor and auxiliary-data changes,
- to serve the consistent evaluation and validation of level 2 data processing over multiple seasonal cycle,
- to evaluate consistently the long-term degradation of the instrument,
- to support the development of a level 1C processor and product, mitigating the effects of long-term instrument degradation [RD5], and
- to serve the preparation and execution of atmospheric composition and climate monitoring studies (extension of the GOME-1 and SCIAMACHY datasets).

All reprocessed onboard measurements crucial for the evaluation of the long terms performance, like dark measurements, the spectral calibration and the etalon correction show a signal evolution which is solely related to instrument events for G2RP-R2 (see Sections 7.1–7.4). Dark signal offsets and dark signal-derived noise values are essentially constant, whereas detector leakage signal is increasing within the predicted limits of 1 BU/s per year [RD12]. The spectral signal is stable for G2RP-R2 and changing only at sub-detector pixel level closely related to the on-board optical bench temperature variations. The processing of etalon correction spectra for G2RP-R2 has been demonstrated to be consistent over the whole reference period using WLS reference spectra and the observed changes in etalon pattern are linked to long-term changes of the instrument (like degradation) or triggered and related to instrument events (PLSOL and throughput test).

We have focused our validation on the evaluation of Stokes fraction and polarisation correction quality (Sections 7.5 and 7.8) because the most significant changes between PPF 4.0 (R1) and PPF 5.3 (R2) are related to PMD calibration and Stokes fraction quality (see Section 5.3). The Stokes fraction show significant discontinuities over the full time period for G2RP-R1 predominantly related to a changing instrument performance, changes in PMD band setting and instrument events. G2RP-R2 demonstrates to remove these discontinuities because of the usage of improved key-data but most important the application of an online Stokes-fraction correction scheme (for details see Section 7.5).

A second strong focus of the validation has been put on the evaluation of the “differential degradation” between signals from the solar/calibration unit optical path and the earthshine path. The differential degradation of the latter impacts the long-term change in reflectivity; the main quantity used for level-2 retrievals. In case both optical paths would degrade in exactly the same way the reflectivity degradation would be zero and level-2 retrievals would be predominantly affected by increasing noise on the derived columns or/and increase in fit residuals (error on the derived column). However, after G2RP-R2 we need to conclude that the differential degradation is even larger than previously evaluated for G2RP-R1, especially after the second throughput test. This however explains why—even though the overall throughput degradation rates for the individual optical paths are much smaller after the second throughput test than before it—level-2 retrieval do still suffer from the influence of reflectivity degradation as evaluated in Sections 7.7.3, 7.7.4, and 7.8.4 (see also [RD21]). The empirical evaluation of degradation rates at only a few wavelengths over the complete spectrum can be used as a reference for the evaluation of a level 1C processor and product, for mitigating the effects of long-term instrument degradation. The latter was, however, not part of the scope of this campaign.

The evaluation of differences of key-parameter series between R2 and the previous campaign settings (R1+) have demonstrated that the consistency of the dataset has significantly improved together with the quality of individual parameters (like Stokes fractions and PMD signal related key-data; see Section 7.8). Level 1B data from G2RP-R2 is therefore expected to improve on the quality of long-term data-series derived from it.

#### **8.1.1 Product Validation Open Issues**

None (TBC).

#### **8.1.2 Processor Open Issues**

None.

#### **8.1.3 Instrument Performance**

Anomalous degradation of instrument throughput [RD5].

#### **8.1.4 Calibration Key Data**

Update for reanalysed GOME-2 FM3 / Metop-A is not part of G2RP-2. However, the major changes to key-data for FM3 which are included in the re-analysed dataset (Issue 6) by SSST/Galileo/TNO have already been introduced for PPF 5.3 by EUMETSAT before issuing of G2RP-R2 and are therefore included here. Changes between products from PPF 5.3.0 (R2) and products using the official TNO-reanalysed dataset are on the order of 1% below 290 nm and only for very high solar zenith and viewing angles. For lower wavelengths, the differences at large viewing and high solar zenith angle are well below 0.5 %.

See the GOME-2 newsletter #29 on this web page:

[www.eumetsat.int](http://www.eumetsat.int) > [Service Status](#) > [Product Quality Monitoring](#) > [GOME-2 Newsletter](#)

## **8.2 Recommendations**

It is recommended that all partners make use of the G2PR-R2 dataset of January 2007 to January 2012 for long-term level 2 activities addressing long-term data quality and climate-related activities. This dataset is consistent with the current operational processor GOME-2 PPF 5.3.